

Color superconductivity in dense quark matter

Mark G. Alford* and Andreas Schmitt†

Department of Physics, Washington University, St Louis, MO 63130, USA

Krishna Rajagopal‡

Center for Theoretical Physics, Massachusetts Institute of Technology, Cambridge, MA 02139, USA

Thomas Schäfer§

Department of Physics, North Carolina State University, Raleigh, NC 27695, USA

(Dated: 28 Sep 2007)

Matter at high density and low temperature is expected to be a color superconductor, which is a degenerate Fermi gas of quarks with a condensate of Cooper pairs near the Fermi surface that induces color Meissner effects. At the highest densities, where the QCD coupling is weak, rigorous calculations are possible, and the ground state is a particularly symmetric state, the color-flavor locked (CFL) phase. The CFL phase is a superfluid, an electromagnetic insulator, and breaks chiral symmetry. The effective theory of the low-energy excitations in the CFL phase is known and can be used, even at more moderate densities, to describe its physical properties. At lower densities the CFL phase may be disfavored by stresses that seek to separate the Fermi surfaces of the different flavors, and comparison with the competing alternative phases, which may break translation and/or rotation invariance, is done using phenomenological models. We review the calculations that underlie these results, and then discuss transport properties of several color-superconducting phases and their consequences for signatures of color superconductivity in neutron stars.

Contents

I. Introduction	2	IV. Weak-coupling QCD calculations	15
A. General outline	2	A. The gap equation	16
B. Inevitability of color superconductivity	3	B. Quasiparticle excitations	18
C. Quark Cooper pairing	5	C. Pressure and condensation energy	20
D. Chemical potentials and neutrality constraints	5	D. Weak coupling solution of the gap equation	20
E. Stresses on BCS pairing	6	E. Gap and critical temperature at weak coupling	22
F. Overview of the quark matter phase diagram	6	F. Color and electromagnetic Meissner effect	23
II. Matter at the highest densities	7	G. Chromomagnetic instability	25
A. Color-flavor locked (CFL) quark matter	7	V. Effective theories of the CFL phase	26
1. Color-flavor locking and chiral symmetry breaking	8	A. High density effective theory	27
2. Superfluidity	8	1. Effective Lagrangian	27
3. Gauge symmetry breaking and electromagnetism	8	2. Non-Fermi liquid effects and the gap equation	28
4. Low-energy excitations	9	3. Mass terms	29
5. Why CFL is favored	9	B. Ginzburg-Landau theory	29
B. Intermediate density: stresses on the CFL phase	10	C. Goldstone bosons in the CFL phase	30
C. Kaon condensation: the CFL- K^0 phase	11	1. Effective Lagrangian	30
III. Below CFL densities	11	2. Mass terms	32
A. Two-flavor pairing: the 2SC phase	11	D. Kaon condensation	33
B. The unstable gapless phases	12	E. Fermions in the CFL phase	34
C. Crystalline color superconductivity	13	F. Goldstone boson currents	35
D. Meson supercurrent (“curCFL- K^0 ”)	13	G. Other effective theories	36
E. Single-flavor pairing	13	VI. NJL model comparisons among candidate phases below CFL densities	36
F. Gluon condensation	14	A. Model, pairing ansatz, and homogeneous phases	37
G. Secondary pairing	14	B. Crystalline phases	40
H. Mixed phases	14	C. Rigidity of crystalline color superconducting quark matter	44
I. Relation to cold atomic gases	15	VII. Transport properties and neutrino processes	45
		A. Viscosity and thermal conductivity	46
		1. CFL phase	46
		2. Other phases	47
		B. Neutrino emissivity and specific heat	48
		1. CFL phase	48
		2. Other phases	48
		VIII. Color superconductivity in neutron stars	50

*Electronic address: alford@wuphys.wustl.edu

†Electronic address: aschmitt@wuphys.wustl.edu

‡Electronic address: krishna@lns.mit.edu

§Electronic address: tmschaef@unity.ncsu.edu

A. Mass-radius relation	51
B. Signatures of the compactness of neutron stars	52
C. Cooling	52
D. r -modes limiting pulsar spins	54
E. Supernova neutrinos	55
F. Rigid quark matter and pulsar glitches	55
Acknowledgments	56
References	57

I. INTRODUCTION

A. General outline

The study of matter at ultra-high density is the “condensed matter physics of quantum chromodynamics”. It builds on our understanding of the strong interaction, derived from experimental observation of few-body processes, to predict the behavior of macroscopic quantities in many-body systems where the fundamental particles of the standard model—quarks and leptons—become the relevant degrees of freedom. As in conventional condensed-matter physics, the goal is to map the phase diagram and calculate the properties of the phases. However, in contrast to most areas of condensed matter physics, we can study “asymptotically high” densities, where quantum chromodynamics is weakly coupled, and we can rigorously calculate many properties of quark matter from first principles. We will review those results and describe the progress that has been made in building on this solid foundation to extend our understanding to lower and more phenomenologically relevant densities.

Quark matter occurs in various forms, depending on the temperature T and quark chemical potential μ (see Fig. 1). At high temperatures ($T \gg \mu$) entropy precludes any pattern of order and there is only quark-gluon plasma (QGP), the phase of strongly interacting matter that has no spontaneous symmetry breaking, and which filled the universe for the first microseconds after the big bang. Quark-gluon plasma is also being created in small, very short-lived, droplets in ultrarelativistic heavy ion collisions at the Relativistic Heavy Ion Collider.

In this review we concentrate on the regime of relatively low temperatures, $T \ll \mu$, where we find a rich variety of spontaneous symmetry breaking phases. To create such material in nature requires a piston that can compress matter to super-nuclear densities and hold it while it cools. The only known context where this might happen is in the interior of neutron stars, where gravity squeezes the star to an ultra-high density state where it remains for millions of years. This gives time for weak interactions to equilibrate, and for the temperature of the star to drop far below the quark chemical potential. We do not currently know whether quark matter exists in the cores of neutron stars. One of the reasons for studying color superconductivity is to improve our understanding of how a quark matter core would affect the observable

behavior of a neutron star, and thereby resolve this uncertainty.

When we speak of matter at the highest densities, we shall always take the high density limit with up, down and strange quarks only. We do so because neutron star cores are not dense enough (by more than an order of magnitude) to contain any charm or heavier quarks, and our ultimate goal is to gain insight into quark matter at densities that may be found in nature. For the same reason we focus on temperatures below about ten MeV, which are appropriate for neutron stars that are more than a few seconds old.

As we will explain in some detail, at low temperatures and the highest densities we expect to find a degenerate liquid of quarks, with Cooper pairing near the Fermi surface that spontaneously breaks the color gauge symmetry (“color superconductivity”). Speculations about the existence of a quark matter phase at high density go back to the earliest days of the quark model of hadrons (Boccaletti *et al.*, 1966; Itoh, 1970; Ivanenko and Kurdgelaidze, 1965; Pacini, 1966), and the possibility of quark Cooper pairing was noted even before there was a comprehensive theory of the strong interaction (Ivanenko and Kurdgelaidze, 1969, 1970). After the development of quantum chromodynamics (QCD), with its property of asymptotic freedom (Gross and Wilczek, 1973; Politzer, 1973), it became clear that a quark matter phase would exist at sufficiently high density (Collins and Perry, 1975; Kislinger and Morley, 1976) and the study of quark Cooper pairing was pioneered by Barrois and Frautschi (Barrois, 1977, 1979; Frautschi, 1978), who first used the term “color superconductivity”, and by Bailin and Love (Bailin and Love, 1979, 1984), who classified many of the possible pairing patterns. Iwasaki and Iwado (Iwasaki, 1995; Iwasaki and Iwado, 1995) performed mean-field calculations of single-flavor pairing in a Nambu-Jona-Lasinio (NJL) model, but it was not until the prediction of large pairing gaps (Alford *et al.*, 1998; Rapp *et al.*, 1998) and the color-flavor locked (CFL) phase (Alford *et al.*, 1999b) that the phenomenology of color-superconducting quark matter became widely studied. At present there are many reviews of the subject from various stages in its development (Alford, 2001; Alford and Rajagopal, 2006; Bailin and Love, 1984; Buballa, 2005a; Hong, 2001; Hsu, 2000; Huang, 2005; Nardulli, 2002; Rajagopal and Wilczek, 2000; Reddy, 2002; Ren, 2004; Rischke, 2004; Schäfer, 2003b; Shovkovy, 2005), and the reader may wish to consult them for alternative presentations with different emphases. As these reviews make clear, the last decade has seen dramatic progress in our understanding of dense matter. We are now able to obtain, directly from QCD, rigorous and quantitative answers to the basic question: “What happens to matter if you squeeze it to arbitrarily high density?”. In Sec. IV we will show how QCD becomes analytically tractable at arbitrarily high density: the coupling is weak and the physics of confinement

never arises, since long-wavelength magnetic interactions are cut off, both by Landau damping and by the Meissner effect. As a result, matter at the highest densities is known to be in the CFL phase, whose properties (see Sec. II) are understood rigorously from first principles. There is a well-developed effective field theory describing the low energy excitations of CFL matter (see Sec. V), so that at any density at which the CFL phase occurs, even if this density is not high enough for a weak-coupling QCD calculation to be valid, many phenomena can nevertheless be described quantitatively in terms of a few parameters, via the effective field theory.

It should be emphasized that QCD at arbitrarily high density is more fully understood than in any other context. High energy scattering, for example, can be treated by perturbative QCD, but making contact with observables brings in poorly understood nonperturbative physics via structure functions and/or fragmentation functions. Or, in quark-gluon plasma in the high temperature limit much of the physics is weakly-coupled but the lowest energy modes remain strongly coupled with nonperturbative physics arising in the nonabelian color-magnetic sector. We shall see that there are no analogous difficulties in the analysis of CFL matter at asymptotic densities.

If the CFL phase persists all the way down to the transition to nuclear matter then we have an exceptionally good theoretical understanding of the properties of quark matter in nature. However, less symmetrically paired phases of quark matter may well intervene in the intermediate density region between nuclear and CFL matter (Sec. I.E). We enumerate some of the possibilities in Sec. III. In principle this region could also be understood from first principles, using brute-force numerical methods (lattice QCD) to evaluate the QCD path integral, but unfortunately current lattice QCD algorithms are defeated by the fermion sign problem in the high-density low-temperature regime (Schmidt, 2006).¹ This means we have to use models, or try to derive information from astrophysical observations. In Sec. VI we sketch an example of a (Nambu–Jona-Lasinio) model analysis within which one can compare some of the possible intermediate-density phases suggested in Sec. I.E. We finally discuss the observational approach, which involves elucidating the properties of the suggested phases of quark matter (Secs. VI.C and VII), and then finding astrophysical signatures by which their presence inside neutron stars might be established or ruled out using astronomical observations (Sec. VIII).

B. Inevitability of color superconductivity

At sufficiently high density and low temperature it is a good starting point to imagine that quarks form a degenerate Fermi liquid. Because QCD is asymptotically free — the interaction becomes weaker as the momentum transferred grows — the quarks near the Fermi surface are almost free, with weak QCD interactions between them. (Small-angle quark-quark scattering via a low-momentum gluon is no problem because it is cut off by Landau damping, which, together with Debye screening, keeps perturbation theory at high density much better controlled than at high temperature (Pisarski and Rischke, 1999a; Son, 1999).) The quark-quark interaction is certainly attractive in some channels, since we know that quarks bind together to form baryons. As we will now argue, these conditions are sufficient to guarantee color superconductivity at sufficiently high density.

At zero temperature, the thermodynamic potential (which we will loosely refer to as the “free energy”) is $\Omega = E - \mu N$, where E is the total energy of the system, μ is the chemical potential, and N is the number of fermions. If there were no interactions then the energy required to add a particle to the system would be the Fermi energy $E_F = \mu$, so adding or subtracting particles or holes near the Fermi surface would cost zero free energy. With a weak attractive interaction in any channel, if we add a pair of particles (or holes) with the quantum numbers of the attractive channel, the free energy is lowered by the potential energy of their attraction. Many such pairs will therefore be created in the modes near the Fermi surface, and these pairs, being bosonic, will form a condensate. The ground state will be a superposition of states with different numbers of pairs, breaking the fermion number symmetry. This argument, originally developed by Bardeen, Cooper, and Schrieffer (BCS) (Bardeen *et al.*, 1957) is completely general, and can be applied to electrons in a metal, nucleons in nuclear matter, ³He atoms, cold fermionic atoms in a trap, or quarks in quark matter.

The application of the BCS mechanism to pairing in dense quark matter is in a sense more direct than in its original setting. The dominant interaction between electrons in a metal is the repulsive Coulomb interaction, and it is only because this interaction is screened that the attraction mediated by phonons comes into play. This means that the effective interactions that govern superconductivity in a metal depend on band structure and other complications and are very difficult to determine accurately from first principles. In contrast, in QCD the “color Coulomb” interaction is attractive between quarks whose color wave function is antisymmetric, meaning that superconductivity arises as a direct consequence of the primary interaction in the theory. This has two important consequences. First, at asymptotic densities where the QCD interaction is weak we can derive the gap parameter and other properties of color super-

¹ Condensation of Cooper pairs of quarks has been studied on the lattice in 2-color QCD (Alles *et al.*, 2006; Fukushima and Iida, 2007; Hands *et al.*, 2006, 1999; Kogut *et al.*, 2001, 1999, 2000, 2002; Nishida *et al.*, 2004), for high isospin density rather than baryon density (Kogut and Sinclair, 2002; Son and Stephanov, 2001; Splittorff *et al.*, 2001) and in NJL-type models (Hands and Walters, 2004).

conducting quark matter rigorously from the underlying microscopic theory. Second, at accessible densities where the QCD interaction is stronger the ratio of the gap parameter to the Fermi energy will be much larger than in conventional BCS superconducting metals. Thus, superconductivity in QCD is more robust, both in the theoretical sense and in the phenomenological sense, than superconductivity in metals.

It has long been known that, in the absence of pairing, an unscreened static magnetic interaction results in a “non-Fermi-liquid” (Baym *et al.*, 1990; Boyanovsky and de Vega, 2001a,b; Brown *et al.*, 2000a; Chakravarty *et al.*, 1995; Gerhold *et al.*, 2004; Holstein *et al.*, 1973; Ipp *et al.*, 2004, 2006; Manuel, 2000a,b; Nayak and Wilczek, 1994; Polchinski, 1994; Vanderheyden and Ollitrault, 1997). However, in QCD the magnetic interaction is screened at nonzero frequency (Landau damping) and this produces a particularly mild form of non-Fermi-liquid behavior, as we describe in Sec. V.A.2. In the absence of pairing but in the presence of interactions, there are still quark quasiparticles and there is still a “Fermi surface”, and the BCS argument goes through. This argument is rigorous at high densities, where the QCD coupling g is small. The energy scale below which non-Fermi liquid effects would become strong enough to modify the quasiparticle picture qualitatively is parametrically of order $\exp(-\text{const}/g^2)$ whereas the BCS gap that results from pairing is parametrically larger, of order $\exp(-\text{const}/g)$ as we shall see in Sec. IV. This means that pairing occurs in a regime where the basic logic of the BCS argument remains valid.

Since pairs of quarks cannot be color singlets, the Cooper pair condensate in quark matter will break the local color symmetry $SU(3)_c$, hence the term “color superconductivity”. The quark pairs play the same role here as the Higgs particle does in the standard model: the color-superconducting phases can be thought of as Higgs phases of QCD. Here, the gauge bosons that acquire a mass through the process of spontaneous symmetry breaking are the gluons, giving rise to color Meissner effects. It is important to note that quarks, unlike electrons, have color and flavor as well as spin degrees of freedom, so many different patterns of pairing are possible. This leads us to expect a panoply of different possible color superconducting phases.

As we shall discuss in Sec. II, at the highest densities we can achieve an *ab initio* understanding of the properties of dense matter, and we find that its preferred state is the CFL phase of three-flavor quark matter, which is unique in that *all* the quarks pair (all flavors, all colors, all spins, all momenta on the Fermi surfaces) and all the nonabelian gauge bosons are massive. The suppression of these infrared degrees of freedom eliminates the possibility of new phenomena emerging at low momenta, and ensures that, at sufficiently high density, the CFL ground state, whose only infrared degrees of freedom are Goldstone bosons and an abelian photon, is stable. In this regime, quantitative calculations of observable prop-

erties of CFL matter can be done from first principles; there are no remaining nonperturbative gaps in our understanding.

As the density decreases, the effect of the strange quark mass becomes more noticeable, imposing stresses that may modify the Cooper pairing and the CFL phase may be replaced by other forms of color superconducting quark matter. Furthermore, as the attractive interaction between quarks becomes stronger at lower densities, correlations beyond the two-body correlation that yields Cooper pairing may become important, and at some point the ground state will no longer be a Cooper-paired state of quark matter, but something quite different. Indeed, by the time we decrease the density down to that of nuclear matter, the average separation between quarks has increased to the point that the interactions are strong enough to bind quarks into nucleons. It is worth noting that quark matter is in this regard different from Cooper-paired ultracold fermionic atoms (to be discussed in Sec. III.I). For fermionic atoms, as the interaction strength increases there is a crossover from BCS-paired fermions to a Bose-Einstein condensate (BEC) of tightly-bound, well-separated, weakly-interacting diatoms (molecules). In QCD, however, the color charge of a diquark is the same as that of an antiquark, so diquarks will interact with each other as strongly as quarks, and there will not be a literal analogue of the BCS/BEC crossover seen in fermionic atoms. In QCD, the neutral bound states at low density that are (by QCD standards) weakly interacting are nucleons, containing three quarks not two.

We shall work with $N_c = 3$ colors throughout. In the limit $N_c \rightarrow \infty$ with fixed Λ_{QCD} (i.e fixed $g^2 N_c$), Cooper pairing is not necessarily energetically preferred. A strong competitor for the large- N_c ground state is the chiral density wave (CDW), a condensate of quark-hole pairs, each with total momentum $2p_F$ (Deryagin *et al.*, 1992). Quark-hole scattering is enhanced by a factor of N_c over quark-quark scattering, but, unlike Cooper pairing, it only uses a small fraction of the Fermi surface, and in the case of short range forces the CDW phase is energetically favored in one-dimensional systems, but not in two or more spatial dimensions (Shankar, 1994). However, in QCD in the large N_c limit the equations governing the CDW state become effectively one-dimensional because the gluon propagator is not modified by the medium, so the quark-hole interaction is dominated by almost collinear scattering. Since pairing gaps are exponentially small in the coupling but medium effects only vanish as a power of N_c , the CDW state requires an exponentially large number of colors. It is estimated that for $\mu \sim 1$ GeV, quark-hole pairing becomes favored over Cooper pairing when $N_c \gtrsim 1000$ (Shuster and Son, 2000). Recent work (McLerran and Pisarski, 2007) discusses aspects of physics at large N_c at lower densities that may also be quite different from physics at $N_c = 3$.

Before turning to a description of CFL pairing in Sec. II and less-symmetrically paired forms of color supercon-

ducting quark matter in Sec. III, we discuss some generic topics that arise in the analysis of color-superconducting phases: the gap equations, neutrality constraints, the resultant stresses on Cooper pairing, and the expected overall form of the phase diagram.

C. Quark Cooper pairing

The quark pair condensate can be characterized in a gauge-variant way by the expectation value of the one-particle-irreducible quark-quark two-point function, also known as the “anomalous self-energy”,

$$\langle \psi_{ia}^\alpha \psi_{jb}^\beta \rangle = P_{ij}^{\alpha\beta} \Delta \quad (1)$$

Here ψ is the quark field operator, color indices α, β range over red, green, and blue (r, g, b), flavor indices i, j range over up, down and strange (u, d, s), and a, b are the spinor Dirac indices. The angle brackets denote the one-particle-irreducible part of the quantum-mechanical ground-state expectation value. In general, both sides of this equation are functions of momentum. The color-flavor-spin matrix P characterizes a particular pairing channel, and Δ is the gap parameter which gives the strength of the pairing in this channel. A standard BCS condensate is position-independent (so that in momentum space the pairing is between quarks with equal and opposite momentum) and a spin singlet (so that the gap is isotropic in momentum space). However, as we will see later, there is good reason to expect non-BCS condensates as well as BCS condensates in high-density quark matter.

Although (1) defines a gauge-variant quantity, it is still of physical relevance. Just as electroweak symmetry breaking is most straightforwardly understood in the unitary gauge where the Higgs vacuum expectation value is uniform in space, so color superconductivity is typically analyzed in the unitary gauge where the quark pair operator has a uniform color orientation in space. We then relate the gap parameter Δ to the spectrum of the quark-like excitations above the ground state (“quasiquarks”), which is gauge-invariant.

In principle, a full analysis of the phase structure of quark matter in the μ - T plane would be performed by writing down the free energy Ω , which is a function of the temperature, the chemical potentials for all conserved quantities, and the gap parameters for all possible condensates, including the quark pair condensates but also others such as chiral condensates of the form $\langle \bar{q}q \rangle$. We impose neutrality with respect to gauge charges (see Sect. I.D below) and then within the neutral subspace we minimize the free energy with respect to the strength of the condensate:

$$\frac{\partial \Omega}{\partial \Delta} = 0, \quad \frac{\partial^2 \Omega}{\partial \Delta^2} > 0. \quad (2)$$

We have written this gap equation and stability condition somewhat schematically since for many patterns of

pairing there will be gap parameters with different magnitudes in different channels. The free energy must then be minimized with respect to each of the gap parameters, yielding a coupled set of gap equations. The solution to (2) with the lowest free energy that respects the neutrality constraints discussed below yields the favored phase.

D. Chemical potentials and neutrality constraints

Why do we describe “matter at high density” by introducing a large chemical potential μ for quark number but no chemical potentials for other quantities? The answer is that this reflects the physics of neutron stars, which are the main physical arena that we consider. Firstly, on the long timescales relevant to neutron stars, the only global charges that are conserved in the standard model are quark number and lepton number, so only these can be coupled to chemical potentials (we shall discuss gauged charges below). Secondly, a neutron star is permeable to lepton number because neutrinos are so light and weakly-interacting that they can quickly escape from the star, so the chemical potential for lepton number is zero. Electrons are present because they carry electric charge, for which there is a nonzero potential. In the first few seconds of the life of a neutron star the neutrino mean free path may be short enough to sustain a nonzero lepton number chemical potential, but we will not discuss that scenario.

Stable bulk matter must be neutral under all gauged charges, whether they are spontaneously broken or not. Otherwise, the net charge density would create large electric fields, making the energy non-extensive. In the case of the electromagnetic gauge symmetry, this simply requires zero charge density, $Q = 0$. The correct formal requirement concerning the color charge of a large lump of matter is that it should be a color *singlet*, i.e., its wavefunction should be invariant under a general color gauge transformation. However, it is sufficient for us to impose color *neutrality*, meaning equality in the numbers of red, green, and blue quarks. This is a less stringent constraint (singlet \Rightarrow neutral but neutral $\not\Rightarrow$ singlet) but the projection of a color neutral state onto a color singlet costs no extra free energy in the thermodynamic limit (Amore *et al.*, 2002). In general there are 8 possible color charges, but because the Cartan subalgebra of $SU(3)_c$ is two-dimensional it is always possible to transform to a gauge where all are zero except Q_3 and Q_8 , the charges associated with the diagonal generators $T_3 = \frac{1}{2} \text{diag}(1, -1, 0)$ and $T_8 = \frac{1}{2\sqrt{3}} \text{diag}(1, 1, -2)$ in (r, g, b) space (Buballa and Shovkovy, 2005; Rajagopal and Schmitt, 2006). In this review, we only discuss such gauges. So to impose color neutrality we just require $Q_3 = Q_8 = 0$.

In nature, electric and color neutrality are enforced by the dynamics of the electromagnetic and QCD gauge fields, whose zeroth components serve as chemical potentials coupled to the charges Q, Q_3, Q_8 , and which

are naturally driven to values that set these charges to zero (Alford and Rajagopal, 2002; Dietrich and Rischke, 2004; Gerhold and Rebhan, 2003; Iida and Baym, 2001; Kryjevski, 2003). In an NJL model with fermions but no gauge fields (see Sec. VI) one has to introduce the chemical potentials μ_e , μ_3 and μ_8 by hand in order to enforce color and electric neutrality. The neutrality conditions are then

$$\begin{aligned} Q &= \frac{\partial\Omega}{\partial\mu_e} = 0 \\ Q_3 &= -\frac{\partial\Omega}{\partial\mu_3} = 0 \\ Q_8 &= -\frac{\partial\Omega}{\partial\mu_8} = 0. \end{aligned} \quad (3)$$

(Note that we define an electrostatic potential μ_e that is coupled to the *negative* electric charge Q , so that in typical neutron star conditions, where there is a finite density of electrons rather than positrons, μ_e is positive.)

Finally we should note that enforcing local neutrality is appropriate for uniform phases, but there are also non-uniform charge-separated phases (“mixed phases”), consisting of positively and negatively charged domains which are neutral on average. These are discussed further in Sec. III.H.

E. Stresses on BCS pairing

The free energy argument that we gave in Sec. I.B for the inevitability of BCS pairing in the presence of an attractive interaction relies on the assumption that the quarks that pair with equal and opposite momenta can each be arbitrarily close to their common Fermi surface. However, as we will see in Sec. II, the neutrality constraint, combined with the mass of the strange quark and the requirement that matter be in beta equilibrium, tends to pull apart the Fermi momenta of the different flavors of quarks, imposing an extra energy cost (“stress”) on the formation of Cooper pairs involving quarks of different flavors. This raises the possibility of non-BCS pairing in some regions of the phase diagram.

To set the stage here, let us discuss a simplified example: consider two massless species of fermions, labeled 1 and 2, with different chemical potentials μ_1 and μ_2 , and an attractive interaction between them that favors cross-species BCS pairing with a gap parameter Δ . It will turn out that to a good approximation the color-flavor locked pairing pattern contains three such sectors, so this example captures the essential physics we will encounter in later sections. We define the average chemical potential and the stress parameter

$$\begin{aligned} \bar{\mu} &= \frac{1}{2}(\mu_1 + \mu_2) \\ \delta\mu &= \frac{1}{2}(\mu_1 - \mu_2). \end{aligned} \quad (4)$$

As long as the stress $\delta\mu$ is small enough relative to Δ , BCS pairing between species 1 and 2 can occur,

locking their Fermi surfaces together and ensuring that they occur in equal numbers. At the Chandrasekhar-Clogston point (Chandrasekhar, 1962; Clogston, 1962), where $\delta\mu = \Delta/\sqrt{2}$, the two-species model undergoes a first-order transition to the unpaired phase. At this point BCS pairing still exists as a locally stable state, with a completely gapped spectrum of quasiparticles. When $\delta\mu$ reaches Δ the spectrum becomes gapless at momentum $p = \bar{\mu}$, indicating that cross-species BCS pairing is no longer favored at all momenta (Alford *et al.*, 2004b). If the two species are part of a larger pairing pattern, the Chandrasekhar-Clogston transition can be shifted, and we shall see that in the two-species subsectors of the CFL pattern it is shifted to $\delta\mu > \Delta$. The onset of gaplessness is therefore the relevant threshold for our purposes, and it always occurs at $\delta\mu = \Delta$, independent of the larger context in which the two flavors pair. This follows from the fact that BCS pairing only occurs if the energy gained from turning a 1 quark into a 2 quark with the same momentum (namely $\mu_1 - \mu_2$) is less than the cost of breaking the Cooper pair formed by these quarks, which is 2Δ (Rajagopal and Wilczek, 2001). Thus the 1-2 Cooper pairs are energetically stable (or metastable) as long as $\delta\mu < \Delta$. A more detailed treatment of this illustrative example can be found in (Alford and Wang, 2005).

This example uses massless quarks, but it can easily be modified to include the leading effect of a quark mass M . A difference in the masses of the pairing quarks also stresses the pairing, because it gives them different Fermi momenta at the same chemical potential, so the quarks in a 1-2 Cooper pair, which have equal and opposite momenta, will not both be close to their Fermi energies. The leading-order effect is easily calculated, since for a quark near its Fermi surface it acts like a shift in the quark chemical potential by $-M^2/(2\bar{\mu})$ (given that Fermi momentum $p_F \approx \bar{\mu}$ to this order).

Returning from our toy model to realistic quark matter, the quark flavors that are potentially relevant at neutron-star densities are the light up (u) and down (d) quarks, with current masses m_u and m_d that are $\lesssim 5$ MeV, and a medium-weight flavor, the strange (s) quark, with current mass $m_s \sim 90$ MeV. Their effective “constituent” masses in the vacuum are hundreds of MeV larger, but are expected to decrease with increasing quark density. We shall refer to the density-dependent constituent masses as $M_{u,d,s}$ and shall typically neglect M_u and M_d . As our toy model has illustrated, however, the strange quark mass M_s will contribute to stresses on cross-flavor pairing, and those stresses will become more severe as the density (and hence $\bar{\mu}$) decreases. This will be a major theme of later sections.

F. Overview of the quark matter phase diagram

Fig. 1 shows a schematic phase diagram for QCD that is consistent with what is currently known. Along the

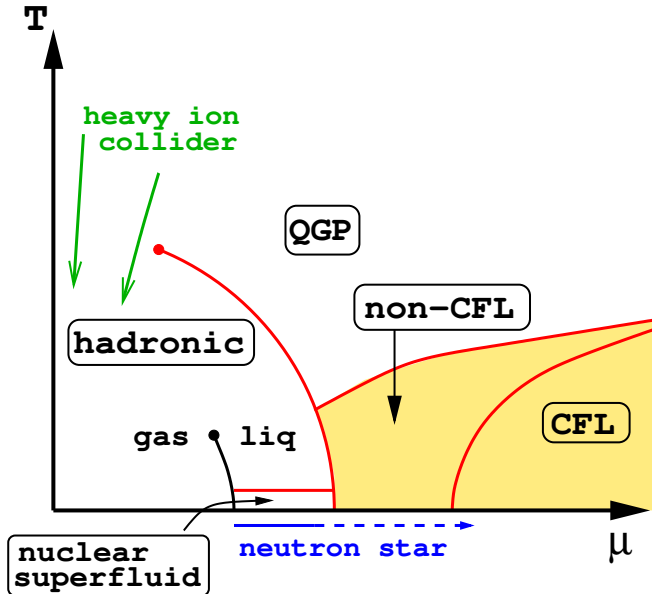


FIG. 1 (Color online) A schematic outline for the phase diagram of matter at ultra-high density and temperature. The CFL phase is a superfluid (like cold nuclear matter) and has broken chiral symmetry (like the hadronic phase).

horizontal axis the temperature is zero, and the density is zero up to the onset transition where it jumps to nuclear density, and then rises with increasing μ . Neutron stars are in this region of the phase diagram, although it is not known whether their cores are dense enough to reach the quark matter phase. Along the vertical axis the temperature rises, taking us through the crossover from a hadronic gas to the quark-gluon plasma. This is the regime explored by high-energy heavy-ion colliders.

At the highest densities we find the color-flavor locked color-superconducting phase,² in which the strange quark participates symmetrically with the up and down quarks in Cooper pairing. This is described in more detail in Secs. II, IV, and V. It is not yet clear what happens at intermediate density, and in Secs. III and VI we will discuss the factors that disfavor the CFL phase at intermediate densities, and survey the color superconducting phases that have been hypothesized to occur there.

Various aspects of color superconductivity at high temperatures have been studied, including the phase structure (see Sec. VI.A), spectral functions, pair-forming and -breaking fluctuations, possible precursors to condensation such as pseudogaps, and various collective phenomena (Abuki *et al.*, 2002; Fukushima and Iida,

2005; Hatsuda *et al.*, 2006; Kitazawa *et al.*, 2002, 2004, 2005a,b, 2007; Voskresensky, 2004; Yamamoto *et al.*, 2007). However, this review centers on quark matter at neutron star temperatures, and throughout Secs. II and III we restrict ourselves to the phases of quark matter at zero temperature. This is because most of the phases that we discuss are expected to persist up to critical temperatures that are well above the core temperature of a typical neutron star, which drops below 1 MeV within seconds of its birth before cooling down through the keV range over millions of years.

II. MATTER AT THE HIGHEST DENSITIES

A. Color-flavor locked (CFL) quark matter

Given that quarks form Cooper pairs, the next question is who pairs with whom? In quark matter at sufficiently high densities, where the up, down and strange quarks can be treated on an equal footing and the disruptive effects of the strange quark mass can be neglected, the most symmetric and most attractive option is the color-flavor locked phase, where quarks of all three colors and all three flavors form conventional zero-momentum spinless Cooper pairs. This pattern, anticipated in early studies of alternative condensates for zero-density chiral symmetry breaking (Srednicki and Susskind, 1981), is encoded in the quark-quark self-energy (Alford *et al.*, 1999b)

$$\begin{aligned} \langle \psi_i^\alpha C \gamma_5 \psi_j^\beta \rangle &\propto \Delta_{\text{CFL}}(\kappa+1)\delta_i^\alpha \delta_j^\beta + \Delta_{\text{CFL}}(\kappa-1)\delta_j^\alpha \delta_i^\beta \\ &= \Delta_{\text{CFL}} \epsilon^{\alpha\beta A} \epsilon_{ijA} + \Delta_{\text{CFL}} \kappa (\delta_i^\alpha \delta_j^\beta + \delta_j^\alpha \delta_i^\beta) \end{aligned} \quad (5)$$

The symmetry breaking pattern is

$$\begin{aligned} [SU(3)_c] \times U(1)_B \\ \times \underbrace{[SU(3)_L \times SU(3)_R]}_{\supset [U(1)_Q]} \rightarrow \underbrace{[SU(3)_{c+L+R}]}_{\supset [U(1)_{\bar{Q}}]} \times \mathbb{Z}_2 \end{aligned} \quad (6)$$

Color indices α, β and flavor indices i, j run from 1 to 3, Dirac indices are suppressed, and C is the Dirac charge-conjugation matrix. Gauge symmetries are in square brackets. Δ_{CFL} is the CFL gap parameter. The Dirac structure $C \gamma_5$ is a Lorentz singlet, and corresponds to parity-even spin-singlet pairing, so it is antisymmetric in the Dirac indices. The two quarks in the Cooper pair are identical fermions, so the remaining color+flavor structure must be symmetric. The dominant color-flavor component in (5) transforms as $(\bar{\mathbf{3}}_A, \bar{\mathbf{3}}_A)$, antisymmetric in both. The subdominant term, multiplied by κ , transforms as $(\mathbf{6}_S, \mathbf{6}_S)$. It is almost certainly not energetically favored on its own (all the arguments in Sec. II.A.5 for the color triplet imply repulsion for the sextet), but in the presence of the dominant pairing it breaks no additional symmetries, so κ is in general small but not zero (Alford *et al.*, 1999b; Pisarski and Rischke, 1999c; Schäfer, 2000a; Shovkovy and Wijewardhana, 1999).

² As explained in Sec. I.A, we fix $N_f = 3$ at all densities, to maintain relevance to neutron star interiors. Pairing with arbitrary N_f has been studied (Schäfer, 2000a). For N_f a multiple of three one finds multiple copies of the CFL pattern; for $N_f = 4, 5$ the pattern is more complicated.

1. Color-flavor locking and chiral symmetry breaking

A particularly striking feature of the CFL pairing pattern is that it breaks chiral symmetry. Because of color-flavor locking, chiral symmetry remains broken up to arbitrarily high densities in three-flavor quark matter. The mechanism is quite different from the formation of the $\langle\bar{\psi}\psi\rangle$ condensate that breaks chiral symmetry in the vacuum by pairing left-handed (L) quarks with right-handed (R) antiquarks. The CFL condensate pairs L quarks with each other and R quarks with each other (quarks in a Cooper pair have opposite momentum, and zero net spin, hence the same chirality) and so it might naively appear chirally symmetric. However, the Kronecker deltas in (5) connect color indices with flavor indices, so that the condensate is not invariant under color rotations, nor under flavor rotations, but only under simultaneous, equal and opposite, color and flavor rotations. Color is a vector symmetry, so the compensating flavor rotation must be the same for L and R quarks, so the axial part of the flavor group, which is the chiral symmetry, is broken by the locking of color and flavor rotations to each other (Alford *et al.*, 1999b). Such locking is familiar from other contexts, including the QCD vacuum, where a condensate of quark-antiquark pairs locks $SU(3)_L$ to $SU(3)_R$ breaking chiral symmetry “directly”, and the B phase of superfluid ^3He , where the condensate transforms non-trivially under rotations of spin and orbital angular momentum, but is invariant under simultaneous rotations of both.

The breaking of the chiral symmetry is associated with an expectation value for a gauge-invariant order parameter with the structure $\bar{\psi}\bar{\psi}\psi\psi$ (see Sec. V). There is also a subdominant “conventional” chiral condensate $\langle\bar{\psi}\psi\rangle \ll \langle\psi C\gamma_5\psi\rangle$ (Schäfer, 2000a). These gauge-invariant observables distinguish the CFL phase from the QGP, and if a lattice QCD algorithm applicable at high density ever becomes available, they could be used to map the presence of color-flavor locking in the phase diagram.

We also expect massless Goldstone modes associated with chiral symmetry breaking (see Secs. II.A.4 and V). In the real world there is small explicit breaking of chiral symmetry from the current quark masses, so the order parameters will not go to zero in the QGP, and the Goldstone bosons will be light but not massless.

2. Superfluidity

The CFL pairing pattern spontaneously breaks the exact global baryon number symmetry $U(1)_B$, leaving only a discrete \mathbb{Z}_2 symmetry under which all quark fields are multiplied by -1 . There is an associated gauge-invariant 6-quark order parameter with the flavor and color structure of two Lambda baryons, $\langle\Lambda\Lambda\rangle$ where $\Lambda = \epsilon^{abc}\epsilon_{ijk}\psi_i^a\psi_j^b\psi_k^c$. This order parameter distinguishes the CFL phase from the QGP, and there is an associated massless Goldstone boson that makes the CFL

phase a superfluid, see Sec. V.C. The vortices that result when CFL quark matter is rotated have been studied in (Balachandran *et al.*, 2006; Forbes and Zhitnitsky, 2002; Iida and Baym, 2002; Nakano *et al.*, 2007).

3. Gauge symmetry breaking and electromagnetism

As explained above, the CFL condensate breaks the $SU(3)_c \times SU(3)_L \times SU(3)_R$ symmetry down to the diagonal group $SU(3)_{c+L+R}$ of simultaneous color and flavor rotations. Color is a gauge symmetry, and one of the generators of $SU(3)_{L+R}$ is the electric charge, which generates the $U(1)_Q$ gauge symmetry. This means that the unbroken $SU(3)_{c+L+R}$ contains one gauged generator, corresponding to an unbroken $U(1)_{\tilde{Q}}$ which consists of a simultaneous electromagnetic and color rotation. The rest of the color group is broken, so by the Higgs mechanism seven gluons and one gluon-photon linear combination become massive via the Meissner effect. The orthogonal gluon-photon generator \tilde{Q} remains unbroken, because every diquark in the condensate has $\tilde{Q} = 0$. The mixing angle is $\cos\theta \equiv g/\sqrt{g^2 + 4e^2/3}$ where e and g are the QED and QCD couplings. Because $e \ll g$ the angle is close to zero, meaning that the \tilde{Q} photon is mostly the original photon with a small admixture of gluon.

The \tilde{Q} photon is massless. Given small but nonzero quark masses, there are no gapless \tilde{Q} -charged excitations; the lightest ones are the pseudoscalar pseudo-Goldstone bosons π^\pm and K^\pm (see Secs. II.A.4 and V), so for temperatures well below their masses the CFL phase is a transparent insulator, in which \tilde{Q} -electric and magnetic fields satisfy Maxwell’s equations with a dielectric constant and index of refraction that can be calculated directly from QCD (Litim and Manuel, 2001),

$$n = 1 + \frac{e^2 \cos^2 \theta}{9\pi^2} \frac{\mu^2}{\Delta_{\text{CFL}}^2}. \quad (7)$$

(This result is valid as long as $n - 1 \ll 1$.) Apart from the fact that $n \neq 1$, the emergence of the \tilde{Q} photon is an exact QCD-scale analogue of the TeV-scale spontaneous symmetry breaking that gave rise to the photon as a linear combination of the W_3 and hypercharge gauge bosons, with the diquark condensate at the QCD scale playing the role of the Higgs condensate at the TeV scale.

If one could shine a beam of ordinary light on a lump of CFL matter in vacuum, some would be reflected and some would enter, refracted, as a beam of \tilde{Q} -light. The reflection and refraction coefficients are known (Manuel and Rajagopal, 2002) (see also (Alford and Good, 2004)). The static limit of this academic result is relevant: if a volume of CFL matter finds itself in a static magnetic field as within a neutron star, surface currents are induced such that a fraction of this field is expelled via the Meissner effect for the non- \tilde{Q} component of Q , while a fraction is admitted as \tilde{Q} -magnetic field (Alford *et al.*, 2000b). The magnetic field within the CFL volume is not confined to flux tubes, and is not

frozen as in a conducting plasma: CFL quark matter is a color superconductor but it is an electromagnetic insulator.

All Cooper pairs have zero net \tilde{Q} -charge, but some have neutral constituents (both quarks \tilde{Q} -neutral) and some have charged constituents (the two quarks have opposite \tilde{Q} -charge). The \tilde{Q} -component of an external magnetic field will not affect the first type, but it will affect the pairing of the second type, so external magnetic fields can modify the CFL phase to the so-called magnetic CFL (“MCFL”) phase. The MCFL phase has a different gap structure (Ferrer *et al.*, 2005, 2006) and a different effective theory (Ferrer and de la Incera, 2007b). The original analyses of the MCFL phase were done for rotated magnetic fields \tilde{B} large enough that all quarks are in the lowest Landau level; solving the gap equations at lower \tilde{B} shows that the gap parameters in the MCFL phase exhibit de Haas-van Alphen oscillations, periodic in $1/\tilde{B}$ (Fukushima and Warringa, 2007; Noronha and Shovkovy, 2007).

4. Low-energy excitations

The low-energy excitations in the CFL phase are: the 8 light pseudoscalars arising from broken chiral symmetry, the massless Goldstone boson associated with superfluidity, and the \tilde{Q} -photon. The pseudoscalars form an octet under the unbroken $SU(3)$ color+flavor symmetry, and can naturally be labeled according to their \tilde{Q} -charges as pions, kaons, and an η . The effective Lagrangian that describes their interactions, and the QCD calculation of their masses and decay constants will be discussed in Sec. V. We shall find, in particular, that even though the quark-antiquark condensate is small, the pion decay constant is large, $f_\pi \sim \mu$.

The symmetry breaking pattern (6) does not include the spontaneous breaking of the $U(1)_A$ “symmetry” because it is explicitly broken by instanton effects. However, at large densities these effects become arbitrarily small, and the spontaneous breaking of $U(1)_A$ will have an associated order parameter and a ninth pseudo-Goldstone boson with the quantum numbers of the η' . This introduces the possibility of a second type of vortices (Forbes and Zhitnitsky, 2002; Son *et al.*, 2001).

Among the gapped excitations, we find the quark-quasiparticles which fall into an $\mathbf{8} \oplus \mathbf{1}$ of the unbroken global $SU(3)_{c+L+R}$, so there are two gap parameters Δ_1 and Δ_8 . The singlet has the larger gap $\Delta_1 = (2 + \mathcal{O}(\kappa))\Delta_8$. We also find an octet of massive vector mesons, which are the gluons that have acquired mass via the Higgs mechanism. The symmetries of the 3-flavor CFL phase are the same as those one would expect for 3-flavor hypernuclear matter, and even the pattern of gapped excitations is remarkably similar, differing only in the absence of a ninth massive vector meson. It is therefore possible that there is no phase transition between hypernuclear matter and CFL quark matter

(Schäfer and Wilczek, 1999c). This hadron-quark continuity can arise in nature only if the strange quark is so light that there is a hypernuclear phase, and this phase is characterized by proton- Ξ^- , neutron- Ξ^0 and $\Sigma^+ - \Sigma^-$ pairing, which can then continuously evolve into CFL quark matter upon further increasing the density (Alford *et al.*, 1999a).

5. Why CFL is favored

The dominant component of the CFL pairing pattern is the color $\mathbf{\bar{3}}_A$, flavor $\mathbf{\bar{3}}_A$, and Dirac $C\gamma_5$ (Lorentz scalar). There are many reasons to expect the color $\mathbf{\bar{3}}_A$ to be favored. First, this is the most attractive channel for quarks interacting via single-gluon exchange which is the dominant interaction at high densities where the QCD coupling is weak; second, it is also the most attractive channel for quarks interacting via the instanton-induced 't Hooft interaction, which is important at lower densities; third, qualitatively, combining two quarks that are each separately in the color- $\mathbf{3}$ representation to obtain a diquark that is a color- $\mathbf{\bar{3}}_A$ lowers the color-flux at large distances; and, fourth, phenomenologically, the idea that baryons can be modeled as bound states of a quark and a color-antisymmetric diquark, taking advantage of the attraction in this diquark channel, has a long history and has had a recent renaissance (Anselmino *et al.*, 1993; Close and Tornqvist, 2002; Jaffe, 1977; Jaffe and Wilczek, 2003; Selem and Wilczek, 2006).

It is also easy to understand why pairing in the Lorentz-scalar channel is favorable: it leaves rotational invariance unbroken, allowing for quarks at all angles on the entire Fermi-sphere to participate coherently in the pairing. Many calculations have shown that pairing is weaker in channels that break rotational symmetry (Alford *et al.*, 2003, 1998; Buballa *et al.*, 2003; Iwasaki and Iwado, 1995; Schäfer, 2000b; Schmitt *et al.*, 2002). There is also a rotationally invariant pairing channel with negative parity described by the order parameter $\langle \psi C \psi \rangle$. Perturbative gluon exchange interactions do not distinguish between positive and negative parity diquarks, but non-perturbative instanton induced interactions do, favoring the positive parity channel (Alford *et al.*, 1998; Rapp *et al.*, 1998, 2000).

Once we have antisymmetry in color and in Dirac indices, we are forced to antisymmetrize in flavor indices, and the most general color-flavor structure that the arguments above imply should be energetically favored is

$$\langle \psi_i^\alpha C \gamma_5 \psi_j^\beta \rangle \propto \epsilon^{\alpha\beta A} \epsilon_{ijB} \phi_B^A. \quad (8)$$

CFL pairing corresponds to $\phi_B^A = \delta_B^A$, and this is the only pattern that pairs all the quarks and leaves an entire $SU(3)$ global symmetry unbroken. The 2SC pattern is $\phi_B^A = \delta_3^A \delta_B^3$, in which only u and d quarks of two colors pair (Alford *et al.*, 1998; Bailin and Love, 1984; Barrois, 1979; Rapp *et al.*, 1998), see Sec. III.A. As

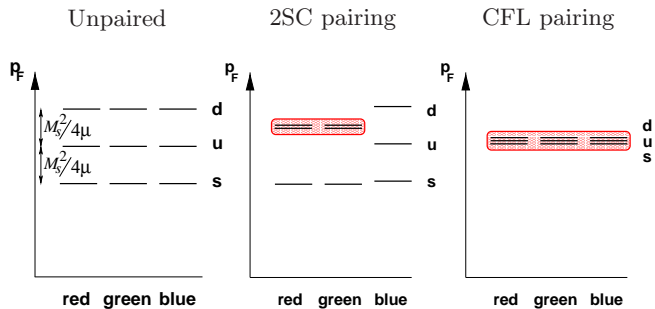


FIG. 2 (Color online) Illustration of the splitting apart of the Fermi momenta of the various colors and flavors of quarks (exaggerated for easy visibility). In the unpaired phase, requirements of neutrality and weak interaction equilibration cause separation of the Fermi momenta of the various flavors. The splittings increase with decreasing density, as μ decreases and $M_s(\mu)$ increases. In the 2SC phase, up and down quarks of two colors pair, locking their Fermi momenta together. In the CFL phase, all colors and flavors pair and have a common Fermi momentum.

long as the strange quark mass can be neglected (the parametric criterion turns out to be $\Delta_{\text{CFL}} \gg M_s^2/\mu$, see Sec. III.B) calculations comparing patterns of the structure (8) always find the CFL phase to have the highest condensation energy, making it the favored pattern. This has been confirmed in weak-coupling QCD calculations valid at high density (Evans *et al.*, 2000; Schäfer, 2000a; Shovkovy and Wijewardhana, 1999), in the Ginzburg-Landau approximation (Iida and Baym, 2001), and in many calculations using Nambu–Jona-Lasinio models (Alford *et al.*, 1999a,b; Rapp *et al.*, 2000; Schäfer and Wilczek, 1999c). In the high-density limit where $\Delta \gg M_s^2/\mu$ and $\Delta \ll \mu$ we can expand in powers of Δ/μ and explicitly compare CFL to 2SC pairing. The CFL condensation energy is $(8\Delta_8^2 + \Delta_1^2)\mu^2/(4\pi^2)$ which is $12\Delta_{\text{CFL}}^2\mu^2/(4\pi^2)$ when $\kappa \ll 1$ (see Sec. II.A.4) whereas the condensation energy in the 2SC phase is only $4\Delta_{\text{2SC}}^2\mu^2/(4\pi^2)$. We shall see later that the 2SC gap parameter turns out to be larger than the CFL gap parameter by a factor of $2^{1/3}$, so up to corrections of order κ the CFL condensation energy is larger than that in the 2SC phase by a factor of $3 \times 2^{-2/3}$. At lower densities the condensation energies become smaller, and we cannot neglect negative M_s^4 terms which are energy penalties induced by the neutrality requirement. Their coefficient is larger for CFL than for 2SC, partly (but usually not completely) cancelling the extra condensation energy—see Fig. 3 and Sec. III.A.

B. Intermediate density: stresses on the CFL phase

As we noted in section I.E, BCS pairing between two species is suppressed if their chemical potentials are sufficiently different. In real-world quark matter such stresses arise from the strange quark mass, which gives

the strange quark a lower Fermi momentum than the down quark at the same chemical potentials μ and μ_e , and from the neutrality requirement, which gives the up quark a different chemical potential from the down and strange quarks at the same μ and μ_e . Once flavor equilibrium under the weak interactions is reached, we find that all three flavors prefer to have different Fermi momenta at the same chemical potentials. This is illustrated in Fig. 2, which shows the Fermi momenta of the different species of quarks.

In the unpaired phase (Fig. 2, left panel), the strange quarks have a lower Fermi momentum because they are heavier, and to maintain electrical neutrality the number of down quarks is correspondingly increased. To lowest order in the strange quark mass, the separation between the Fermi momenta is $\delta p_F = M_s^2/(4\mu)$, so the splitting becomes larger as the density is reduced, and smaller as the density is increased. The phase space at the Fermi surface is proportional to μ^2 , so the resultant difference in quark number densities is $n_d - n_u = n_u - n_s \propto \mu^2 \delta p_F \sim \mu M_s^2$. Electrons are also present in weak equilibrium, with $\mu_e = M_s^2/(4\mu)$, so their charge density is parametrically of order $\mu_e^3 \sim M_s^6/\mu^3 \ll \mu M_s^2$, meaning that they are unimportant in maintaining neutrality.

In the CFL phase all the colors and flavors pair with each other, locking all their Fermi momenta together at a common value (Fig. 2, right panel). This is possible as long as the energy cost of forcing all species to have the same Fermi momentum is compensated by the pairing energy that is released by the formation of the Cooper pairs. Still working to lowest order in M_s^2 , we can say that parametrically the cost is $\mu^2 \delta p_F^2 \sim M_s^4$, and the pairing energy is $\mu^2 \Delta_{\text{CFL}}^2$, so we expect CFL pairing to become disfavored when $\Delta_{\text{CFL}} \lesssim M_s^2/\mu$. In fact, the CFL phase remains favored over the unpaired phase as long as $\Delta_{\text{CFL}} > M_s^2/4\mu$ (Alford and Rajagopal, 2002), but already becomes unstable against unpairing when $\Delta_{\text{CFL}} \gtrsim M_s^2/2\mu$ (see Sec. III.B). NJL model calculations (Abuki *et al.*, 2005; Alford *et al.*, 2005c; Alford and Rajagopal, 2002; Blaschke *et al.*, 2005; Fukushima *et al.*, 2005; Ruster *et al.*, 2005) find that if the attractive interaction were strong enough to induce a 100 MeV CFL gap when $M_s = 0$ then the CFL phase would survive all the way down to the transition to nuclear matter. Otherwise, there must be a transition to some other quark matter phase: this is the “non-CFL” region shown schematically in Fig. 1. When the stress is small, the CFL pairing can bend rather than break, developing a condensate of K^0 mesons, described in Sec. II.C below. When the stress is larger, however, CFL pairing becomes disfavored. A comprehensive survey of possible BCS pairing patterns shows that all of them suffer from the stress of Fermi surface splitting (Rajagopal and Schmitt, 2006), so in the intermediate-density “non-CFL” region we expect more exotic non-BCS pairing patterns. In Sec. III we give a survey of possibilities that have been explored.

C. Kaon condensation: the CFL- K^0 phase

Bedaque and Schäfer (Bedaque and Schäfer, 2002) showed that when the stress is not too large (high density), it may simply modify the CFL pairing pattern by inducing a flavor rotation of the condensate. This modification can be interpreted as a condensate of “ K^0 ” mesons. The K^0 meson carries negative strangeness (it has the same strangeness as a \bar{s} quark), so forming a K^0 condensate relieves the stress on the CFL phase by reducing its strangeness content. At large density kaon condensation occurs for $M_s \gtrsim m^{1/3}\Delta^{2/3}$, where m is mass of the light (u and d) quarks. At moderate density the critical strange quark mass is increased by instanton contribution to the kaon mass (Schäfer, 2002a). Kaon condensation was initially demonstrated using an effective theory of the Goldstone bosons, but with some effort can also be seen in an NJL calculation (Buballa, 2005b; Forbes, 2005). The CFL- K^0 phase is a superfluid; it is a neutral insulator; all its quark modes are gapped (as long as $M_s^2/(2\mu) < \Delta$); it breaks chiral symmetry. In all these respects it is similar to the CFL phase. Once we turn on small quark masses, different for all flavors, the $SU(3)_{c+L+R}$ symmetry of the CFL phase is reduced by explicit symmetry breaking to just $U(1)_{\bar{Q}} \times U(1)_{\bar{Y}}$, with \bar{Y} a linear combination of a diagonal color generator and hypercharge. In the CFL- K^0 phase, the kaon condensate breaks $U(1)_{\bar{Y}}$ spontaneously. This modifies the spectrum of both quarks and Goldstone modes, and thus can affect transport properties.

III. BELOW CFL DENSITIES

As we discussed in the introduction (end of Sec. I.A) and above (Sec. II.B), at intermediate densities the CFL phase suffers from stresses induced by the strange quark mass, combined with beta-equilibration and neutrality requirements. It can only survive down to the transition to nuclear matter (occurring at quark chemical potential $\mu = \mu_{\text{nuc}}$) if the pairing is strong enough: roughly $\Delta_{\text{CFL}} > M_s(\mu_{\text{nuc}})^2/2\mu_{\text{nuc}}$, ignoring strong interaction corrections, which are presumably important in this regime. It is therefore quite possible that other pairing patterns occur at intermediate densities, and in this section we survey some of the possibilities that have been suggested.

Fig. 3 shows a comparison of the free energies of some of these phases. We have chosen $\Delta_{\text{CFL}} = 25$ MeV, so there is a window of non-CFL pairing between nuclear density and the region where the CFL phase becomes stable. (For stronger pairing, $\Delta_{\text{CFL}} \sim 100$ MeV, there would be no such window.) The curves for the CFL, 2SC, gCFL, g2SC, and crystalline phases (2PW, CubeX and 2Cube45z) are obtained from an NJL model as described in Sec. VI. The curves for the CFL- K^0 and meson supercurrent (curCFL- K^0) phases are calculated using the CFL effective theory with parameters chosen by match-

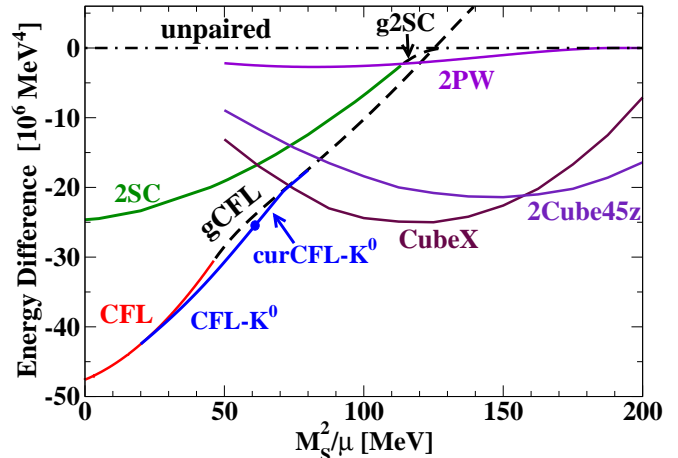


FIG. 3 (Color online) Free energy of various phases of dense 3-flavor quark matter, assuming $\Delta_{\text{CFL}} = 25$ MeV. The homogeneous phases are CFL and 2SC, their gapless analogs gCFL and g2SC, and the kaon-condensed phase CFL- K^0 . The true ground state must have a free energy below that of the gCFL phase, which is known to be unstable. The inhomogeneous phases are curCFL- K^0 , which is CFL- K^0 with meson supercurrents, and 2PW, CubeX, and 2Cube45z, which are crystalline color superconducting phases. The transition from CFL- K^0 to curCFL- K^0 is marked with a dot. In 2PW the condensate is a sum of only two plane waves. CubeX and 2Cube45z involve more plane waves, their condensation energies are larger but less reliably determined, so their curves should be assumed to have error bands comparable in size to the difference between them.

ing to weak-coupling QCD, as described in Sec. V, except that the gap was chosen to match $\Delta_{\text{CFL}} = 25$ MeV. The phases displayed in Fig. 3 are discussed in the following sections.

A. Two-flavor pairing: the 2SC phase

After CFL, 2SC is the most straightforward less-symmetrically paired form of quark matter, and was one of the first patterns to be analyzed (Alford *et al.*, 1998; Bailin and Love, 1979, 1984; Barrois, 1979; Rapp *et al.*, 1998). In the 2SC phase, quarks with two out of three colors (red and green, say) and two out of three flavors, pair in the standard BCS fashion. The flavors with the most phase space near their Fermi surfaces, namely u and d , are the ones that pair, leaving the strange and blue quarks unpaired (middle panel of Fig. 2). According to NJL models, if the coupling is weak then there is no 2SC region in the phase diagram (Steiner *et al.*, 2002). This can be understood by an expansion in powers of M_s , which finds that the CFL \rightarrow 2SC transition occurs at the same point as the 2SC \rightarrow unpaired transition, leaving no 2SC window (Alford and Rajagopal, 2002) (this is the situation in Fig. 3). However, NJL models with stronger coupling leave open the possibility

of a 2SC window in the “non-CFL” region of the phase diagram (Abuki and Kunihiro, 2006; Ruster *et al.*, 2005). (These calculations have to date not included the possibility of meson current or crystalline color superconducting phases, discussed below, that may prove more favorable.)

The 2SC pairing pattern, corresponding to $\phi_B^A = \delta_3^A \delta_B^3$ in (8), is $\langle \psi_i^\alpha C \gamma_5 \psi_j^\beta \rangle \propto \Delta_{2\text{SC}} \epsilon_{ij3} \epsilon^{\alpha\beta 3}$, where the symmetry breaking pattern, assuming massless up and down quarks, is

$$\begin{aligned} & [SU(3)_c] \times \underbrace{SU(2)_L \times SU(2)_R \times U(1)_B \times U(1)_S}_{\supset [U(1)_{\tilde{Q}}]} \\ \rightarrow & [SU(2)_{rg}] \times \underbrace{SU(2)_L \times SU(2)_R \times U(1)_{\tilde{B}} \times U(1)_S}_{\supset [U(1)_{\tilde{Q}}]} \end{aligned} \quad (9)$$

using the same notation as in Eq. (6). The unpaired massive strange quarks introduce a $U(1)_S$ symmetry. The color $SU(3)_c$ gauge symmetry is broken down to an $SU(2)_{rg}$ red-green gauge symmetry, whose confinement distance rises exponentially with density, as $\Delta^{-1} \exp(\text{const } \mu / (g\Delta))$ (Rischke *et al.*, 2001) (see also (Casalbuoni *et al.*, 2002b; Ouyed and Sannino, 2001)). An interesting feature of 2SC pairing is that no global symmetries are broken. The condensate is a singlet of the $SU(2)_L \times SU(2)_R$ flavor symmetry, and baryon number survives as \tilde{B} , a linear combination of the original baryon number and the broken diagonal T_8 color generator. Electromagnetism, originally a linear combination of B , S , and I_3 (isospin), survives as an unbroken linear combination \tilde{Q} of \tilde{B} , S , and I_3 . 2SC quark matter is therefore a color superconductor but is neither a superfluid nor an electromagnetic superconductor, and there is no order parameter that distinguishes it from the unpaired phase or the QGP (Alford *et al.*, 1998). With respect to the unbroken $U(1)_{\tilde{Q}}$ gauge symmetry, the 2SC phase is a conductor not an insulator because some of the ungapped blue and strange quarks are \tilde{Q} -charged.

B. The unstable gapless phases

As was noted in Sec. II.B, and can be seen in Fig. 3, the CFL phase becomes unstable when $\mu \approx \frac{1}{2} M_s^2 / \Delta_{\text{CFL}}$. At this point the pairing in the gs - bd sector suffers the instability discussed in Sec. I.E, and it becomes energetically favorable to convert gs quarks into bd quarks (both near their common Fermi momentum).³ If we restrict

ourselves to diquark condensates that are spatially homogeneous, the result is a modification of the pairing in which there is still pairing in all the color-flavor channels that characterize CFL, but gs - bd Cooper pairing ceases to occur in a range of momenta near the Fermi surface (Alford *et al.*, 2004b, 2005c; Fukushima *et al.*, 2005). In this range of momenta there are bd quarks but no gs quarks, and quark modes at the edges of this range are ungapped, hence this is called a gapless phase (“gCFL”). Such a phenomenon was first proposed for two flavor quark matter (“g2SC”) (Shovkovy and Huang, 2003), see also (Gubankova *et al.*, 2003). It has been confirmed in NJL analyses such as those in (Abuki *et al.*, 2005; Abuki and Kunihiro, 2006; Alford *et al.*, 2005b, 2004a,b, 2005c; Fukushima *et al.*, 2005; Ruster *et al.*, 2004, 2005), which predict that at densities too low for CFL pairing there will be gapless phases.

In Fig. 3, where $\Delta_{\text{CFL}} = 25$ MeV, we see the transition from CFL to gCFL at $M_s^2/\mu \approx 2\Delta_{\text{CFL}} = 50$ MeV. (It is interesting to note that, whereas the CFL phase is a \tilde{Q} -insulator, the gCFL phase is a \tilde{Q} -conductor, because it has a small electron density, balanced by unpaired bu quarks from a very thin momentum shell of broken bu - rs pairing; the CFL \rightarrow gCFL transition is the analogue of an insulator to metal transition at which a “band” that was unfilled in the insulating phase drops below the Fermi energy, making the material a metal.) The gCFL phase then remains favored beyond the value $M_s^2/\mu \approx 4\Delta_{\text{CFL}} = 100$ MeV at which the CFL phase would become unfavored relative to completely unpaired quark matter (Alford and Rajagopal, 2002).

However, it turns out that in QCD the gapless phases, both g2SC (Giannakis and Ren, 2005a; Huang and Shovkovy, 2004b) and gCFL (Casalbuoni *et al.*, 2005b; Fukushima, 2005), are unstable at zero temperature. (Increasing the temperature above a critical value removes the instability; the critical value varies dramatically between phases, from a fraction of an MeV to of order 10 MeV (Fukushima, 2005).) The instability manifests itself in an imaginary Meissner mass m_M for some of the gluons. m_M^2 is the low-momentum current-current two-point function, and $m_M^2/(g^2\Delta^2)$ (where the strong interaction coupling is g) is the coefficient of the gradient term in the effective theory of small fluctuations around the ground-state condensate, so a negative value indicates an instability towards spontaneous breaking of translational invariance (Fukushima, 2006; Hashimoto, 2006; Huang, 2006; Iida and Fukushima, 2006; Reddy and Rupak, 2005). Calculations in a simple two-species model (Alford and Wang, 2005) show that gapless charged fermionic modes generically lead to imaginary m_M .

The instability of the gapless phases indicates that there must be other phases of even lower free energy, that occur in their place in the phase diagram. The nature of those phases is not reliably determined at present; likely candidates are discussed below.

³ The onset of gaplessness occurs at the μ at which $\frac{1}{2}(\mu_{bd} - \mu_{gs}) = \Delta_{\text{CFL}}$, as explained in Sec. I.E. Note that in the CFL phase $(\mu_{bd} - \mu_{gs}) = M_s^2/\mu$, twice its value in unpaired quark matter because of the nonzero color chemical potential $\mu_8 \propto M_s^2/\mu$ required by color neutrality in the presence of CFL pairing (Alford and Rajagopal, 2002; Steiner *et al.*, 2002).

C. Crystalline color superconductivity

The Meissner instability of the gCFL phase points to a breaking of translational invariance, and crystalline color superconductivity represents a possible resolution of that instability. The basic idea, first proposed in condensed matter physics (Fulde and Ferrell, 1964; Larkin and Ovchinnikov, 1965) and more recently analyzed in the context of color superconductivity (Alford *et al.*, 2001a; Bowers and Rajagopal, 2002; Casalbuoni and Nardulli, 2004), is to allow the different quark flavors to have different Fermi momenta, thus accommodating the stress of the strange quark mass, and to form Cooper pairs with nonzero momentum, each quark lying close to its respective Fermi surface. The price one must pay for this arrangement is that only fermions in certain regions on the Fermi surface can pair. Pairs with nonzero momenta chosen from some set of wave vectors \mathbf{q}_a yield condensates that vary in position space like $\sum_a \exp(i\mathbf{q}_a \cdot \mathbf{x})$, forming a crystalline pattern whose Bravais lattice is the set of \mathbf{q}_a .

Analyses to date have focused on u - d and u - s pairing, neglecting pairing of d and s because the separation of their Fermi momenta is twice as large (Fig. 2). If the $\langle ud \rangle$ condensate includes only pairs with a single nonzero momentum \mathbf{q} , this means that in position space the condensate is a single plane-wave and means that in momentum space pairing is allowed on a single ring on the u Fermi surface and a single ring on the opposite side of the d Fermi surface. The simplest “crystalline” phase of three-flavor quark matter that has been analyzed (Casalbuoni *et al.*, 2005a; Mannarelli *et al.*, 2006b) includes two such single-plane wave condensates (“2PW”), one $\langle ud \rangle$ and one $\langle us \rangle$. The favored orientation of the two \mathbf{q} ’s is parallel, keeping the two “pairing rings” on the u Fermi surface (from the $\langle us \rangle$ and $\langle ud \rangle$ condensates) as far apart as possible (Mannarelli *et al.*, 2006b). This simple pattern of pairing leaves much of the Fermi surfaces unpaired, and it is much more favorable to choose a pattern in which the $\langle us \rangle$ and $\langle ud \rangle$ condensates each include pairs with more than one \mathbf{q} -vector, thus more than one ring and more than one plane wave. Among such more realistic pairing patterns, the two that appear most favorable have either four \mathbf{q} ’s per condensate that together point at the eight corners of a cube in momentum space (“CubeX”) or eight \mathbf{q} ’s per condensate that each point at the corners of separate cubes, rotated relative to each other by 45 degrees (“2Cube45z”) (Rajagopal and Sharma, 2006b). It has been shown that the chromomagnetic instability is no longer present in these phases (Ciminale *et al.*, 2006). The free energies of the 2PW, CubeX and 2Cube45z phases as calculated within an NJL model (see Sec. VI) are shown in Fig. 3. The calculation is an expansion in powers of $(\Delta/\delta p_F)^2$ which in the CubeX and 2Cube45z phases turns out to be of order a tenth to a quarter. According to results obtained in a calculation done to third order in this expansion parameter, the CubeX and 2Cube45z condensa-

tion energies are large enough that one or other of them is favored over a wide range of M_s^2/μ as illustrated in Fig. 3. The uncertainty in each is of the same order as the difference between them, so one cannot yet say which is favored, but the overall scale is plausible (one would expect condensation energies an order of magnitude bigger than that of the 2PW state). We discuss crystalline color superconductivity in greater detail in Sec. VI.

D. Meson supercurrent (“curCFL- K^0 ”)

Kaon condensation alone does not remove the gapless modes that occur in the CFL phase when M_s becomes large enough, but it does affect the number of gapless modes and the onset value of M_s . In the CFL- K^0 phase, the electrically charged (bs) mode becomes gapless at $M_s^2/\mu \approx 8\Delta/3$ (compared to 2Δ in the CFL phase), and the electrically neutral (bd) mode becomes gapless for $M_s^2/\mu \approx 4\Delta$ (Kryjevski and Schäfer, 2005; Kryjevski and Yamada, 2005). (In an NJL model analysis (Forbes, 2005), the charged mode in the CFL- K^0 phase becomes gapless at $M_s^2/\mu \approx 2.44\Delta$ for $\Delta = 25$ MeV as in Fig. 3). The gapless CFL- K^0 phase has an instability which is similar to the instability of the gCFL phase. This instability can be viewed as a tendency towards spontaneous generation of Goldstone boson (kaon) currents (Kryjevski, 2005; Schäfer, 2006). The currents correspond to a spatial modulation of the kaon condensate. There is no net transfer of any charge because the Goldstone boson current is counterbalanced by a backflow of ungapped fermions. The meson supercurrent ground state is lower in energy than the CFL- K^0 state and the magnetic screening masses are real (Gerhold *et al.*, 2007). Because the ungapped fermion mode is electrically charged, both the magnitude of the Goldstone boson current needed to stabilize the phase and the magnitude of the resulting energy gain relative to the phase without a current are very small. Goldstone boson currents can also be generated in the gCFL phase without K^0 condensation. In this case gauge invariance implies that the supercurrent state is equivalent to a single plane-wave LOFF state, but the analyses can be carried out in the limit that the gap is large compared to the magnitude of the current (Gerhold and Schäfer, 2006). This analysis is valid near the onset of the gCFL phase, but not for larger mismatches, where states with multiple currents are favored.

E. Single-flavor pairing

If the stress due to the strange quark mass is large enough then there may be a range of quark matter densities where no pairing between different flavors is possible, whether spatially uniform or inhomogeneous. From Fig. 3 we can estimate that this will occur when $M_s^2/(\mu\Delta_{\text{CFL}}) \gtrsim 10$, so it requires a large effective strange

quark mass and/or small CFL pairing gap. The best available option in this case is Cooper pairing of each flavor with itself. Single-flavor pairing may also arise among the strange quarks in a 2SC phase, since they are not involved in two-flavor pairing. We will discuss these cases separately below.

To maintain fermionic antisymmetry of the Cooper pair wavefunction, single-flavor pairing phases have to either be symmetric in color, which greatly weakens or eliminates the attractive interaction, or symmetric in Dirac indices, which compromises the uniform participation of the whole Fermi sphere. As a result, they have much lower critical temperatures than multi-flavor phases such as the CFL or 2SC phases, perhaps as large as a few MeV, more typically in the eV to many keV range (Alford *et al.*, 2003, 1998; Buballa *et al.*, 2003; Schäfer, 2000b; Schmitt, 2005; Schmitt *et al.*, 2002).

Matter in which each flavor only pairs with itself has been studied using NJL models and weakly-coupled QCD. These calculations agree that the energetically favored state is color-spin-locked (CSL) pairing for each flavor (Bailin and Love, 1979; Schäfer, 2000b; Schmitt, 2005). CSL pairing involves all 3 colors, with the color direction of each Cooper pair correlated with its spin direction, breaking $SU(3)_c \times SO(3)_{\text{rot}} \rightarrow SO(3)_{c+\text{rot}}$. The phase is isotropic, with rotational symmetry surviving as a group of simultaneous spatial and color rotations. Other possible phases exhibiting spin-one, single-flavor, pairing include the polar, planar, and A phases described in (Schäfer, 2000b; Schmitt, 2005) (for an NJL model treatment see (Alford *et al.*, 2003)). Some of these phases exhibit point or line nodes in the energy gap at the Fermi surface, and hence do break rotational symmetry.

If 2SC pairing occurs with strange quarks present, one might expect the strange quarks of all three colors to undergo CSL self-pairing, yielding an isotropic “2SC+CSL” pattern. However, the 2SC pattern breaks the color symmetry, and in order to maintain color neutrality, a color chemical potential is generated, which splits the Fermi momentum of the blue strange quarks away from that of the red and green strange quarks. This is a small effect, but so is the CSL pairing gap, and NJL model calculations indicate that the color chemical potential typically destroys CSL pairing of the strange quarks (Alford and Cowan, 2006). The system falls back on the next best alternative, which is spin-one pairing of the red and green strange quarks.

Because their gaps and critical temperatures can range as low as the eV scale, single-flavor pairing phases in compact stars would appear relatively late in the life of the star, and might cause dramatic changes in its behavior. For example, unlike the CFL and 2SC phases, many single-flavor-paired phases are electrical superconductors (Schmitt *et al.*, 2003), so their appearance could significantly affect the magnetic field dynamics of the star.

F. Gluon condensation

In the 2SC phase (unlike in the CFL phase) the magnetic instability arises at a lower value of the stress on the BCS pairing than that at which the onset of gapless pairing occurs. In this 2SC regime, analyses done using a Ginzburg-Landau approach indicate that the instability can be cured by the appearance of a chromoelectric condensate (Gorbar *et al.*, 2006a, 2007, 2006b; Hashimoto and Miransky, 2007). The 2SC condensate breaks the color group down to the $SU(2)_{rg}$ red-green subgroup, and five of the gluons become massive vector bosons via the Higgs mechanism. The new condensate involves some of these massive vector bosons, and because they transform non-trivially under $SU(2)_{rg}$ it now breaks that gauge symmetry. Because they are electrically charged vector particles, rotational symmetry is also broken, and the phase is an electrical superconductor. Alternatively, it has been suggested (Ferrer and de la Incera, 2007a) that the gluon condensate may be inhomogeneous with a large spontaneously-induced \vec{Q} magnetic field.

G. Secondary pairing

Since the Meissner instability is generically associated with the presence of gapless fermionic modes, and the BCS mechanism implies that any gapless fermionic mode is unstable to Cooper pairing in the most attractive channel, one may ask whether the instability could be resolved without introducing spatial inhomogeneity simply by “secondary pairing” of the gapless quasiparticles, which would then acquire their own gap Δ_s (Hong, 2005; Huang and Shovkovy, 2003). Furthermore, there is a mode in the gCFL phase whose dispersion relation is well approximated as quadratic, $\epsilon \propto (k - \text{const})^2$, yielding a greatly increased density of states at low energy (diverging as $\epsilon^{-1/2}$), so its secondary pairing is much stronger than would be predicted by BCS theory: $\Delta_s \propto G^2$ for an effective four-fermion coupling strength G , as compared with the standard BCS result $\Delta \propto \exp(-\text{const}/G)$ (Hong, 2005). This result is confirmed by an NJL study in a two-species model (Alford and Wang, 2006), but the secondary gap Δ_s was found to be still much smaller than the primary gap Δ_p , so it does not generically resolve the magnetic instability (in the temperature range $\Delta_s \ll T \ll \Delta_p$, for example).

H. Mixed phases

Another way for a system to deal with a stress on its pairing pattern is to form a mixed phase, which is a charge-separated state consisting of positively and negatively charged domains which are neutral on average. The coexisting phases have a common pressure and a common value of the charge chemical potential which is not equal to the neutrality value for either phase

(Glendenning, 1992; Ravenhall *et al.*, 1983). The size of the domains is determined by a balance between surface tension (which favors large domains) and electric field energy (which favors small domains). Separation of color charge is expected to be suppressed by the very high energy cost of color electric fields, but electric charge separation is quite possible, and may occur at the interface between color-superconducting quark matter and nuclear matter (Alford *et al.*, 2001b) and an interface between quark matter and the vacuum (Alford *et al.*, 2006; Jaikumar *et al.*, 2006a), just as it occurs at interfaces between nuclear matter and a nucleon gas (Ravenhall *et al.*, 1983). Mixed phases are a generic phenomenon, since, in the approximation where Coulomb energy costs are neglected, any phase can always lower its free energy density by becoming charged (this follows from the fact that free energies are concave functions of chemical potentials). In this approximation, if two phases A and B can coexist at the same pressure with opposite charge densities then such a mixture will always be favored over a uniform neutral phase of either A or B. For a pedagogical discussion, see (Alford *et al.*, 2005c). Surface and Coulomb energy costs can cancel this energy advantage, however, and have to be calculated on a case-by-case basis.

In quark matter it has been found that as long as we require local color neutrality such mixed phases are not the favored response to the stress imposed by the strange quark mass (Alford *et al.*, 2004a,b). Phases involving color charge separation have been studied (Neumann *et al.*, 2003) but it seems likely that the energy cost of the color-electric fields will disfavor them.

I. Relation to cold atomic gases

An interesting class of systems in which stressed superconductivity can be studied experimentally is trapped atomic gases in which two different hyperfine states (“species”) of the atom pair with each other (Giorgini *et al.*, 2007). This is a useful experimental model because the stress and interaction strength are both under experimental control, unlike quark matter where one physical variable (μ) controls both the coupling strength and the stress. The atomic pairing stress can be adjusted by changing the relative number of atoms of the two species (“polarization”). The scattering length of the atoms can be controlled using Feshbach resonances, making it possible to vary the strength of the inter-atomic attraction from weak (where BCS pairing occurs) through the unitarity limit (where a bound state forms) to strong (Bose-Einstein condensation of diatomic molecules).

The theoretical expectation is that, in the weak coupling limit, there will be BCS pairing as long as $\delta\mu$, the chemical potential difference between the species, is small enough. The BCS phase is unpolarized because the Fermi surfaces are locked together. A first-order

transition from BCS to crystalline (LOFF) pairing is expected at $\delta\mu = \Delta_0/\sqrt{2}$, where Δ_0 is the BCS gap at $\delta\mu = 0$; then at $\delta\mu_c$ a continuous transition to the unpaired phase (Chandrasekhar, 1962; Clogston, 1962; Fulde and Ferrell, 1964; Larkin and Ovchinnikov, 1965). For the single plane wave LOFF state $\delta\mu_c \simeq 0.754\Delta_0$, but for multiple plane wave states $\delta\mu_c$ may be larger.

Experiments with cold trapped atoms near the unitary limit (strong coupling) have seen phase separation between an unpolarized superfluid and a polarized normal state (Chin *et al.*, 2006; Partridge *et al.*, 2006; Zwerlein *et al.*, 2006). If one ignores the crystalline phase (perhaps only favored at weak coupling (Mannarelli *et al.*, 2006a; Sheehy and Radzihovsky, 2006, 2007)) this is consistent with the theoretical expectation for the BCS regime: the net polarization forces the system to phase separate, yielding a mixture of BCS and unpaired phases with $\delta\mu$ fixed at the first order transition between them (Bedaque *et al.*, 2003; Carlson and Reddy, 2005). It remains an exciting possibility that crystalline superconducting (LOFF) phases of cold atoms may be observed: this may require experiments closer to the BCS regime.

In the strong coupling limit the superfluid consists of tightly bound molecules. Adding an extra atom requires energy Δ . For $|\delta\mu| > \Delta$ the atomic gas is a homogeneous mixture of an unpolarized superfluid and a fully polarized Fermi gas, so the system is a stable gapless superfluid. This means that in strong coupling polarization can be carried by a gapless superfluid, whereas in weak coupling even a small amount of polarization leads to the appearance of a mixed BCS/LOFF phase. It is not known what happens at intermediate coupling, but one possibility is that the gapless superfluid and the LOFF phase are connected by a phase transition (Son and Stephanov, 2006). This transition would correspond to a magnetic instability of the gapless superfluid.

IV. WEAK-COUPLING QCD CALCULATIONS

We have asserted in Secs. I and II that at sufficiently high densities it is possible to do controlled calculations of properties of CFL quark matter directly from the QCD Lagrangian. We describe how to do such calculations in this section. We shall focus on the calculation of the gap parameter, but shall also discuss the critical temperature T_c for the transition from the CFL phase to the quark-gluon plasma and the Meissner and Debye masses that control color-magnetic and color-electric effects in the CFL phase. Phenomena that are governed by the massless Goldstone bosons and/or the light pseudo-Goldstone bosons are most naturally described by first constructing the appropriate effective theory and then, if at sufficiently high densities, calculating its parameters directly from the QCD Lagrangian. We defer these analyses to Sec. V.

Although the weak-coupling calculations that we describe in this section are only directly applicable in the

CFL phase, we shall present them in a sufficiently general formalism that they can be applied to other spatially homogeneous phases also, including for example the 2SC and CSL phases. These phases can be analyzed at weak-coupling either just by ansatz, or by introducing such a large strange quark mass that CFL pairing is disfavored even at enormous densities. Such calculations provide insights into the properties of these phases, even though they do not occur in the QCD phase diagram at high enough densities for a weak-coupling approach to be applicable. To keep our notation general, we shall refer to the gap parameter as Δ ; in the CFL phase, $\Delta_{\text{CFL}} \equiv \Delta$.

We shall see that at weak coupling the expansion parameter that controls the calculation of $\log(\Delta/\mu)$ is at best g , certainly not g^2 . (The leading term is of order $1/g$; the $\log g$ and g^0 terms have also been calculated. The $\mathcal{O}(g \log g)$ and $\mathcal{O}(g)$ terms are nonzero, and have not yet been calculated. Beyond $\mathcal{O}(g)$, it is possible that fractional powers of g may arise in the series.) We therefore expect the weak-coupling calculations to be quantitatively reliable only at densities for which $g(\mu) < 1$, which corresponds to densities many orders of magnitude greater than that at the centers of neutron stars. Indeed, it has been shown (Rajagopal and Shuster, 2000) that some of the $\mathcal{O}(g)$ contributions start to decline in magnitude relative to the g^0 term only for $g(\mu) \lesssim 0.8$ which corresponds, via the two-loop QCD beta function, to $\mu \gtrsim 10^8$ MeV meaning densities 15-16 orders of magnitude greater than those at the centers of compact stars. The reader may therefore be tempted to see this section as academic. From a theoretical point of view, it is exceptional to have an instance where the properties of a superconducting phase can be calculated rigorously from a fundamental short-distance theory, making this exploration a worthy pursuit even if academic. From a practical point of view, the quantitative understanding that we derive from calculations reviewed in this section provides a completely solid foundation from which we can extrapolate downwards in μ . The effective field theory described in Sec. V gives us a well-defined way of doing so as long as we stay within the CFL phase, meaning that we can come down from $\mu > 10^8$ MeV all the way down to $\mu \sim M_s^2/(2\Delta_{\text{CFL}})$. Finally, we shall gain qualitative insights into the CFL phase and other color superconducting phases, insights that guide our thinking at lower densities.

The QCD Lagrangian is given by

$$\mathcal{L} = \bar{\psi}(i\gamma^\mu D_\mu + \hat{\mu}\gamma_0 - \hat{m})\psi - \frac{1}{4}G_a^{\mu\nu}G_{\mu\nu}^a. \quad (10)$$

Here, ψ is the quark spinor in Dirac, color, and flavor space, i.e., a $4N_c N_f$ -component spinor, and $\bar{\psi} \equiv \psi^\dagger \gamma_0$. The covariant derivative acting on the fermion field is $D_\mu = \partial_\mu + igT_a A_\mu^a$, where g is the strong coupling constant, A_μ^a are the gauge fields, $T^a = \lambda^a/2$ ($a = 1, \dots, 8$) are the generators of the gauge group $SU(3)_c$, and λ^a are the Gell-Mann matrices. The field strength tensor is $G_a^{\mu\nu} = \partial_\mu A_\nu^a - \partial_\nu A_\mu^a + gf^{abc}A_\mu^b A_\nu^c$ with the $SU(3)_c$ struc-

ture constants f^{abc} . The chemical potential $\hat{\mu}$ and the quark mass $\hat{m} = \text{diag}(m_u, m_d, m_s)$ are diagonal matrices in flavor space. If weak interactions are taken into account flavor is no longer conserved and there are only two chemical potentials, one for quark (baryon) number, μ , and one for electric charge, μ_e . At the very high densities of interest in this section, the constituent quark masses are essentially the same as the current quark masses m_u , m_d and m_s meaning that we need not distinguish between them. Furthermore, at asymptotic densities we can neglect even the strange quark mass, so throughout most of this section we shall set $m_u = m_d = m_s = 0$.

If the coupling is small then the natural starting point is a free Fermi gas of quarks. In a degenerate quark gas all states with momenta $p < p_F = (\mu^2 - m_q^2)^{1/2}$ are occupied, and all states with $p > p_F$ are empty. Because of Pauli-blocking, interactions mainly modify states in the vicinity of the Fermi surface. Since the Fermi momentum is large, typical interactions between quarks near the Fermi surface involve large momentum transfer and are governed by the weak coupling $g(\mu)$. Interactions in which quarks scatter by only a small angle involve only a small momentum transfer and are therefore potentially dangerous. However, small momenta correspond to large distances, and medium modifications of the exchanged gluons are therefore important. In a dense medium, electric gluons are Debye screened at momenta $q \sim g\mu$. The dominant interaction for momenta below the screening scale is due to unscreened, almost static, magnetic gluons. In a hot quark-gluon gas, interactions between magnetic gluons become nonperturbative for momenta less than $g^2 T$. This phenomenon does not take place in a very dense quark liquid, and gluon exchanges with arbitrarily small momenta remain perturbative. On a qualitative level this can be attributed to the absence of Bose enhancement factors in soft gluon propagators. A more detailed explanation will be given in Sec. V.A.2. The unscreened magnetic interactions nevertheless make the fluid a “non-Fermi liquid” at temperatures above the critical temperature for color superconductivity. We shall discuss this also in Sec. V.A.2, where we shall see that these non-Fermi liquid effects do not spoil the basic logic of the BCS argument that diquark condensation must occur in the presence of an attractive interaction, but are crucial in the calculation of the gap that results.

A. The gap equation

As discussed in Sec. I.B, any attractive interaction in a many-fermion system leads to Cooper pairing. QCD at high density provides an attractive interaction via one-gluon exchange. In terms of quark representations of $SU(3)_c$, the attractive channel is the anti-symmetric anti-triplet $\bar{\mathbf{3}}_A$, appearing by “pairing” two color triplets: $\mathbf{3} \otimes \mathbf{3} = \bar{\mathbf{3}}_A \oplus \mathbf{6}_S$. Consequently, only quarks of different colors form Cooper pairs. There is an induced pairing in the symmetric sextet channel

6_S . However, this pairing is much weaker (Alford *et al.*, 1999a,b; Pisarski and Rischke, 1999c; Schäfer, 2000a; Shovkovy and Wijewardhana, 1999), and we shall largely neglect it in the following. As in an electronic superconductor, Cooper pairing results in an energy gap in the quasiparticle excitation spectrum. Its magnitude at zero temperature Δ is crucial for the phenomenology of a superconductor. In addition, it also sets the scale for the critical temperature T_c of the phase transition which can be expected to be of the same order as Δ (in BCS theory, $T_c = 0.57\Delta$). Over the course of the next five subsections, we shall discuss the QCD gap equation, which is used to determine both Δ and T_c .

Our starting point is the partition function

$$\mathcal{Z} = \int \mathcal{D}A \mathcal{D}\bar{\psi} \mathcal{D}\psi e^{i\mathcal{S}}, \quad (11)$$

with the action $\mathcal{S} = \int d^4x \mathcal{L}$ and the Lagrangian (10). In the following we shall only sketch the derivation of the gap equation. Details following the same lines can be found in (Manuel, 2000b; Pisarski and Rischke, 1999b, 2000a; Rischke, 2004; Schmitt, 2004, 2005; Schmitt *et al.*, 2002).

We begin by introducing Nambu-Gorkov spinors. This additional two-dimensional structure proves convenient in the theoretical description of a superconductor or a superfluid, see for instance (Abrikosov *et al.*, 1963; Fetter and Walecka, 1971). It allows for the introduction of a source that couples to quark bilinears (as opposed to quark-anti-quark bilinears). Spontaneous symmetry breaking is realized by taking the limit of a vanishing source. The Nambu-Gorkov basis is given by

$$\Psi = \begin{pmatrix} \psi \\ \psi_C \end{pmatrix}, \quad \bar{\Psi} = (\bar{\psi}, \bar{\psi}_C), \quad (12)$$

where $\psi_C = C\bar{\psi}^T$ is the charge-conjugate spinor, obtained by multiplication with the charge conjugation matrix $C \equiv i\gamma^2\gamma^0$. In a free fermion system, the new basis is a pure doubling of degrees of freedom with the inverse fermion propagator consisting of the original free propagators,

$$S_0^{-1} = \begin{pmatrix} [G_0^+]^{-1} & 0 \\ 0 & [G_0^-]^{-1} \end{pmatrix} \quad (13)$$

where $[G_0^\pm]^{-1}(X, Y) \equiv -i(i\gamma^\mu\partial_\mu \pm \mu\gamma_0)\delta^{(4)}(X - Y)$. Here and in the following capital letters denote four-vectors, e.g., $X \equiv (x_0, \mathbf{x})$. The effect of a nonzero diquark condensate can now be taken into account through adding a suitable source term to the action and computing the effective action Γ as a functional of the gluon and fermion propagators D and S (Abuki, 2003; Miransky *et al.*, 2001; Rischke, 2004;

Rüster and Rischke, 2004; Schmitt, 2004; Takagi, 2003):

$$\begin{aligned} \Gamma[D, S] &= -\frac{1}{2}\text{Tr} \log D^{-1} - \frac{1}{2}\text{Tr}(D_0^{-1}D - 1) \\ &+ \frac{1}{2}\text{Tr} \log S^{-1} + \frac{1}{2}\text{Tr}(S_0^{-1}S - 1) \\ &+ \Gamma_2[D, S]. \end{aligned} \quad (14)$$

This functional is called the “2PI effective action” since the contribution $\Gamma_2[D, S]$ consists of all two-particle irreducible diagrams (Baym, 1962; Cornwall *et al.*, 1974; Luttinger and Ward, 1960). This formalism is particularly suitable for studying spontaneous symmetry breaking in a self-consistent way. The ground state of the system is obtained by finding the stationary point of the effective action. The stationarity conditions yield Dyson-Schwinger equations for the gauge boson and fermion propagators,

$$D^{-1} = D_0^{-1} + \Pi, \quad (15a)$$

$$S^{-1} = S_0^{-1} + \Sigma, \quad (15b)$$

where the gluon and fermion self-energies are the functional derivatives of Γ_2 at the stationary point,

$$\Pi \equiv -2\frac{\delta\Gamma_2}{\delta D}, \quad \Sigma \equiv 2\frac{\delta\Gamma_2}{\delta S}. \quad (16)$$

Writing the second of these equations as $\Gamma_2[S] = (1/4)\text{Tr}(\Sigma S)$, we can then use the Dyson-Schwinger equation (15b) to evaluate the fermionic part of the effective action at the stationary point, obtaining the pressure

$$P = \frac{1}{2}\text{Tr} \log S^{-1} - \frac{1}{4}\text{Tr}(1 - S_0^{-1}S). \quad (17)$$

We shall return to this expression for the pressure in Sec. IV.C.

Here, we proceed to analyze the Dyson-Schwinger equation (15b) for the fermion propagator. We denote the entries of the 2×2 matrix Σ in Nambu-Gorkov space as

$$\Sigma \equiv \begin{pmatrix} \Sigma^+ & \Phi^- \\ \Phi^+ & \Sigma^- \end{pmatrix}, \quad (18)$$

where the off-diagonal elements are related via $\Phi^- = \gamma_0(\Phi^+)^\dagger\gamma_0$. One can invert the Dyson-Schwinger equation formally to obtain the full fermion propagator in the form

$$S = \begin{pmatrix} G^+ & F^- \\ F^+ & G^- \end{pmatrix}, \quad (19)$$

where the fermion propagators for quasiparticles and charge-conjugate quasiparticles are

$$G^\pm = \{[G_0^\pm]^{-1} + \Sigma^\pm - \Phi^\mp([G_0^\mp]^{-1} + \Sigma^\mp)^{-1}\Phi^\pm\}^{-1}, \quad (20)$$

and the so-called anomalous propagators, typical for a superconducting system, are given by

$$F^\pm = -([G_0^\mp]^{-1} + \Sigma^\mp)^{-1}\Phi^\pm G^\pm. \quad (21)$$

They can be thought of as describing the propagation of a charge-conjugate particle (i.e., a hole) with propagator $([G_0^-]^{-1} + \Sigma^-)^{-1}$ that is converted into a particle with propagator G^+ , via the condensate Φ^+ . (Or, a particle that is converted into a hole via the condensate.) The essence of superconductivity or superfluidity is the existence of a difermion condensate that makes the quasiparticle excitations superpositions of elementary states with fermion-number $\dots, -5, -3, -1, 1, 3, 5, \dots$; we see the formalism accommodating this phenomenon here.

We shall approximate Γ_2 by only taking into account two-loop diagrams. Upon taking the functional derivative with respect to S , this corresponds to a one-loop self-energy Σ . We show Σ diagrammatically in Fig. 4. We shall argue later that this approximation is sufficient to calculate $\log(\Delta/\mu)$ up to terms of order g^0 . Upon making this approximation, the gap equation takes the form shown in the lower panel of Fig. 4, namely

$$\Phi^+(K) = g^2 \int_Q \gamma^\mu T_a^T F^+(Q) \gamma^\nu T_b D_{\mu\nu}^{ab}(K - Q), \quad (22)$$

in momentum space, where $D_{\mu\nu}^{ab}(K - Q)$ is the gluon propagator.

Note that in the derivation of the gap equation we have assumed the system to be translationally invariant. This assumption fails for crystalline color superconductors, see Sec. VI. There has been some work on analyzing a particularly simple crystalline phase in QCD at asymptotically high densities and weak coupling (Leibovich *et al.*, 2001), but the formalism we are employing does not allow us to incorporate it into our presentation and, anyway, this subject remains to date largely unexplored.

B. Quasiparticle excitations

Before we proceed with solving the gap equation, it is worthwhile to derive the dispersion relations for the fermionic quasiparticle excitations in a color superconductor. That is, we suppose that the gap parameter(s) Δ have been obtained in the manner that we shall describe below and ask what are the consequences for the quasiparticle dispersion relations. Based on experience with ordinary superconductors or superfluids, we expect (and shall find) gaps in the dispersion relations for the fermionic quasiparticles. We may also expect that in some color superconducting phases, quasiparticles with different colors and flavors, or different linear combinations of color and flavor, differ in their gaps and dispersion relations. Indeed, some gaps may vanish or may be nonzero only in certain directions in momentum space.

The quasiparticle dispersion relations are encoded within the anomalous self-energy Φ^+ , defined in (18), which satisfies the gap equation (22). We shall assume that Φ^+ can be written in the form

$$\Phi^+(K) = \sum_{e=\pm} \Delta^{(e)}(K) \mathcal{M} \Lambda_{\mathbf{k}}^{(e)}, \quad (23)$$

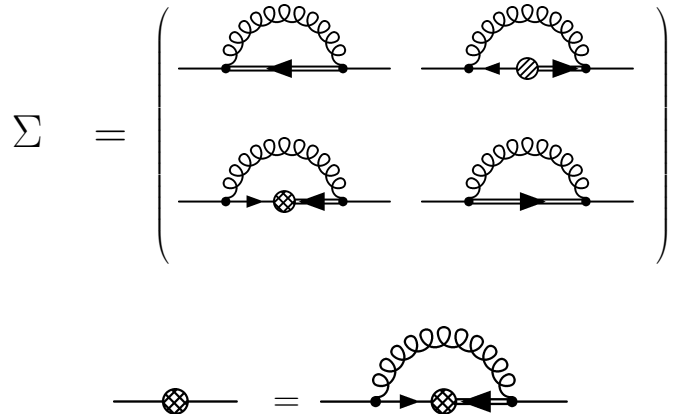


FIG. 4 Upper panel: Diagrammatic representation of the quark self-energy in Nambu-Gorkov space. Curly lines correspond to the gluon propagator D . The quasiparticle propagators G^+ and G^- are denoted by double lines with an arrow pointing to the left and right, respectively. The anomalous propagators F^\pm in the off-diagonal entries are drawn according to their structure given in Eq. (21): thin lines correspond to the term $([G_0^\mp]^{-1} + \Sigma^\mp)^{-1}$, while the cross-hatched and hatched circles denote the gap matrices Φ^+ and Φ^- , respectively. Lower panel: The QCD gap equation (22) is obtained by equating Φ^+ with the lower left entry of the self-energy depicted in the upper panel (the other off-diagonal component yields an equivalent equation for Φ^-).

where \mathcal{M} is a matrix in color, flavor and Dirac space, and $\Lambda_{\mathbf{k}}^{(e)} \equiv (1 + e\gamma_0 \boldsymbol{\gamma} \cdot \hat{\mathbf{k}})/2$ are projectors onto states of positive ($e = +$) or negative ($e = -$) energy. The corresponding gap functions are denoted as $\Delta^{(e)}(K)$ and will be determined by the gap equation. Here and in the following the energy superscript is denoted in parentheses to distinguish it from the superscript that denotes components in Nambu-Gorkov space. In our presentation we shall assume that \mathcal{M} is momentum-independent, corresponding to a condensate of Cooper pairs with angular momentum $J = 0$, but the formalism can easily be extended to allow a momentum-dependent $\mathcal{M}_{\mathbf{k}}$ as required for example in the analysis of the CSL phase and we shall quote results for this case also. Note that in Eq. (23) we are assuming that every nonzero entry in \mathcal{M} is associated with the same gap functions $\Delta^{(e)}$; the formalism would have to be generalized to analyze phases in which there is more than one independent gap function, as for example in the gCFL phase.

We shall analyze color superconducting phases whose color, flavor and Dirac structure takes the form

$$\mathcal{M}_{ij}^{\alpha\beta} = \phi_A^B \epsilon^{\alpha\beta A} \epsilon_{ijB} \gamma_5, \quad (24)$$

where the γ_5 Dirac structure selects a positive parity condensate, where, as described in Secs. I and II, the antisymmetric color matrix is favored since QCD is attractive in this channel and the antisymmetric flavor matrix is then required, and where ϕ is a 3×3 matrix. We note that because the full flavor symmetry is the chiral

$SU(3)_L \times SU(3)_R$ symmetry, the matrix ϕ is actually a pair (ϕ^L, ϕ^R) . In this section we shall assume $\phi^R = \phi^L$. The case $\phi^R \neq \phi^L$, which corresponds to a meson condensate in the CFL phase, is discussed in Sec. V.C.

The excitation spectrum is given by the poles of the propagator S in (19). (We shall see that the diagonal and the off-diagonal entries in S have the same poles.) It will turn out that the Hermitian matrix $\mathcal{M}\mathcal{M}^\dagger$ determines which quasiparticles are gapped and determines the ratios among the magnitudes of (possibly) different gaps. It is convenient to write this matrix via its spectral representation

$$\mathcal{M}\mathcal{M}^\dagger = \sum_r \lambda_r \mathcal{P}_r, \quad (25)$$

where λ_r are the eigenvalues and \mathcal{P}_r the projectors onto the corresponding eigenstates.

The final preparation that we must discuss prior to computing the propagator is that we approximate the diagonal elements of the quark self-energy as (Brown *et al.*, 2000c; Gerhold and Rebhan, 2005; Manuel, 2000b)

$$\Sigma^\pm \simeq \gamma_0 \Lambda_{\mathbf{k}}^{(\pm)} \frac{g^2}{18\pi^2} k_0 \log \frac{48e^2 m_g^2}{\pi^2 k_0^2}, \quad (26)$$

where $m_g^2 = N_f g^2 \mu^2 / (6\pi^2)$ is the square of the effective gluon mass at finite density, and e is the Euler constant. The expression (26) is the low energy approximation to the one-loop self-energy, valid for $k_0 \sim \Delta \ll m_g$, for the positive energy ($e = +$) states. Taking the low energy approximation to Σ^\pm and neglecting the self-energy correction to the negative energy states will prove sufficient to determine $\log(\Delta/\mu)$ up to order g^0 .

With all the groundwork in place, we now insert G_0 , Σ from (26), and Φ from (23) into (20) and (21), and hence (19), and use (25) to simplify the result. We find that the diagonal entries in the fermion propagator S are given by

$$G^\pm = \left([G_0^\mp]^{-1} + \Sigma^\mp \right) \sum_{e,r} \frac{\mathcal{P}_r \Lambda_{\mathbf{k}}^{(\mp e)}}{[k_0/Z^{(e)}(k_0)]^2 - [\epsilon_{k,r}^{(e)}]^2}, \quad (27)$$

while the anomalous propagators are

$$F^+(K) = - \sum_{e,r} \frac{\gamma_0 \mathcal{M} \gamma_0 \mathcal{P}_r \Lambda_{\mathbf{k}}^{(-e)} \Delta^{(e)}}{[k_0/Z^{(e)}(k_0)]^2 - [\epsilon_{k,r}^{(e)}]^2}, \quad (28a)$$

$$F^-(K) = - \sum_{e,r} \frac{\mathcal{M}^\dagger \mathcal{P}_r \Lambda_{\mathbf{k}}^{(e)} (\Delta^{(e)})^*}{[k_0/Z^{(e)}(k_0)]^2 - [\epsilon_{k,r}^{(e)}]^2}. \quad (28b)$$

In writing these expressions, we have defined the wave function renormalization factor

$$Z^{(+)}(k_0) \equiv \left(1 + \frac{g^2}{18\pi^2} \log \frac{48e^2 m_g^2}{\pi^2 k_0^2} \right)^{-1}, \quad (29)$$

for the positive energy $e = +$ components, originating from the self-energy (26). (By neglecting the negative energy contribution to Σ^\pm in (26), we are setting the negative energy wave function renormalization $Z^{(-)}(k_0) = 1$.) We have furthermore defined

$$\epsilon_{k,r}^{(e)} \equiv \sqrt{(ek - \mu)^2 + \lambda_r |\Delta^{(e)}|^2}. \quad (30)$$

The r 'th quasiparticle and antiquasiparticle energies are then given by solving $k_0 = Z^{(e)}(k_0) \epsilon_{k,r}^{(e)}$ for k_0 . To leading order in g , wave function renormalization can be neglected and the quasiparticle and antiquasiparticle energies are given by the $\epsilon_{k,r}^{(e)}$ themselves. We see from (30) that the antiparticles have $\epsilon > \mu$ — in fact, for k near μ they have $\epsilon \sim 2\mu$. They therefore never play an important role at high density. This justifies our neglect of the negative energy Σ^\pm and hence of $Z^{(-)}$. And, it justifies the further simplification that we shall henceforth employ, setting the antiparticle gap to zero, $\Delta^{(-)} = 0$, and denoting $\Delta \equiv \Delta^{(+)}$. We shall also use the notation $Z(k_0) \equiv Z^{(+)}(k_0)$ and $\epsilon_{k,r} \equiv \epsilon_{k,r}^{(+)}$. We then see that the minimum value of $\epsilon_{k,r}$ occurs at the Fermi surface, where $k = \mu$, and is given by $\sqrt{\lambda_r} \Delta$ which is conventionally referred to as the gap, again neglecting wave function renormalization. We see that although we must solve the gap equation in order to determine the magnitude of the gap parameter Δ , as we will do in Secs. IV.D and IV.E, the ratios among the actual gaps in the quasiparticle spectra that result are determined entirely by the λ_r 's, namely the eigenvalues of $\mathcal{M}\mathcal{M}^\dagger$.

We close this subsection by evaluating the pattern of quasiparticle gaps explicitly for the CFL and 2SC phases. We list the order parameters ϕ_A^B , eigenvalues λ_r , and corresponding projectors \mathcal{P}_r for these two phases in Table I. In the CFL phase, one finds the eigenvalues $\lambda_1 = 4$ with degeneracy $\text{Tr}[\mathcal{P}_1] = 1$ and $\lambda_2 = 1$ with degeneracy $\text{Tr}[\mathcal{P}_2] = 8$. This means that all nine quasiparticles are gapped. There is an octet with gap Δ , and a singlet with gap 2Δ . The octet Cooper pairs are *gu-rd*, *bd-gs*, *bu-rs*, as well as two linear combinations of the three quarks *ru-gd-bs*. (Here, *gu* refers to a green up quark, etc.) The singlet Cooper pair with twice the gap is the remaining orthogonal combination of *ru-gd-bs*. In the 2SC phase, on the other hand, we find four quasiparticles with $\lambda_1 = 1$ and hence gap Δ and 5 quasiparticles with $\lambda_2 = 0$ that are unpaired. The gapped quasiparticles involve the first two colors, red and green, and the first two flavors, up and down. The Cooper pairs have color-flavor structure *ru-gd* and *gu-rd*. (Note that all these color-flavor combinations depend on the chosen basis of the color and flavor (anti)triplets. This basis is fixed by Eq. (24); applying color (flavor) rotations to $\epsilon^{\alpha\beta A}$ (ϵ_{ijB}) would change the basis and yield different, physically equivalent, color-flavor combinations for the 2SC and CFL phases.)

The formalism of this section can easily be applied to patterns of pairing in which $\mathcal{M}_{\mathbf{k}}$ depends on the direction of the quark momentum \mathbf{k} . Such phases arise if the Cooper pairs carry total angular momentum $J = 1$. This

phase	ϕ_A^B	λ_1	λ_2	$(\mathcal{P}_1)_{\alpha\beta}^{ij}$	$(\mathcal{P}_2)_{\alpha\beta}^{ij}$
CFL	δ_A^B	4 (1-fold)	1 (8-fold)	$\delta_\alpha^i \delta_\beta^j / 3$	$\delta_{\alpha\beta} \delta^{ij} - \delta_\alpha^i \delta_\beta^j / 3$
2SC	$\delta_{A3} \delta^{B3}$	1 (4-fold)	0 (5-fold)	$(\delta_{\alpha\beta} - \delta_{\alpha 3} \delta_{\beta 3})(\delta^{ij} - \delta^{i3} \delta^{j3})$	$\delta_{\alpha 3} \delta_{\beta 3} \delta^{i3} \delta^{j3}$

TABLE I Color-flavor structure of CFL and 2SC phases: Order parameters ϕ_A^B , eigenvalues λ_r of the matrix $\mathcal{M}\mathcal{M}^\dagger$, and corresponding projectors \mathcal{P}_r , derived from Eq. (24). Color (flavor) indices are denoted $\alpha, \beta, (i, j)$.

allows for pairing between quarks of the same flavor, as discussed in Sec. III.E. Depending on the specific structure of $\mathcal{M}_{\mathbf{k}}$, the eigenvalues λ_r may become momentum dependent and lead to nodes in the gap function along certain directions in momentum space.

C. Pressure and condensation energy

We can now return to our expression (17) for the pressure P (equivalently, the thermodynamic potential since $\Omega = -P$) for a color superconductor and use the results of Sec. IV.B to evaluate it for a superconducting phase of the form (24). We first substitute the expressions (27) and (28) for the fermion propagator (19) in the pressure (17). In order to obtain a result that is valid at both nonzero and zero temperature, it is then convenient to switch to Euclidean space, and perform the sum over Matsubara frequencies. Upon doing the trace over Nambu-Gorkov, color, flavor, and Dirac space we find

$$P = \sum_{e,r} \int \frac{d^3k}{(2\pi)^3} \text{Tr}[\mathcal{P}_r] \left\{ \epsilon_{k,r}^{(e)} + 2T \log \left(1 + e^{-\epsilon_{k,r}^{(e)}/T} \right) - \frac{\lambda_r |\Delta|^2}{2\epsilon_{k,r}^{(e)}} \tanh \left(\frac{\epsilon_{k,r}^{(e)}}{2T} \right) \right\}. \quad (31)$$

Including the effects of wave function renormalization would modify this expression at order g . In most contexts, we shall only consider the pressure (31) at zero temperature. In this case, with $\sum_r \text{Tr}[\mathcal{P}_r] = N_c N_f$,

$$P = N_c N_f \frac{\mu^4}{12\pi^2} + \delta P. \quad (32)$$

where we denote the pressure difference of the color-superconducting phase compared to the unpaired phase by δP . If we make the simplifying assumption (corrected in the next subsection) that the gap function is a constant in momentum space in the vicinity of the Fermi surface, we find the easily interpretable result

$$\delta P = \frac{\mu^2}{4\pi^2} \sum_r \text{Tr}[\mathcal{P}_r] \lambda_r \Delta^2. \quad (33)$$

At $T = 0$ this quantity is the condensation energy density of the color-superconducting state. The fact that $\delta P > 0$ implies that the superconducting state is favored relative to the normal phase. We observe that δP is proportional to the sum of the energy gap squared of the r -th branch, multiplied by the corresponding degeneracy $\text{Tr}[\mathcal{P}_r]$.

We can use the result (33) to understand how to compare the favorability of different patterns of color superconducting pairing: the phase with lowest free energy (highest δP) is favored. As an example, in the CFL phase $\delta P = (\mu^2/(4\pi^2))(8 \cdot 1 + 1 \cdot 4)\Delta_{\text{CFL}}^2$ while in the 2SC phase $\delta P = (\mu^2/(4\pi^2))(4 \cdot 1 + 0 \cdot 5)\Delta_{\text{2SC}}^2$ suggesting that the CFL phase is favored. (We shall make this conclusion firm in Sec. IV.E, where we shall find that Δ_{CFL} is smaller than Δ_{2SC} but only by a factor of $2^{1/3}$. This factor will also turn out to be determined entirely by the λ_r 's and $\text{Tr}[\mathcal{P}_r]$'s.)

In principle, in order to generalize the conclusion that the CFL phase is favored one has to compare the condensation energies of all possible phases described by the order parameter \mathcal{M} in Eq. (24). This is difficult because ϕ is an arbitrary complex 3×3 matrix. At asymptotic densities, however, we can neglect the strange quark mass and treat the quarks as degenerate in mass. The resulting $SU(3)_c \times SU(3)_f$ symmetry simplifies the task. (f is L or R for ϕ_L or ϕ_R .) The matrix ϕ transforms under color-flavor rotations as $\phi \rightarrow U^T \phi V$ with $U \in SU(3)_c$, $V \in SU(3)_f$. This means that two order parameters ϕ and $U^T \phi V$ describe the same physics. Now note that for any ϕ there exists a transformation (U, V) such that $U^T \phi V$ is diagonal. Therefore, we need consider only diagonal matrices ϕ . Choosing all diagonal elements to be nonzero corresponds to the maximum number of gapped quasiparticles. Hence, once we show (below) that Δ_{2SC} is not much larger than Δ_{CFL} it is easy to understand that the CFL phase with $\phi = \mathbf{1}$, yielding an order parameter that is invariant under the largest possible subgroup of the original symmetries, is the ground state at asymptotically large densities.

At lower densities, the flavor symmetry is explicitly broken by the mass of the strange quark (the symmetries are further broken by different chemical potentials due to neutrality constraints). In this case, the above argument fails and non-diagonal matrices ϕ become possible candidates for the ground state (Malekzadeh, 2006; Rajagopal and Schmitt, 2006).

D. Weak coupling solution of the gap equation

We are now in a position to solve the QCD gap equation (22) for an order parameter with a given matrix structure \mathcal{M} . The matrix structure of the gap equation (22) is handled by multiplying both sides of the equation by $\mathcal{M}^\dagger \Lambda_{\mathbf{k}}^{(+)}$ and taking the trace over color, flavor, and Dirac indices.

The gap equation is sensitive to gluon modes with small momentum ($p \ll m_g$) and even smaller energy ($p_0 \sim p^3/m_g^2 \ll p$), meaning that medium effects in the gluon propagator have to be taken into account. In the low momentum limit, the gluon propagator takes on the standard hard-dense loop approximation form (Braaten and Pisarski, 1992), which we shall give below in Eqs. (36) and (37) upon simplifying it as appropriate for $p_0 \ll p$. In order to obtain $\log(\Delta/\mu)$ to order g^0 , it suffices to keep only the leading terms in the propagator in the $p_0 \ll p$ limit. We shall work in Coulomb gauge. Gauge independence of the gap in a generalized Coulomb gauge was established in (Pisarski and Rischke, 2002), and a more formal proof of gauge invariance was given in (Gerhold and Rebhan, 2003; Hou *et al.*, 2004). The gap equation reads

$$\Delta_{k,r} = \frac{g^2}{4} \int \frac{d^3q}{(2\pi)^3} \sum_s Z(\epsilon_{q,s}) \frac{\Delta_{q,s}}{\epsilon_{q,s}} \tanh\left(\frac{\epsilon_{q,s}}{2T}\right) \times \left[D_\ell(p) \mathcal{T}_{00}^s(\mathbf{k}, \mathbf{q}) + D_t(p, \epsilon_{q,s}, \epsilon_{k,r}) \mathcal{T}_t^s(\mathbf{k}, \mathbf{q}) \right], \quad (34)$$

where we have abbreviated $P \equiv K - Q$ and have denoted the gap function on the quasiparticle mass shell by $\Delta_{k,r} \equiv \Delta(\epsilon_{k,r}, \mathbf{k})$. We have denoted the traces over color, flavor, and Dirac space by

$$\mathcal{T}_{\mu\nu}^s(\mathbf{k}, \mathbf{q}) \equiv -\frac{\text{Tr} \left[\gamma_\mu T_a^T \gamma_0 \mathcal{M}_{\mathbf{q}} \gamma_0 \mathcal{P}_s \Lambda_{\mathbf{q}}^{(-)} \gamma_\nu T_a \mathcal{M}_{\mathbf{k}}^\dagger \Lambda_{\mathbf{k}}^{(+)} \right]}{\text{Tr} \left[\mathcal{M}_{\mathbf{k}} \mathcal{M}_{\mathbf{k}}^\dagger \Lambda_{\mathbf{k}}^{(+)} \right]}, \quad (35)$$

and $\mathcal{T}_t^s(\mathbf{k}, \mathbf{q}) \equiv -(\delta^{ij} - \hat{p}^i \hat{p}^j) \mathcal{T}_{ij}^s(\mathbf{k}, \mathbf{q})$. The two terms inside the square bracket in Eq. (34) correspond to the contributions from electric and magnetic gluons. The dominant contribution comes from almost static gluons with $p_0 \ll p$. The static electric and almost static magnetic gluon propagator give

$$D_\ell(p) \equiv \frac{2}{p^2 + 3m_g^2} \quad (36)$$

$$D_t(p, \epsilon, \epsilon') \equiv \frac{p^4}{p^6 + M_g^4(\epsilon + \epsilon')^2} + (\epsilon' \rightarrow -\epsilon'), \quad (37)$$

where $M_g^2 \equiv (3\pi/4)m_g^2$. With the gap equation now stated fully explicitly, all that remains is to solve it.

We can solve (34) for the zero temperature gap Δ on the Fermi surface. Or, we can solve for T in the $\Delta \rightarrow 0$ limit, thus obtaining the critical temperature T_c . Solving for Δ , we find that it has a weak coupling expansion of the form

$$\log\left(\frac{\Delta}{\mu}\right) = -\frac{b_{-1}}{g} - \bar{b}_0 \log(g) - b_0 - \dots \quad (38)$$

In our treatment of the fermion propagator, the gluon propagator, and in our truncation of the self-energy in Fig. 4 to one loop (for example neglecting vertex renormalization) we have been careful to keep all effects that

contribute to b_0 , but we have neglected many that contribute at order $g \log g$ and g . The formalism that we have presented can be used to evaluate b_{-1} , \bar{b}_0 and b_0 , and we shall describe the results in Sec. IV.E.

Before turning to quantitative results, it is worth highlighting the origin and the importance of the leading $-1/g$ behavior in (38), namely the fact that $(\Delta/\mu) \sim \exp(-\text{constant}/g)$. If in the gap equation of Fig. 4 we were to replace the exchanged gluon by a contact interaction, we would obtain a gap equation of the form

$$\Delta \propto g^2 \int d\xi \frac{\Delta}{\sqrt{\xi^2 + \Delta^2}} \quad (39)$$

with $\xi \equiv k - \mu$. This always has the solution $\Delta = 0$; to seek nonzero solutions, we cancel Δ from both sides of the equation. Then, if Δ were 0, the remaining integral would diverge logarithmically at small ξ . Therefore, we find a nonzero Δ for any positive nonzero g no matter how small, with $\Delta \propto \exp(-\text{constant}/g^2)$. This is the original BCS argument for superconductivity as a consequence of an attractive interaction at a Fermi surface. However, once we restore the gluon propagator the argument is modified. The crucial point is that magnetic gluon exchange is an unscreened long-range interaction, meaning that the angular integral will diverge logarithmically at forward scattering in the absence of any mechanism that screens the magnetic interaction. The gap equation therefore takes the form

$$\Delta \propto g^2 \int d\xi \frac{\Delta}{\sqrt{\xi^2 + \Delta^2}} d\theta \frac{\mu^2}{\theta \mu^2 + \delta^2} \quad (40)$$

where θ is the angle between the external momentum \mathbf{k} and the loop momentum \mathbf{q} and where δ is some quantity with the dimensions of mass that cuts off the logarithmic collinear divergence of the angular integral. In the superconducting phase this divergence will at the least be cut off by the Meissner effect, which screens gluon modes with $p < \Delta$ (since the Cooper pairs have size $1/\Delta$) giving $\delta \sim \Delta$. This yields $\Delta \sim g^2 \Delta (\log \Delta)^2$ and hence a nonzero gap $\Delta \sim \exp(-\text{constant}/g)$. This consequence of the long-range nature of the magnetic gluon exchange was first discovered by Barrois (Barrois, 1979). However, pursuing the argument as just stated yields the wrong value of the constant b_{-1} ; it was Son who realized that the collinear divergence is cut off by Landau damping at a larger value of the angle θ than that at which the Meissner effect does so. Loosely speaking, Landau damping leads to $\delta \sim (\Delta m_g^2)^{1/3} \gg \Delta$. Son was then able to calculate the coefficients of the $1/g$ term and of the logarithm in (38) (Son, 1999). The calculation of the constant b_0 was initiated in (Hong *et al.*, 2000; Hsu and Schwetz, 2000; Pisarski and Rischke, 2000a,b; Schäfer and Wilczek, 1999d) and completed in (Brown *et al.*, 2000b; Wang and Rischke, 2002). Higher order terms are expected to be of order $g \log g$, order g , and at higher order still may contain fractional powers and logarithms of g , see Sec. V.A.2.

The $(\Delta/\mu) \propto \exp(-\text{constant}/g)$ behavior means that the color superconducting gap is parametrically larger at $\mu \rightarrow \infty$ than it would be for any four-fermion interaction. Furthermore, asymptotic freedom ensures that $1/g(\mu)^2$ increases logarithmically with μ , which means that $\exp[-\text{constant}/g(\mu)]$ decreases more slowly than $1/\mu$ at large μ . We can therefore conclude that Δ increases with increasing μ at asymptotically large μ , although of course Δ/μ decreases.

We conclude this subsection with a derivation of the correct value of the coefficient b_{-1} , namely the constant in $(\Delta/\mu) \propto \exp(-\text{constant}/g)$. This coefficient turns out to be independent of the spin-color-flavor structure \mathcal{M} , and it is therefore simplest to present its derivation in the 2SC phase, in which there is only one gap parameter $\Delta_k \equiv \Delta_{k,r=1}$, $\epsilon_k \equiv \epsilon_{k,r=1}$. The leading behavior of the gap is completely determined by magnetic gluon exchanges. We can also approximate the trace term by its value in the forward direction $\mathcal{T}_t(\mathbf{k}, \mathbf{q}) \simeq \mathcal{T}_t(\mathbf{k}, \mathbf{k}) = 2/3$ and set the wave function renormalization $Z(q_0) = 1$ (in the forward limit we also find $\mathcal{T}_{00}(\mathbf{k}, \mathbf{q}) \simeq \mathcal{T}_t(\mathbf{k}, \mathbf{q})$). Carrying out the angular integrals in the gap equation gives

$$\Delta_k = \frac{g^2}{18\pi^2} \int dq \frac{\Delta_q}{\epsilon_q} \frac{1}{2} \log \left(\frac{\mu^2}{|\epsilon_q^2 - \epsilon_k^2|} \right). \quad (41)$$

Soon observed that at this order we can replace the logarithm by $\max\{\log(\mu/\epsilon_k), \log(\mu/\epsilon_q)\}$. Introducing logarithmic variables $x = \log[2\mu/(\xi_k + \epsilon_k)]$ with $\xi_k = |k - \mu|$, the integral equation (41) can be written as a differential equation

$$\Delta''(x) = -\frac{g^2}{18\pi^2} \Delta(x), \quad (42)$$

with the boundary conditions $\Delta(0) = 0$ and $\Delta'(x_0) = 0$. Here, $x_0 = \log(2\mu/\Delta)$ determines the gap on the Fermi surface. The solution is

$$\Delta(x) = \Delta \sin \left(\frac{gx}{3\sqrt{2}\pi} \right), \quad \Delta = 2\mu \exp \left(-\frac{3\pi^2}{\sqrt{2}g} \right), \quad (43)$$

and thus $b_{-1} = 3\pi^2/\sqrt{2}$. We see that in the weak-coupling limit the gap function is peaked near the Fermi surface, with a width that is much smaller than μ but much larger than Δ .

E. Gap and critical temperature at weak coupling

The gap on the Fermi surface of a color superconductor at zero temperature can be written as

$$\Delta = \mu g^{-b_0} e^{-b_0} \exp \left(-\frac{3\pi^2}{\sqrt{2}g} \right), \quad (44)$$

to order g^0 in the weak-coupling expansion of $\log(\Delta/\mu)$. We have derived the coefficient b_{-1} in the exponent above, starting from a simplified version of the gap equation (34), with no wave function renormalization and a

simplified gluon propagator. Upon restoring these effects, analysis of the gap equation (34) yields

$$g^{-b_0} e^{-b_0} = g^{-5} 512\pi^4 \left(\frac{2}{N_f} \right)^{5/2} e^{-b'_0} e^{-d} e^{-\zeta}. \quad (45)$$

In the following we shall define and explain the origin of each of the terms in this equation; we shall not present a complete derivation.

- The factor g^{-5} and the numerical factor in Eq. (45) are due to large angle magnetic as well as electric gluon exchanges and are independent of the pattern of pairing in the color superconducting phase, i.e. independent of \mathcal{M} .
- The factor

$$e^{-b'_0} = \exp \left(-\frac{\pi^2 + 4}{8} \right) \simeq 0.177 \quad (46)$$

arises from the wave function renormalization factor $Z(q_0)$ in (26) (Brown *et al.*, 2000b; Wang and Rischke, 2002) and is also independent of \mathcal{M} and hence the same for all color superconducting phases.

- The factors that we have written as $e^{-d}e^{-\zeta}$ are different in different color superconducting phases. The factor e^{-d} is due to the angular structure of the gap. For the $J = 0$ condensates whose gap equation we have derived, $e^{-d} = 1$. Upon redoing the angular integrals for spin-1 condensates, we find that they are strongly suppressed (Schäfer, 2000b; Schmitt, 2005; Schmitt *et al.*, 2002). For spin-1 pairing patterns in which quarks of the same chirality form Cooper pairs, $d = 6$. A smaller suppression occurs when quarks of opposite chirality pair, $d = 4.5$. Superpositions of these states yield values of d between these limits. Regardless, perturbative QCD predicts spin-1 gaps to be two to three orders of magnitude smaller than spin-0 gaps.
- The factor $e^{-\zeta}$ depends on \mathcal{M} , the color-flavor-spin matrix that describes the pattern of pairing in a particular color superconducting phase. In a phase in which $\mathcal{M}\mathcal{M}^\dagger$ has two different eigenvalues λ_1 and λ_2 , describing $\text{Tr}[\mathcal{P}_1]$ and $\text{Tr}[\mathcal{P}_2]$ quasiparticles respectively, we find

$$\zeta = \frac{1}{2} \frac{\langle \text{Tr}[\mathcal{P}_1] \lambda_1 \log \lambda_1 + \text{Tr}[\mathcal{P}_2] \lambda_2 \log \lambda_2 \rangle}{\langle \text{Tr}[\mathcal{P}_1] \lambda_1 + \text{Tr}[\mathcal{P}_2] \lambda_2 \rangle}, \quad (47)$$

where the angular brackets denote an angular average (trivial for $J = 0$ phases). In the CFL phase, $\lambda_1 = 1$ and $\text{Tr}[\mathcal{P}_1] = 8$ while $\lambda_2 = 4$ and $\text{Tr}[\mathcal{P}_2] = 1$, meaning that there are 8 quasiparticles with gap Δ and 1 with gap 2Δ . Evaluating Eq. (47), we find $e^{-\zeta} = 2^{-1/3}$ in the CFL phase (Schäfer, 2000a). In the 2SC phase, $e^{-\zeta} = 1$. Note that the ratio

$\Delta_{\text{CFL}}/\Delta_{\text{2SC}}$ is also $2^{-1/3}$ in an NJL model analysis (Rajagopal and Wilczek, 2000); this result depends on the structure of the condensates not on the nature of the interaction. From $\Delta_{\text{CFL}}/\Delta_{\text{2SC}} = 2^{-1/3}$ we can conclude the discussion begun in Sec. IV.C, noting now that the condensation energy in the CFL phase is larger than that in the 2SC phase by a factor $3 \cdot 2^{-2/3}$.

- We can also determine the admixture of a color symmetric condensate in the CFL phase. In this case we have to use a two-parameter ansatz for the gap and solve two coupled gap equations. The color-symmetric gap parameter Δ_6 is parametrically small compared to the color-antisymmetric gap $\Delta_{\bar{3}}$, and the two gap equations decouple. We find $\Delta_6/\Delta_{\bar{3}} = \sqrt{2} \log(2)g/(36\pi)$ which is suppressed by both the coupling constant g and a large numerical factor.

In evaluating (44) and (45), it suffices at present to evaluate g at the scale μ . The effect of choosing $g(a\mu)$ with a either some purely numerical constant or some constant proportional to g or $\log \Delta$ is order g , meaning that we cannot and need not determine a within our present calculation of $\log \Delta$ to order g^0 . For a numerical estimate of the effects of a running g on Δ , see (Schäfer, 2004). The effects are not as large as envisioned in (Beane *et al.*, 2001).

We shall discuss a systematic approach to the calculation of corrections beyond $\mathcal{O}(g^0)$ in $\log(\Delta/\mu)$ in Sec. V.A.2. There are a number of effects that have been considered, and were shown not to contribute at $\mathcal{O}(g^0)$, but for which the actual size of the $\mathcal{O}(g)$ (or higher) correction is not known. These include vertex corrections (Brown *et al.*, 2000a), the imaginary part of the gap function (Feng *et al.*, 2006; Reuter, 2006), and the modification of the gluon propagator due to the Meissner effect (Rischke, 2001).

It is instructive to extrapolate the perturbative results to lower baryon densities for which the running coupling constant is not small. Taking $\mu \simeq 400 - 500$ MeV, and a strong coupling constant $g \simeq 3.5$ (note that $g = 3.56$ at $\mu = 400$ MeV according to the two-loop QCD beta function, which of course should not be taken seriously at these low densities) one obtains $\Delta \simeq 20$ MeV. This is comparable to (but on the small side of) the range of typical gaps $\Delta \sim (20 - 100)$ MeV (Rajagopal and Wilczek, 2000) obtained using models in which the interaction between quarks is described via a few model parameters whose values are chosen based upon consideration of zero-density physics, like the NJL models that we shall discuss in Sec. VI or numerical solutions of the Dyson-Schwinger equations (Marhauser *et al.*, 2007; Nickel *et al.*, 2006b). This qualitative agreement between two completely different approaches, one based on using a model to extrapolate from $\mu = 0$ to $\mu = 400 - 500$ MeV and the other based on applying a rigorous calculation that is valid for $\mu > 10^8$ MeV where the QCD coupling is weak

at $\mu = 400 - 500$ MeV gives us confidence that we understand the magnitude of Δ , the fundamental energy scale that characterizes color superconductivity. Furthermore, the one nonperturbative interaction in QCD whose contribution to Δ has been evaluated reliably at high density, namely that due to the 't Hooft interaction induced by instantons, serves to increase Δ , bringing the high density computation into even better agreement with the model-based approaches (Alford *et al.*, 1998; Berges and Rajagopal, 1999; Carter and Diakonov, 1999; Rapp *et al.*, 1998, 2000; Schäfer, 2004).

Finally, we can use the gap equation (34) to extract the critical temperature T_c . The result is

$$\frac{T_c}{\Delta} = \frac{e^\gamma}{\pi} e^\zeta, \quad (48)$$

where $\gamma \simeq 0.577$ is the Euler-Mascheroni constant. This should be compared to the BCS result $T_c/\Delta = e^\gamma/\pi \simeq 0.57$. We observe that deviations from the BCS ratio occur in the case of two-gap structures and/or anisotropic gaps. Nevertheless, since e^ζ is of order one, the critical temperature is always of the same order of magnitude as the zero-temperature gap. We see that for the 2SC phase T_c/Δ is as in BCS theory, whereas in the CFL phase this ratio is larger by a factor of $2^{1/3}$. It therefore turns out that T_c is the same in the CFL and 2SC phases.

These estimates of T_c neglect gauge field fluctuations, making them valid only at asymptotic densities. We shall see in Sec. V.B that including the gauge field fluctuations turns the second order phase transition that we find by analyzing (34) into a first order phase transition, and increases T_c by a factor $1 + \mathcal{O}(g)$, see Eq. (74).

F. Color and electromagnetic Meissner effect

One of the characteristic properties of a superconductor is the Meissner effect, the fact that an external magnetic field does not penetrate into the superconductor. The external field is shielded by supercurrents near the interface between the normal phase and the superconducting phase. The inverse penetration length defines a mass scale which can be viewed as an effective magnetic gauge boson mass.

This effect can also be described as the Anderson-Higgs phenomenon (Anderson, 1963; Higgs, 1964). The difermion condensate acts as a composite Higgs field which breaks all or part of the gauge symmetry of the theory. The gauge fields acquire a mass from the Higgs vacuum expectation value, and the would-be Goldstone bosons become the longitudinal components of the gauge fields. A well known example in particle physics is provided by the electroweak sector of the standard model. The $SU(2)_L \times U(1)_Y$ gauge symmetry of the electroweak standard model is broken down to $U(1)_Q$ by the expectation value of an $SU(2)$ Higgs doublet which carries hypercharge. There are three massive gauge bosons, the W^\pm and the Z boson. The Z is a linear combination of

the original I_3 and Y gauge bosons. The orthogonal linear combination is the photon, which remains massless because the Higgs condensate is electrically neutral.

The gauge symmetry in QCD is $SU(3)_c \times U(1)_Q$. Different color superconducting order parameters realize different Higgs phases. The color gauge group may be partially or fully broken, and mixing between diagonal gluons and photons can occur. In the following we shall concentrate on the 2SC and CFL phases and briefly mention other phases at the end of the section. Our starting point is the one-loop gauge boson polarization tensor (Litim and Manuel, 2001; Rischke, 2000a,b; Rischke and Shovkovy, 2002; Son and Stephanov, 2000a),

$$\Pi_{ab}^{\mu\nu}(P) \equiv \frac{1}{2V} \sum_K \text{Tr}[\hat{\Gamma}_a^\mu S(K) \hat{\Gamma}_b^\nu S(K-P)], \quad (49)$$

where

$$\hat{\Gamma}_a^\mu \equiv \begin{cases} \text{diag}(g\gamma^\mu T_a, -g\gamma^\mu T_a^T) & \text{for } a = 1, \dots, 8, \\ \text{diag}(e\gamma^\mu Q, -e\gamma^\mu Q) & \text{for } a = 9. \end{cases} \quad (50)$$

Here, Q is the electric charge matrix $Q = \text{diag}(2/3, -1/3, -1/3)$, and e the electromagnetic coupling constant. The polarization function can be defined as the second derivative of the thermodynamic potential with respect to an external gauge field. This quantity is equal to the derivative of the induced charge/current with respect to the gauge field. Electric charge screening is governed by the zero momentum limit of the Π_{00} component of the polarization tensor. The Meissner effect is related to a non-vanishing zero momentum limit of the spatial components Π_{ij} . We can define electric (Debye) and magnetic screening masses as

$$m_{D,ab}^2 \equiv -\lim_{p \rightarrow 0} \Pi_{ab}^{00}(0, \mathbf{p}), \quad (51a)$$

$$m_{M,ab}^2 \equiv \frac{1}{2} \lim_{p \rightarrow 0} (\delta^{ij} - \hat{p}^i \hat{p}^j) \Pi_{ab}^{ij}(0, \mathbf{p}). \quad (51b)$$

A calculation of the full momentum dependence of $\Pi_{\mu\nu}$ in the 2SC and CFL phases can be found in (Rischke, 2001) and (Malekzadeh and Rischke, 2006), respectively. One result that we shall need in Sec. V.C is the electric screening mass for gluons in the CFL phase, which is given by

$$m_{D,aa}^2 = \frac{21 - 8 \log 2}{36} \frac{g^2 \mu^2}{\pi^2}. \quad (52)$$

The numerical factor $21 - 8 \log 2$ can be written as $15 + (6 - 8 \log 2)$, where the first term comes from diagrams in which the gluon couples to two octet quasiparticles and the second from coupling to one octet and one singlet quasiparticle. The $\log 2$ factor is the log of the ratio of the singlet and octet gaps.

In the following, we shall discuss the Meissner masses. Results for the CFL phase (Casalbuoni *et al.*, 2001b;

Rischke, 2000a; Son and Stephanov, 2000a; Zarembo, 2000) and the 2SC phase (Casalbuoni *et al.*, 2002b; Rischke, 2000b) are summarized in Table II, where we also list the screening masses for the single-flavor CSL phase (Schmitt *et al.*, 2003, 2004).

We observe that the chromomagnetic screening masses are of order $g\mu$. This means that the screening length is much shorter than the coherence length $\xi = 1/\Delta$, and color superconductivity is type I, see Sec. V.B. The fact that the screening masses are independent of the gap does not contradict the fact that there is no magnetic screening in the normal phase. Magnetic screening disappears for energies and momenta larger than the gap. Therefore, if the $\Delta \rightarrow 0$ limit is taken before the limit $p \rightarrow 0$ then the magnetic screening vanishes, as expected. Of course, magnetic screening masses also vanish as the temperature approaches T_c .

We also note that $m_{M,ab}^2$ is a 9×9 matrix, and the physical masses are determined by the eigenvalues of this matrix. In the CFL phase, all magnetic gluons acquire the same nonzero mass, reflecting the residual $SU(3)_{c+L+R}$. In the 2SC phase, the Meissner masses of the gluons 1 through 3 vanish, reflecting the symmetry breaking pattern $SU(3)_c \rightarrow SU(2)_c$. The unscreened gluons correspond to the generators of the unbroken $SU(2)_c$, as they only see the first two colors, red and green. Cooper pairs are red-green singlets and so cannot screen these low momentum gluons.

In both 2SC and CFL phases, the off-diagonal masses vanish except for the eighth gluon and the photon, $m_{M,\gamma 8}^2 = m_{M,8\gamma}^2 \neq 0$. The two-by-two part of the gauge boson mass matrices that describe the eighth gluon and the photon has one vanishing eigenvalue and one nonzero eigenvalue. The eigenvectors are characterized by a mixing angle θ , given in the last column of Table II. This angle defines the new gauge fields,

$$\tilde{A}_\mu^8 = \cos \theta A_\mu^8 + \sin \theta A_\mu, \quad (53a)$$

$$\tilde{A}_\mu = -\sin \theta A_\mu^8 + \cos \theta A_\mu, \quad (53b)$$

where A_μ^8 and A_μ denote the fields for the eighth gluon and the photon, respectively. The \tilde{A}_μ^8 gauge boson feels a Meissner effect; it is the analogue of the massive Z -boson in the electroweak standard model. The \tilde{A}_μ gauge boson, on the other hand, experiences no Meissner effect because the diquark condensate is \tilde{Q} -neutral. This is the photon of the unbroken Abelian $U(1)_{\tilde{Q}}$ gauge symmetry, consisting of simultaneous color and flavor (i.e. electromagnetic) rotations. The \tilde{A}_μ field satisfies Maxwell's equations. Because $g \gg e$, the mixing angle is very small and the \tilde{A}_μ photon contains only a small admixture of the original eighth gluon.

In contrast, $J = 1$ color superconductors show an electromagnetic Meissner effect (Schmitt *et al.*, 2003, 2004). For example, in the CSL phase there is no mixing between the gluons and the photon, as can be seen in the last row of Table II. The photon acquires a mass since the electromagnetic group is spontaneously broken. Other

candidate spin-1 phases, such as the polar, planar, or A phase involve mixing but also (except for a one-flavor system) exhibit an electromagnetic Meissner effect. This difference in phenomenology of spin-0 vs. spin-1 color superconductors may have consequences in compact stars (Aguilera, 2007).

G. Chromomagnetic instability

We have just seen in Sec. IV.F that color superconductors have nonzero Meissner masses for some gluons and/or the photon, indicating a color or electromagnetic Meissner effect. However, as we discussed previously, in Sec. III.B, if the CFL phase is stressed by a nonzero strange quark mass to the point that Cooper pairs break, the resulting gapless CFL (gCFL) phase found in analyses that presume a translationally invariant condensate exhibits *imaginary* Meissner masses (Casalbuoni *et al.*, 2005b; Fukushima, 2005). This phenomenon was first discovered in the simpler gapless 2SC (g2SC) phase (Huang and Shovkovy, 2004a,b) and can be understood in either the gCFL or g2SC context via a simplified analysis involving two quark species only (Alford and Wang, 2005) that we introduced in Sec. I.E and shall pursue here. The negative Meissner mass squared implies that these phases are unstable toward the spontaneous generation of currents, that break translation invariance. In this section we shall review the calculation of the Meissner mass in a gapless color superconductor.

We have seen in Sec. II that the introduction of a nonzero strange quark mass, combined with the requirement that matter be neutral and in beta equilibrium, serve to exert a stress on the CFL pairing that is controlled by the parameter $m_s^2/(2\mu)$. This stress seeks to separate the bu and rs Fermi surfaces (and the bd and gs Fermi surfaces) but in the CFL phase they remain locked together in order to gain pairing energy $\propto \Delta$ per Cooper pair. In the gCFL phase, on the other hand, there are unpaired bu and bd quarks in regions of momentum space in which the corresponding rs and gs states are empty — Cooper pairs have been broken yielding gapless excitations. We can describe the resulting chromomagnetic instability generically by picking one of these pairs, calling the quarks 1 and 2, and labelling their effective chemical potentials μ_1 and μ_2 . The quasiparticle dispersion relations are

$$\epsilon_k \equiv \left| \sqrt{(k - \bar{\mu})^2 + \Delta^2} \pm \delta\mu \right|, \quad (54)$$

with the average chemical potential $\bar{\mu}$ and the mismatch in chemical potentials $\delta\mu$ as in Eq. (4). (Note that the leading effect of the strange mass, $\propto m_s^2/(2\mu)$, is included in the effective chemical potential, meaning that we may use the massless dispersion relation of Eq. (54).) For $\mu_1 = \mu_2$ this yields identical dispersion relations for both degrees of freedom (and the same with a minus sign for the corresponding hole degrees of freedom which are

omitted here). This is the usual situation of BCS superconductivity. For $\mu_1 \neq \mu_2$, however, one obtains two different quasiparticle excitations. A qualitative change appears at $\delta\mu = \Delta$. For $\delta\mu > \Delta$ the dispersion relations become gapless at the two momenta

$$k_{\pm} = \bar{\mu} \pm \sqrt{\delta\mu^2 - \Delta^2}, \quad (55)$$

meaning that there are gapless quasiparticles on two spheres in momentum space. In the region of momentum space between these two spheres, the states of species 1 are filled while those of species 2 are empty: the 1-2 pairing has been “breached” (Gubankova *et al.*, 2003). (We have taken $\delta\mu > 0$.) This seems a natural way for the system to respond to the stress $\delta\mu$, by reducing the number of 2 particles relative to the number of 1 particles, albeit at the expense of lost pairing energy. In the larger gCFL context, such a response serves to alleviate the stress introduced by the requirements of neutrality and weak equilibrium.

Gapless superconductivity (Alford *et al.*, 2000a) refers to the circumstance in which two species of fermions are paired in some regions of momentum space but in a shell (breach) in momentum space, bounded by two spherical effective Fermi surfaces, one finds unpaired fermions of just one of the two species. The term does not refer to situations in which some fermion species pair throughout momentum space while others do not pair at all, as for example in the 2SC phase. Nor does it apply to anisotropic superconductors in which the gap parameter vanishes in certain directions on the Fermi surface, as for example in some single-flavor color superconductors or in the curCFL- K^0 and crystalline color superconducting phases. The g2SC and gCFL phases are gapless superconductors, in which the same quarks pair, yielding a nonzero order parameter Δ , while simultaneously featuring gapless excitations. Such phases turn out to suffer from the chromomagnetic instability as we now explain.

The calculation of the Meissner mass can be done starting from Eq. (49). At zero temperature, in this simple context with two fermion species one finds

$$m_M^2 = m_0^2 \left[1 - \frac{\delta\mu \Theta(\delta\mu - \Delta)}{\sqrt{\delta\mu^2 - \Delta^2}} \right], \quad (56)$$

where m_0 is the Meissner mass obtained upon setting $\delta\mu = 0$, removing the stress. This expression shows that the Meissner mass becomes imaginary if and only if the spectrum is gapless.

In essence, this is also what happens in the CFL phase (Casalbuoni *et al.*, 2005b; Fukushima, 2005). In this case, of course, there are nine gauge bosons whose Meissner masses were discussed in Sec. IV.F for the case of pairing in the absence of stress. The Meissner masses for pairing with mismatched Fermi surfaces are complicated and have to be computed numerically in general. However, the reason for the negativity of m_M^2 is the same as in Eq. (56): a negative term $\propto \delta\mu/\sqrt{\delta\mu^2 - \Delta^2}$ appears

	$m_{M,aa}^2$								$m_{M,a\gamma}^2 = m_{M,\gamma a}^2$		$m_{M,\gamma\gamma}^2$	$\tilde{m}_{M,88}^2$	$\tilde{m}_{M,\gamma\gamma}^2$	$\cos^2 \theta$
a	1	2	3	4	5	6	7	8	1-7	8	9			
CFL	ηg^2								0	$-\frac{2}{\sqrt{3}} \eta e g$	$\frac{4}{3} \eta e^2$	$(\frac{4}{3} e^2 + g^2) \eta$	0	$3g^2/(3g^2 + 4e^2)$
2SC	0		$\frac{1}{2} g^2$			$\frac{1}{3} g^2$			0	$\frac{1}{3\sqrt{3}} e g$	$\frac{1}{9} e^2$	$\frac{1}{3} g^2 + \frac{1}{9} e^2$	0	$3g^2/(3g^2 + e^2)$
CSL	βg^2	αg^2	βg^2	βg^2	αg^2	βg^2	αg^2	βg^2	0	0	$6q^2 e^2$	βg^2	$6q^2 e^2$	1

TABLE II Zero-temperature Meissner masses m_M , rotated Meissner masses \tilde{m}_M , and gluon/photon mixing angle θ . The number a labels the gluons ($a = 1, \dots, 8$) and the photon ($a = 9$). All masses are given in units of $N_f \mu^2 / (6\pi^2)$, where $N_f = 3, 2, 1$ in the CFL, 2SC, CSL phases, respectively. We have abbreviated $\eta \equiv (21 - 8 \log 2)/54$, $\alpha \equiv (3 + 4 \log 2)/27$, $\beta \equiv (6 - 4 \log 2)/9$. For the one-flavor CSL phase we denoted the quark electric charge by q . While the rotated photon in the CFL and 2SC phases is massless, the photon acquires a Meissner mass in the CSL phase.

for $\delta\mu > \Delta$. At the onset of gapless modes, $\delta\mu = \Delta$, this term diverges and thus it dominates the Meissner masses at least for $\delta\mu$ close to, but larger than, Δ . This is the story for the gluons A_1, A_2 , but it turns out that the Meissner masses for the gluons A_a , $a = 4, 5, 6, 7$, at first remain well-behaved for values of $\delta\mu$ larger than Δ before eventually also becoming imaginary for sufficiently large mismatches. The gluons A_3, A_8 and the photon mix with each other. Two of the resulting new gauge bosons acquire an imaginary mass, just as the first two gluons. The third combination, $A_{\tilde{Q}}$, remains massless, as expected from symmetry arguments. (The mixing between these gauge bosons is a function of the mismatch and cannot be described by the mixing angle given in Table II.) Although the details are clearly more complicated than in the simple two-species model, the conclusion remains that the chromomagnetic instability occurs if and only if there are gapless modes.

This statement is not always correct, as the analysis of the gapless 2SC phase demonstrates (Huang and Shovkovy, 2004a,b; Kiriyaama, 2006a,b). In this phase, the gluons 1,2 and 3 are massless for arbitrary mismatches, reflecting the unbroken $SU(2)_c$. One combination of the eighth gluon with the photon behaves as in Eq. (56) while the other combination is massless. The Meissner masses for the gluons 4-7, however, are imaginary for $\delta\mu > \Delta$ as before but they are also imaginary in the parameter region $\Delta/\sqrt{2} < \delta\mu < \Delta$. Hence, the 2SC phase is unstable in a region where there are no gapless modes. Possible consequences of this interesting behavior are discussed in (Gorbar *et al.*, 2006b) and have been related to gluon condensation (Gorbar *et al.*, 2006a).

We also know of an example where gapless pairing need not be accompanied by an instability. This is a two-species system where the coupling is allowed to grow so large that the gap becomes of the order of $\bar{\mu}$ and even larger. In this case, a strong coupling regime has been identified where the gapless phase is free of the chromomagnetic instability (Kitazawa *et al.*, 2006). See (Gubankova *et al.*, 2006) for a similar analysis in a non-relativistic system. The scenario in these examples cannot arise in QCD, since long before $\bar{\mu}$ drops so low that $\Delta \gtrsim \bar{\mu}$, quark matter must be replaced by nuclear matter.

The chromomagnetic instability of the gCFL phase

only demonstrates that this phase is unstable; it does not determine the nature of the stable phase. However, the nature of the instability suggests that the stable phase should feature currents, which must be counterpropagating since in the ground state there can be no net current. Among the possible resolutions to the instability that we have enumerated in Sec. III, two stand out by this argument. In the meson supercurrent phase of Sec. III.D, that we shall discuss further in Sec. V.F, the phase of the CFL kaon condensate varies in space, yielding a current (Gerhold and Schäfer, 2006). Ungapped fermion modes carry a counter-propagating current such that the total current vanishes. In the crystalline color superconducting phases of Sec. III.C, that we shall discuss further in Sec. VI, the diquark condensate varies in space in some crystalline pattern constructed as the sum of multiple plane waves. If the total current carried by the condensate is nonzero, it is cancelled by a counter-propagating current carried by the ungapped fermion modes that are also found in the crystalline phases. It is important to note that in both these phases, the ungapped modes have different Fermi surface topologies compared to that in the gCFL phase: they are anisotropic in momentum space, with unpaired fermions accommodated in one or many “caps” rather than in spherically symmetric shells. It turns out that in both these phases, the Meissner masses are real, meaning that these phases do not suffer from a chromomagnetic instability. This was shown in the meson supercurrent phase in (Gerhold *et al.*, 2007) and in the crystalline color superconducting phase in (Ciminale *et al.*, 2006). We compare the free energies of these phases in Fig. 3. These two phases have to date been analyzed “in isolation”. It remains to be seen whether when they are analyzed in a sufficiently general framework that currents of either or both types are possible they are distinct possibilities or different limits of the same more general inhomogeneous phase.

V. EFFECTIVE THEORIES OF THE CFL PHASE

At energies below the gap the response of superconducting quark matter is carried by collective excitations of the superfluid condensate. The lightest of these excitations are Goldstone bosons associated with broken global

symmetries. Effective theories for the Goldstone modes have a number of applications. They can be used to compute low temperature thermodynamic and transport properties, and to study the response to perturbations like nonzero quark masses and lepton chemical potentials. Other light degrees of freedom appear near special points in the phase diagram. Fermion modes become light near the CFL-gCFL transition, and fluctuations of the magnitude of the gap become light near T_c .

Effective field theories can be constructed “top down”, by integrating out high energy degrees of freedom, or “bottom up”, by writing down the most general effective Lagrangian consistent with the symmetries of a given phase. In QCD at moderate or low density the microscopic theory is nonperturbative, and the top down approach is not feasible. In this case the parameters of the effective Lagrangian can be estimated using dimensional analysis or models of QCD. If the density is very large then effective theories can be derived using the top down method. However, even in this case it is often easier to follow the bottom up approach, and determine the coefficients of the effective Lagrangian using matching arguments. Matching expresses the condition that low energy Green functions in the effective and fundamental theory have to agree.

Quark matter at very high density is characterized by several energy scales. In the limit of massless quarks the most important scales are the chemical potential μ , the screening scale m_g , and the pairing gap Δ . In the weak coupling limit we have $\mu \gg m_g \gg \Delta$. This hierarchy of scales can be exploited in order to simplify calculations of the properties of low energy degrees of freedom in the color superconducting phase. For this purpose we introduce an intermediate effective theory, the high density effective theory (HDET), which describes quark and gluon degrees of freedom at energies below m_g . This theory will be described in Secs. V.A.1-V.A.3. Secs. V.B-V.E are devoted to effective theories of the CFL phase that allow us to determine the physics of the its low energy excitations. As we shall see in Secs. VII and VIII, these theories govern the phenomenology of the CFL phase even at densities not high enough for the weak coupling calculation of the gap parameter described in Sec. IV to be reliable. In V.G we briefly mention effective field theories for some other color superconducting phases.

A. High density effective theory

The formalism discussed in Sec. IV can be extended to include higher orders in the coupling constants and the effects of nonzero quark masses. It can also be used to compute more complicated observables, like the dispersion relations of collective excitations. In practice these calculations are quite difficult, because the number of possible gap structures quickly proliferate, and it is difficult to estimate the relative importance of corrections due to the truncation of the Dyson-Schwinger equations,

kinematic approximations, etc., a priori.

There are two, related, strategies for addressing these issues: effective field theories and the renormalization group. Within the effective field theory approach we try to derive an effective Lagrangian for quasi-quarks and gluons near the Fermi surface, together with a power counting scheme that can be used to determine the magnitude of diagrams constructed from the propagators and interaction terms of the theory. This is the strategy that we will describe in Secs. V.A.1-V.A.3 below.

In the renormalization group approach we consider a general effective action for quarks and gluons at high baryon density, and study the evolution of the action as high energy degrees of freedom, energetic gluons and quarks far away from the Fermi surface, are integrated out (Polchinski, 1992; Shankar, 1994). This approach was applied to QCD with short range interactions in (Evans *et al.*, 1999a,b; Schäfer and Wilczek, 1999b). In this case one can show that for typical initial conditions the color antisymmetric, flavor antisymmetric, $J = 0$, BCS interaction does indeed grow faster than all other terms, confirming in another way the arguments of Secs. I and II that these are the channels in which the dominant diquark condensation occurs. In order to use the renormalization group approach more quantitatively, one has to deal with the unscreened long range gluon exchanges, which is more difficult. Son studied the evolution of the BCS interaction using the hard dense loop gluon propagator as an input (Son, 1999). The coupled evolution of static and dynamic screening and the BCS interaction has not been solved yet. A general scheme constructing effective actions by integrating out hard modes was proposed in (Reuter *et al.*, 2004).

1. Effective Lagrangian

Consider the equation of motion of a free quark with a chemical potential μ

$$(\boldsymbol{\alpha} \cdot \mathbf{p} - \mu) \psi_{\pm} = E_{\pm} \psi_{\pm} , \quad (57)$$

where ψ_{\pm} are eigenvectors of $(\boldsymbol{\alpha} \cdot \hat{\mathbf{p}})$ with eigenvalue ± 1 and $E_{\pm} = -\mu \pm p$. If the quark momentum is near the Fermi momentum, $p \sim p_F = \mu$, then the solution ψ_+ describes a low energy excitation $E_+ \sim 0$, whereas $E_- \sim -2\mu$ corresponds to a high energy excitation. In order to construct an effective field theory based on this observation we define low and high-energy components of the quark field (Hong, 2000a,b)

$$\psi_{\pm} = e^{ip_F v_{\mu} x^{\mu}} \left(\frac{1 \pm \boldsymbol{\alpha} \cdot \hat{\mathbf{v}}_F}{2} \right) \psi , \quad (58)$$

where \mathbf{v}_F is the Fermi velocity and $v_{\mu} = (1, \mathbf{v}_F)$. The prefactor removes the rapid phase variation common to all fermions in some patch on the Fermi surface specified by $\hat{\mathbf{v}}_F$. We can insert the decomposition Eq. (58) into the QCD Lagrangian and integrate out the ψ_- field as well

as hard gluon exchanges. This generates an expansion of the QCD Lagrangian in powers of $1/p_F$. At tree level, integrating out the ψ_- fields is equivalent to solving their equation of motion

$$\psi_{-,L} = \frac{1}{2p_F} (i\alpha_{\perp} \cdot \mathbf{D} \psi_{+,L} + \gamma^0 M \psi_{+,R}) , \quad (59)$$

where $\gamma_{\parallel} \equiv \hat{\mathbf{v}}_F (\hat{\mathbf{v}}_F \cdot \boldsymbol{\gamma})$, $\gamma_{\perp} = \boldsymbol{\gamma} - \gamma_{\parallel}$ and M is the quark mass matrix. At $\mathcal{O}(1/p_F)$ the effective Lagrangian for ψ_+ is

$$\begin{aligned} \mathcal{L} = & \psi_{+,L}^{\dagger} (i v^{\mu} D_{\mu}) \psi_{+,L} - \frac{1}{2p_F} \psi_{+,L}^{\dagger} [(\mathcal{D}_{\perp})^2 + M M^{\dagger}] \psi_{+,L} \\ & + (L \leftrightarrow R, M \leftrightarrow M^{\dagger}) + \dots \end{aligned} \quad (60)$$

The low energy expansion was studied in more detail in (Schäfer, 2003a). There are a number of physical effects that have to be included in order to obtain a well-defined expansion. First, four-fermion operators have to be included. These operators naturally appear at $\mathcal{O}(1/p_F^2)$ but their effects are enhanced by the large density of states $N \sim p_F^2$ on the Fermi surface. The most important of these operators is the BCS interaction $[\psi(\mathbf{v})\psi(-\mathbf{v})][\psi^{\dagger}(\mathbf{v}')\psi^{\dagger}(-\mathbf{v}')]$. The coefficient of the BCS operator was determined in (Schäfer, 2003a).

Because of the large density of states it is also necessary to resum quark loop insertions in gluon n-point functions. There is a simple generating functional for these effects, known as the hard dense loop (HDL) effective action (Braaten and Pisarski, 1992)

$$\mathcal{L}_{\text{HDL}} = -\frac{m^2}{2} \sum_v G_{\mu\alpha}^a \frac{v^{\alpha} v^{\beta}}{(v^{\lambda} D_{\lambda})^2} G_{\mu\beta}^a. \quad (61)$$

This is a gauge invariant, but non-local, effective Lagrangian. Expanding \mathcal{L}_{HDL} in powers of the gauge field produces 2, 3, ... gluon vertices. The quadratic term describes dielectric screening of electric modes and Landau damping of magnetic modes. Higher order terms contain corrections to the gluon self interaction in a dense medium.

2. Non-Fermi liquid effects and the gap equation

In this section we shall analyze the low energy expansion in the regime $\Delta < k_0 < m_g$ (Schäfer and Schwenzer, 2006). This energy range gives the dominant contribution to the pairing gap and other low energy constants in the superconducting phase. Since electric fields are screened the interaction is dominated by the exchange of magnetic gluons. The transverse gauge boson propagator is

$$D_{ij}(K) = -\frac{i(\delta_{ij} - \hat{k}_i \hat{k}_j)}{k_0^2 - k^2 + iM_g^2 \frac{k_0}{k}}, \quad (62)$$

where $M_g^2 = (3\pi/4)m_g^2$ and we have assumed that $|k_0| < k$. We observe that the propagator becomes large in the

regime $|k_0| \sim k^3/m_g^2$. If the energy is small, $|k_0| \ll m_g$, then the typical energy is much smaller than the typical momentum,

$$k \sim (m_g^2 |k_0|)^{1/3} \gg |k_0|. \quad (63)$$

This implies that the gluon is very far off its energy shell and not a propagating state. We can compute loop diagrams containing quarks and transverse gluons by picking up the pole in the quark propagator, and then integrate over the cut in the gluon propagator using the kinematics dictated by Eq. (63). In order for a quark to absorb the large momentum carried by a gluon and stay close to the Fermi surface the gluon momentum has to be transverse to the momentum of the quark. This means that the term $k_{\perp}^2/(2\mu)$ in the quark propagator is relevant and has to be kept at leading order. Eq. (63) shows that $k_{\perp}^2/(2\mu) \gg k_0$ as $k_0 \rightarrow 0$. This means that the pole of the quark propagator is governed by the condition $k_{\parallel} \sim k_{\perp}^2/(2\mu)$. We find

$$k_{\perp} \sim g^{2/3} \mu^{2/3} k_0^{1/3}, \quad k_{\parallel} \sim g^{4/3} \mu^{1/3} k_0^{2/3}. \quad (64)$$

In this regime propagators and vertices can be simplified even further. The quark and gluon propagators are

$$S_{\alpha\beta}(K) = \frac{i\delta_{\alpha\beta}}{k_0 - k_{\parallel} - \frac{k_{\perp}^2}{2\mu} + i\epsilon \text{sgn}(k_0)}, \quad (65)$$

$$D_{ij}(K) = \frac{i\delta_{ij}}{k_{\perp}^2 - iM_g^2 \frac{k_0}{k_{\perp}}}, \quad (66)$$

and the quark gluon vertex is $g v_i (\lambda^a/2)$. Higher order corrections can be found by expanding the quark and gluon propagators as well as the HDL vertices in powers of the small parameter $\epsilon \equiv (k_0/m)$.

The regime characterized by Eq. (64) is completely perturbative, i.e. graphs with extra loops are always suppressed by extra powers of $\epsilon^{1/3}$ (Schäfer and Schwenzer, 2006). The power of ϵ can be found by using the fact that loop integrals scale as $(k_0 k_{\parallel} k_{\perp}^2) \sim k_0^{7/3}$, fermion propagators scale as $1/k_{\parallel} \sim 1/k_0^{2/3}$, gluon propagators scale as $1/k_{\perp}^2 \sim 1/k_0^{2/3}$, and the quark-gluon vertex scales as a constant. Quark matter in the regime $\Delta < k_0 < m$ is a non-Fermi liquid. The excitations are quasi-particles with the quantum numbers of quarks, but Green functions scale with fractional powers and logarithms of the energy and the coupling constant (Gerhold and Rebhan, 2005; Ipp *et al.*, 2004; Schäfer and Schwenzer, 2004b).

The corrections to Fermi liquid theory do not upset the logic that underlies the argument that leads to the BCS instability. For quark pairs with back-to-back momenta the basic one gluon exchange interaction has to be summed to all orders, but all other interactions remain perturbative (Schäfer and Schwenzer, 2006). The gap equation that sums the leading order transverse gluon

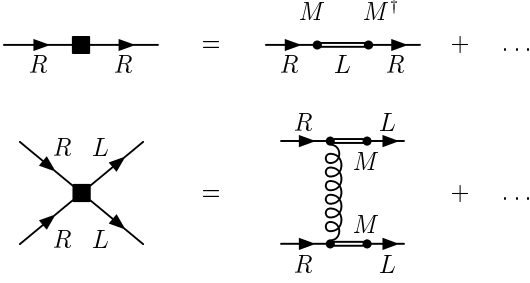


FIG. 5 Mass terms in the high density effective theory. The first diagram shows a $\mathcal{O}(MM^\dagger)$ term that arises from integrating out the ψ_- field in the QCD Lagrangian. The second diagram shows a $\mathcal{O}(M^2)$ four-fermion operator which arises from integrating out ψ_- and hard gluon exchanges.

exchange in the color-anti-symmetric channel is

$$\Delta(p_0) = -i \frac{2g^2}{3} \int \frac{dk_0}{2\pi} \int \frac{dk_\perp^2}{(2\pi)^2} \frac{k_\perp}{k_\perp^3 + iM_g^2(k_0 - p_0)} \times \int \frac{dk_\parallel}{2\pi} \frac{\Delta(k_0)}{k_0^2 + k_\parallel^2 + \Delta(k_0)^2}. \quad (67)$$

This equation is exactly equivalent to Eq. (41). In particular, all the kinematic approximations that were used to derive Eq. (41), like the low energy approximation to the HDL self energies and the forward approximation to the Dirac traces, are built into the effective field theory vertices and propagators. The effective theory can now be used to study corrections to the leading order result. Higher order corrections to the propagators and vertices of the effective theory modify the kernel of the integral equation Eq. (67). The resulting correction to the gap function can be computed perturbatively, without having to solve the integral equation again, using a method that is similar to Rayleigh-Schrödinger perturbation theory (Brown *et al.*, 2000a; Schäfer, 2003a).

The coefficients b_0 and \bar{b}_0 introduced in Sec. IV.D can be determined by matching the four-fermion operators in the effective theory (Schäfer, 2003a). The b_0 term also receives contributions from the fermion wave function renormalization $Z \sim \log(k_0)$. All other terms give corrections beyond $\mathcal{O}(g^0)$ in $\log(\Delta_0/\mu)$. Vertex corrections scale as $\Gamma \sim p_0^{1/3}$ and are suppressed compared to the fermion wave function renormalization. The analogous statement in the case of phonon-induced electronic superconductors is known as Migdal's theorem. Gluon self energy insertions beyond the k_0/k_\perp term included in the leading order propagator are also suppressed by fractional powers of the coupling and the gluon energy.

3. Mass terms

A systematic determination of mass corrections to the high density effective theory is needed for calculations of the Goldstone boson masses in the CFL phase, and in

order to understand the response of the CFL ground state to nonzero quark masses. Mass terms affect both the quark propagator and the quark-quark interaction. From Eq. (59) and (60) we see that integrating out the ψ_- field gives a correction to the energy of the ψ_+ field of the form $MM^\dagger/(2p_F)$. This term can be viewed as an effective flavor dependent chemical potential. We also note that this term is just the first in a tower of operators that arise from expanding out the energy of a free massive quark, $E = (p^2 + m^2)^{1/2}$, for momenta near the Fermi surface. Higher order terms correspond to additional corrections to the chemical potential, the Fermi velocity, and to non-linear terms in the dispersion relation.

There are no mass corrections to the quark-gluon vertex at $\mathcal{O}(1/p_F^2)$. There are, however, mass corrections to the quark-quark interaction. In connection with color superconductivity we are mainly interested in the BCS interaction. The diagram shown in Fig. 5 gives (Schäfer, 2002b)

$$\mathcal{L} = \frac{g^2}{32p_F^4} \left(\psi_{i,L}^{a\dagger} C \psi_{j,L}^{b\dagger} \right) \left(\psi_{k,R}^c C \psi_{l,R}^d \right) \times [(\lambda)^{ac} (\lambda)^{bd} (M)_{ik} (M)_{jl}] + (L \leftrightarrow R, M \leftrightarrow M^\dagger). \quad (68)$$

This is the leading interaction that couples the gap equations for left and right handed fermions. We shall also see that the mass correction to the BCS interaction gives the leading contribution to the mass shift in the condensation energy, and the masses of the Goldstone bosons.

B. Ginzburg-Landau theory

At zero temperature fluctuations of the superconducting state are dominated by fluctuations of the phase of the order parameter. Near the critical temperature the gap becomes small and fluctuations of the magnitude of the gap are important, too. This regime can be described using the Ginzburg-Landau theory. Ginzburg and Landau argued that in the vicinity of a second order phase transition the thermodynamic potential of the system can be expanded in powers of the order parameter and its derivatives. This method was used very successfully in the study of superfluid phases of ^3He .

The Ginzburg-Landau approach was first applied to color superconductivity in (Bailin and Love, 1979). The problem was revisited by (Iida and Baym, 2001), who included the effects of unscreened gluon exchanges and charge neutrality. Consider the s -wave color anti-triplet condensate in QCD with three massless flavors. The order parameter can be written as

$$\langle \psi_i^\alpha C \gamma_5 \psi_j^\beta \rangle = \epsilon^{\alpha\beta A} \epsilon_{ijB} \phi_A^B \quad (69)$$

where ϕ_A^B is a matrix in color-flavor space. Note that here we have included the energy gap into ϕ_A^B , in contrast to Eq. (24), where ϕ_A^B is dimensionless. We have fixed the orientations of left and right-handed condensates. Fluctuations in the relative color-flavor orientation of the left-

and right-handed fermions correspond to the Goldstone modes related to chiral symmetry breaking, and will be considered in Sec. V.C. Therefore, the ansatz (69) implies the assumption that chiral fluctuations near T_c are small compared to non-chiral gap fluctuations and fluctuations of the gauge field. The thermodynamic potential can be expanded as

$$\Omega = \Omega_0 + \alpha \text{Tr}(\phi^\dagger \phi) + \beta_1 [\text{Tr}(\phi^\dagger \phi)]^2 + \beta_2 \text{Tr}([\phi^\dagger \phi]^2) + \kappa \text{Tr}(\nabla \phi \nabla \phi^\dagger) + \dots \quad (70)$$

The coefficients α, β_i, κ can be treated as unknown parameters, or determined in QCD at weak coupling. The weak coupling QCD result is (Iida and Baym, 2001)

$$\alpha = 4N \frac{T - T_c}{T}, \quad \beta_1 = \beta_2 = \frac{7\zeta(3)}{8(\pi T_c)^2} N, \quad (71)$$

$$\kappa = \frac{7\zeta(3)}{8\pi^2 T_c^2} N \quad (72)$$

where $N = \mu^2/(2\pi^2)$ is the density of states on the Fermi surface. This result agrees with the BCS result. Using Eq. (71) we can verify that the ground state is in the CFL phase $\phi_A^B \sim \delta_A^B$. We can also study many other issues, like the gluon screening lengths, the structure of vortices, the effects of electric and color neutrality, and the effects of nonzero quark masses (Iida and Baym, 2002; Iida *et al.*, 2004, 2005).

From the study of electronic superconductors, it is known that the nature of the finite temperature phase transition depends on the ratio $\kappa = \lambda/\xi$ of the screening length λ and the correlation length ξ . If $\kappa > 1/\sqrt{2}$ the superconductor is type II, fluctuations of the order parameter are more important than fluctuations of the gauge field, and the transition is second order. In a type I superconductor the situation is reversed, and fluctuations of the gauge field drive the transition first order (Halperin *et al.*, 1974).

In the weak coupling limit, $\xi \sim 1/\Delta \gg \lambda \sim 1/(g\mu)$ and color superconductivity is strongly type I. The role of gauge field fluctuations was studied in (Bailin and Love, 1984; Giannakis *et al.*, 2004; Giannakis and Ren, 2003; Matsuura *et al.*, 2004; Noronha *et al.*, 2006). The contribution to the thermodynamic potential is

$$\Omega_{fl} = 8T \int \frac{d^3k}{(2\pi)^3} \left\{ \log \left(1 + \frac{m_A^2(k)}{k^2} \right) - \frac{m_A^2(k)}{k^2} \right\}, \quad (73)$$

where $m_A(k)$ is the gauge field screening mass. In QCD the momentum dependence of m_A cannot be neglected. A careful analysis of the thermodynamic potential shows that the transition is indeed first order. The first order transition occurs at a critical temperature T_c^* (Giannakis *et al.*, 2004)

$$\frac{T_c^* - T_c}{T_c} = \frac{\pi^2}{12\sqrt{2}} g, \quad (74)$$

where T_c is the critical temperature of the second order transition obtained upon neglecting gluon fluctuations as in Sec. IV.E. Although the result (74) cannot be trusted quantitatively at accessible densities, say $\mu \sim 400$ MeV where $g \sim 3.6$, it does make it clear that the phase transition between the CFL (or 2SC) phase and the quark-gluon plasma will be strongly first order and will occur at a critical temperature that is significantly elevated relative to the BCS estimate $T_c = 0.57\Delta$. The effects of gluon fluctuations are much more important here than those of photon fluctuations in a conventional Type I superconductor.

C. Goldstone bosons in the CFL phase

1. Effective Lagrangian

In the CFL phase the pattern of chiral symmetry breaking is identical to the one at $T = \mu = 0$. This implies that the effective Lagrangian has the same structure as chiral perturbation theory. The main difference is that Lorentz-invariance is broken and only rotational invariance is a good symmetry. The effective Lagrangian for the Goldstone modes is given by (Casalbuoni and Gatto, 1999)

$$\begin{aligned} \mathcal{L}_{\text{eff}} = & \frac{f_\pi^2}{4} \text{Tr} [\partial_0 \Sigma \partial_0 \Sigma^\dagger - v_\pi^2 \partial_i \Sigma \partial_i \Sigma^\dagger] \\ & + [B \text{Tr}(M \Sigma^\dagger) + h.c.] \\ & + [A_1 \text{Tr}(M \Sigma^\dagger) \text{Tr}(M \Sigma^\dagger) + A_2 \text{Tr}(M \Sigma^\dagger M \Sigma^\dagger) \\ & + A_3 \text{Tr}(M \Sigma^\dagger) \text{Tr}(M^\dagger \Sigma) + h.c.] + \dots \end{aligned} \quad (75)$$

Here $\Sigma = \exp(i\phi^a \lambda^a / f_\pi)$ is the chiral field, f_π is the pion decay constant and M is a complex mass matrix. The fields ϕ^a describe the octet of Goldstone bosons ($\pi^\pm, \pi^0, K^\pm, K^0, \bar{K}^0, \eta$). These Goldstone bosons are an octet under the unbroken $SU(3)_{c+L+R}$ symmetry of the CFL phase and their \tilde{Q} -charges under the unbroken gauge symmetry of the CFL phase are ± 1 and 0 as indicated by the superscripts, meaning that they have the same \tilde{Q} -charges as the Q -charges of the vacuum pseudoscalar mesons. The chiral field and the mass matrix transform as $\Sigma \rightarrow L \Sigma R^\dagger$ and $M \rightarrow L M R^\dagger$ under chiral transformations $(L, R) \in SU(3)_L \times SU(3)_R$. For the present, we have suppressed the singlet fields associated with the breaking of the exact $U(1)_B$ and approximate $U(1)_A$ symmetries. We will give the effective Lagrangian for the massless Goldstone boson associated with superfluidity (i.e. from $U(1)_B$ breaking) below.

The form of the effective Lagrangian follows from the symmetries of the CFL phase. It is nevertheless useful to understand how this Lagrangian arises upon integrating out high energy degrees of freedom. We start from the high density effective Lagrangian in the presence of a

CFL gap term

$$\begin{aligned} \mathcal{L} = & \text{Tr} \left[\psi_L^\dagger (i v^\mu D_\mu) \psi_L \right] \\ & + \frac{\Delta}{2} \left\{ \text{Tr} (X^\dagger \psi_L X^\dagger \psi_L) - [\text{Tr} (X^\dagger \psi_L)]^2 + h.c. \right\} \\ & + (L \leftrightarrow R, X \leftrightarrow Y). \end{aligned} \quad (76)$$

Here, $\psi_{L,R}$ are left and right-handed quark fields which transform as $\psi_L \rightarrow L \psi_L U^T$ and $\psi_R \rightarrow R \psi_R U^T$ under chiral transformations $(L, R) \in SU(3)_L \times SU(3)_R$ and color transformations $U \in SU(3)_c$. We have suppressed the spinor indices and defined $\psi\psi = \psi^\alpha C^{\alpha\beta} \psi^\beta$, where C is the charge conjugation matrix. The traces run over color or flavor indices and X, Y are fields that transform as $X \rightarrow LXU^T$ and $Y \rightarrow RYU^T$. We will assume that the vacuum expectation value is $\langle X \rangle = \langle Y \rangle = 1$. This corresponds to the CFL gap term $\Delta \psi_i^\alpha \psi_j^\beta \epsilon_{\alpha\beta A} \epsilon^{ijA}$. X, Y parametrize fluctuations around the CFL ground state. Note that fluctuations of the type $X = Y$ correspond to the field ϕ introduced in the previous section.

For simplicity we have assumed that the gap term is completely anti-symmetric in flavor. We will derive the effective Lagrangian in the chiral limit $M = M^\dagger = 0$ and study mass terms later. We can redefine the fermion fields according to

$$\chi_L \equiv \psi_L X^\dagger, \quad \chi_R \equiv \psi_R Y^\dagger. \quad (77)$$

In terms of the new fields the Lagrangian takes the form

$$\begin{aligned} \mathcal{L} = & \text{Tr} \left[\chi_L^\dagger (i v^\mu \partial_\mu) \chi_L \right] \\ & - i \text{Tr} \left[\chi_L^\dagger \chi_L X v^\mu (\partial_\mu - i A_\mu^T) X^\dagger \right] \\ & + \frac{\Delta}{2} \left\{ \text{Tr} (\chi_L \chi_L) - [\text{Tr} (\chi_L)]^2 \right\} \\ & + (L \leftrightarrow R, X \leftrightarrow Y). \end{aligned} \quad (78)$$

At energies below the gap we can integrate out the fermions. The fermion determinant generates a kinetic term for the chiral fields X and Y (Casalbuoni and Gatto, 1999)

$$\mathcal{L} = -\frac{f_\pi^2}{2} \text{Tr} \left[(X^\dagger D_0 X)^2 - v_\pi^2 (X^\dagger D_i X)^2 \right] + (X \leftrightarrow Y) \quad (79)$$

For simplicity we have ignored the flavor singlet components of X and Y .

The low energy constants f_π and v_π were calculated by matching the effective theory to weak coupling QCD calculations in (Son and Stephanov, 2000a,b), see also (Beane *et al.*, 2000; Bedaque and Schäfer, 2002; Rho *et al.*, 2000; Zarembo, 2000). The results are

$$f_\pi^2 = \frac{21 - 8 \log 2}{18} \frac{\mu^2}{2\pi^2}, \quad v_\pi^2 = \frac{1}{3}. \quad (80)$$

The simplest way to derive these results, given the results that we have already reviewed in Sec. IV.F, is to

recall that the gluon field acquires a magnetic mass due to the Higgs mechanism and an electric mass due to Debye screening, and then to notice that Eq. (79) shows that the electric mass is $m_D^2 = g^2 f_\pi^2$, while the magnetic mass is $m_M^2 = v_\pi^2 m_D^2$. This means that f_π and v_π are determined by the Debye and Meissner masses for the gluons in the CFL phase that we have presented in Sec. IV.F, see Eq. (52) and Table II.

Since the gluon is heavy, it can also be integrated out. Using Eq. (79) we get

$$A_\mu^T = \frac{i}{2} (X^\dagger \partial_\mu X + Y^\dagger \partial_\mu Y) + \dots \quad (81)$$

This result can be substituted back into the effective Lagrangian. The result is

$$\mathcal{L}_{\text{eff}} = \frac{f_\pi^2}{4} \text{Tr} \left[\partial_0 \Sigma \partial_0 \Sigma^\dagger - v_\pi^2 \partial_i \Sigma \partial_i \Sigma^\dagger \right], \quad (82)$$

where the Goldstone boson field is given by $\Sigma = XY^\dagger$. This shows that the light degrees of freedom correspond to fluctuations of the color-flavor orientation of the left-handed CFL condensate relative to the right-handed one, as expected since these are the fluctuations associated with the spontaneously broken global symmetry.

Finally, we quickly summarize the effective theory for the $U(1)_B$ Goldstone mode. At order $\mathcal{O}((\partial\varphi)^2)$ we get (Son and Stephanov, 2000a,b)

$$\mathcal{L} = \frac{f^2}{2} [(\partial_0 \varphi)^2 - v^2 (\nabla \varphi)^2] + \dots, \quad (83)$$

where the low energy constants f and v are given by

$$f^2 = \frac{6\mu^2}{\pi^2}, \quad v^2 = \frac{1}{3}. \quad (84)$$

The field φ transforms as $\varphi \rightarrow \varphi + \alpha$ under $U(1)_B$ transformation of the quark fields $\psi \rightarrow \exp(i\alpha)\psi$. Because $U(1)_B$ is an Abelian symmetry the two-derivative terms do not contain any Goldstone boson self interactions. These terms are needed in order to compute transport properties of the CFL phase. Son noticed that self-interactions are constrained by Lorentz invariance (of the microscopic theory) and $U(1)_B$ invariance (Son, 2002). The analogous argument for non-relativistic superfluids is described in (Greiter *et al.*, 1989). To leading order in g the effective theory of the $U(1)_B$ Goldstone boson can be written as

$$\mathcal{L} = \frac{3}{4\pi^2} [(\partial_0 \varphi - \mu)^2 - (\nabla \varphi)^2]^2 + \dots, \quad (85)$$

where the omitted terms are of the form $\partial^i \varphi^k$ with $i > k$. Expanding Eq. (85) to second order in derivatives reproduces Eq. (83). In addition to that, Eq. (85) contains the leading three and four boson interactions.

Using microscopic models one can obtain more detailed information on the properties of collective modes. A calculation of the spectral properties of the φ mode in an NJL model at $T = 0$ and $T \neq 0$ can be found in (Fukushima and Iida, 2005).

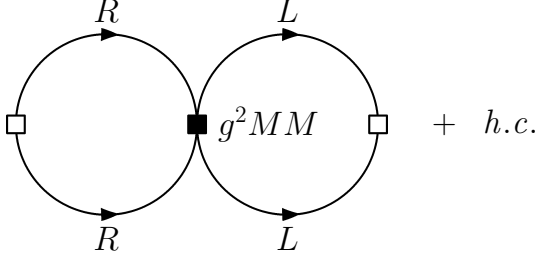


FIG. 6 Contribution of the $\mathcal{O}(M^2)$ BCS four-fermion operator to the condensation energy in the CFL phase. The open squares correspond to insertions of the anomalous self energy Δ .

2. Mass terms

The structure of the mass terms in Eq. (75) is completely determined by chiral symmetry. The coefficients B, A_i can be determined by repeating the steps discussed in the previous section, but keeping the mass terms in the high density effective theory. In practice it is somewhat easier to compute the coefficients of the chiral Lagrangian using matching arguments. For example, we noticed that the easiest way to determine f_π is to compute the gluon screening mass in the microscopic theory.

In Sec. V.A.3 we showed that $X_L \equiv MM^\dagger/(2p_F)$ and $X_R \equiv M^\dagger M/(2p_F)$ act as effective chemical potentials for left and right-handed fermions, respectively. Formally, the effective Lagrangian has an $SU(3)_L \times SU(3)_R$ gauge symmetry under which $X_{L,R}$ transform as the temporal components of non-Abelian gauge fields. We can implement this approximate gauge symmetry in the CFL chiral theory by promoting time derivatives to covariant derivatives (Bedaque and Schäfer, 2002),

$$\partial_0 \Sigma \rightarrow \nabla_0 \Sigma \equiv \partial_0 \Sigma + i \left(\frac{MM^\dagger}{2p_F} \right) \Sigma - i \Sigma \left(\frac{M^\dagger M}{2p_F} \right). \quad (86)$$

The mass dependent terms in the quark-quark interaction contribute to the gap and to the condensation energy. In the chiral theory the shift in the condensation energy due to the quark masses is

$$\mathcal{E} = -B \text{Tr}(M) - A_1 [\text{Tr}(M)]^2 - A_2 \text{Tr}(M^2) - A_3 \text{Tr}(M) \text{Tr}(M^\dagger) + h.c. + \dots \quad (87)$$

The contribution to the condensation energy from the mass correction to the BCS interaction is shown in Fig. 6. The diagram is proportional to the square of the condensate

$$\langle \psi_{i,L}^\alpha C \psi_{j,L}^\beta \rangle = \epsilon^{\alpha\beta A} \epsilon_{ijA} \Delta \frac{3\sqrt{2}\pi}{g} \left(\frac{\mu^2}{2\pi^2} \right), \quad (88)$$

with the dependence on the mass matrix M arising from the contraction of the BCS interaction with the CFL con-

densate. We get

$$\begin{aligned} & \epsilon^{\alpha\beta A} \epsilon_{ijA} (T^a)^{\alpha\gamma} (T^a)^{\beta\delta} (M)_{ik} (M)_{jl} \epsilon^{\gamma\delta B} \epsilon_{klB} \\ & = -\frac{4}{3} \left\{ (\text{Tr}[M])^2 - \text{Tr}[M^2] \right\}, \end{aligned} \quad (89)$$

where $T^a = \lambda^a/2$. We note that the four-fermion operator is proportional to g^2 and the explicit dependence of the diagram on g cancels. We find (Schäfer, 2002b; Son and Stephanov, 2000a,b)

$$\mathcal{E} = -\frac{3\Delta^2}{4\pi^2} \left\{ (\text{Tr}[M])^2 - \text{Tr}[M^2] \right\} + (M \leftrightarrow M^\dagger). \quad (90)$$

This result can be matched against Eq. (87). We find $B = 0$ and

$$A_1 = -A_2 = \frac{3\Delta^2}{4\pi^2} \equiv A, \quad A_3 = 0. \quad (91)$$

The result $A_1 = -A_2$ reflects the fact that the CFL order parameter is anti-symmetric in flavor (pure $\bar{\mathbf{3}}$) to leading order in g . Using Eqs. (86) and (91) we can compute the energies of the flavored Goldstone bosons

$$\begin{aligned} E_{\pi^\pm} &= \mu_{\pi^\pm} + \left[v_\pi^2 p^2 + \frac{4A}{f_\pi^2} (m_u + m_d) m_s \right]^{1/2}, \\ E_{K^\pm} &= \mu_{K^\pm} + \left[v_\pi^2 p^2 + \frac{4A}{f_\pi^2} m_d (m_u + m_s) \right]^{1/2}, \\ E_{K^0, \bar{K}^0} &= \mu_{K^0, \bar{K}^0} + \left[v_\pi^2 p^2 + \frac{4A}{f_\pi^2} m_u (m_d + m_s) \right]^{1/2}, \end{aligned} \quad (92)$$

where

$$\begin{aligned} \mu_{\pi^\pm} &= \mp \frac{m_d^2 - m_u^2}{2\mu}, & \mu_{K^\pm} &= \mp \frac{m_s^2 - m_u^2}{2\mu}, \\ \mu_{K^0, \bar{K}^0} &= \mp \frac{m_s^2 - m_d^2}{2\mu}. \end{aligned} \quad (93)$$

The mass matrix for the remaining neutral Goldstone bosons, which mix, can be found in (Beane *et al.*, 2000; Son and Stephanov, 2000a,b). We observe that the $\mathcal{O}(m)$ terms lead to an inverted mass spectrum with the kaons being lighter than the pions. This can be understood from the microscopic derivation of the chiral Lagrangian. The Goldstone boson field is $\Sigma = XY^\dagger$, and a mode with the quantum number of the pion is given by $\pi^+ \sim \epsilon^{abc} \epsilon^{ade} (d_R^b \bar{s}_R^c) (u_L^d s_L^e)$. The structure of the field operators suggests that the mass is controlled by $(m_u + m_d) m_s$. By the same argument the mass of the K^+ is governed by $(m_u + m_s) m_d$, and $m_K < m_\pi$. We also note that the $\mathcal{O}(m^2)$ terms split the energies of different charge states. This can be understood from the fact that these terms act as an effective chemical potential for flavor. Explicit calculations in an NJL model reproduce f_π in (80) and the results (92), albeit with a different value of A (Kleinhaus *et al.*, 2007; Ruggieri, 2007). This serves as a reminder that in the CFL phase at moderate densities,

the effective theory is valid but the values of coefficients in it may not take on the values obtained by matching to high density calculations.

In perturbation theory the coefficient B of the $\text{Tr}(M\Sigma)$ term is zero. B receives non-perturbative contributions from instantons. Instantons are semi-classical gauge configurations in the Euclidean time functional integral that induce a fermion vertex of the form ('t Hooft, 1976)

$$\mathcal{L} \sim G \det_f(\bar{\psi}_L \psi_R) + h.c., \quad (94)$$

where \det_f denotes a determinant in flavor space. The 't Hooft vertex (94) can be written as the product of the CFL condensate and its conjugate times $\langle \bar{\psi}\psi \rangle$, meaning that in the CFL phase Eq. (94) induces a nonzero quark condensate $\langle \bar{\psi}\psi \rangle$, as well as Goldstone boson masses $m_{GB}^2 \sim m \langle \bar{\psi}\psi \rangle / f_\pi^2$. The instanton has gauge field $A_\mu \sim 1/g$, so its action is $S = 8\pi^2/g^2$. The effective coupling G is proportional to $\exp(-S) \sim \exp(-8\pi^2/g^2)$, where g is the running coupling constant at a scale set by the instanton size ρ .

In dense quark matter perturbative gauge field screening suppresses instantons of size $\rho > 1/\mu$, and the effective coupling G can be computed reliably (Schäfer, 2002a). Combined with the weak coupling result for $\langle \bar{\psi}\psi \rangle$, see Eq. (88), we get

$$B = c \left[\frac{3\sqrt{2}\pi}{g} \Delta \left(\frac{\mu^2}{2\pi^2} \right) \right]^2 \left(\frac{8\pi^2}{g^2} \right)^6 \frac{\Lambda_{QCD}^9}{\mu^{12}}, \quad (95)$$

where $c = 0.155$ and Λ_{QCD} is the QCD scale factor. In terms of B , $\langle \bar{\psi}\psi \rangle = -2B$ and the instanton contribution to the K^0 mass is $\delta m_{K^0}^2 = B(m_d + m_s)/(2f_\pi^2)$ (Manuel and Tytgat, 2000). In the weak coupling limit, $\mu \gg \Lambda_{QCD}$, the instanton contribution is very small. However, because of the strong dependence on Λ_{QCD} the numerical value of B is quite uncertain. Using phenomenological constraints on the instanton size distribution (Schäfer, 2002a) concluded that the instanton contribution to the kaon mass at $\mu = 500$ MeV is of order 10 MeV.

Finally, we summarize the structure of the chiral expansion in the CFL phase. Ignoring non-perturbative effects the effective Lagrangian has the form

$$\mathcal{L} \sim f_\pi^2 \Delta^2 \left(\frac{\partial_0 \Sigma}{\Delta} \right)^k \left(\frac{\vec{\partial} \Sigma}{\Delta} \right)^l \left(\frac{MM^\dagger}{\mu \Delta} \right)^m \left(\frac{MM}{\mu^2} \right)^n. \quad (96)$$

Higher order vertices are suppressed by $\partial\Sigma/\Delta$ whereas Goldstone boson loops are suppressed by powers of $\partial\Sigma/(4\pi f_\pi)$. Since the pion decay constant scales as $f_\pi \sim \mu$ the effects of Goldstone boson loops can be neglected relative to higher order contact interactions. This is different from chiral perturbation theory at zero baryon density. We also note that the quark mass expansion contains two parameters, m^2/μ^2 and $m^2/(\mu\Delta)$. Since $\Delta \ll \mu$ the chiral expansion breaks down if $m^2 \sim \mu\Delta$.

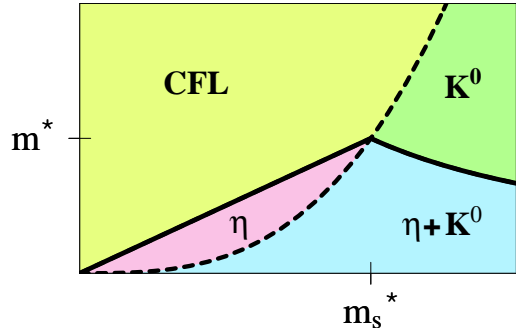


FIG. 7 (Color online) Phase structure of CFL matter as a function of the light quark mass m and the strange quark mass m_s , from (Kryjevski *et al.*, 2005). CFL denotes pure CFL matter, while K^0 and η denote CFL phases with K^0 and/or η condensation. Solid lines are first order transitions, dashed lines are second order. Instanton effects have been neglected.

This is the same scale at which BCS calculations find a transition from the CFL phase to a less symmetric state. We also note that the result for the Goldstone boson energies given in Eq. (92) contains terms of $\mathcal{O}(m^2/\mu^2)$ and $\mathcal{O}([m^2/(\mu\Delta)]^2)$, but neglects corrections of $\mathcal{O}([m^2/\mu^2]^2)$.

The effective Lagrangians (75) and (83) describe the physics of the low momentum pseudo-Goldstone and Goldstone bosons of the CFL phase at any density. We have described the weak coupling computation of the coefficients f_π , v_π , A_1 , A_2 , A_3 , B , f and v as well as the μ_{eff} 's in (93). With the exception of B , all these results are expressed simply in terms of Δ , μ and the quark masses, with g not appearing anywhere. This suggests that the range of validity of these results, when viewed as a function of Δ , is bigger than the range of validity of the weak coupling calculations on which they are based. As we decrease the density down from the very large densities at which the weak coupling calculation of Δ is under control, there is no indication that the relations between the effective theory coefficients and Δ and μ that we have derived in this section break down. The only sense in which we lose control of our understanding of the CFL phase is that we must treat Δ as a parameter, in terms of which all the other effective theory coefficients are known. Since B introduces $U(1)_A$ -breaking physics that is not present at weak coupling and that does not enter the effective theory through any other coupling, it is not well constrained.

D. Kaon condensation

If the effective chemical potential in Eq. (93) becomes larger than the corresponding mass term in Eq. (92), then the energy of a Goldstone boson can become negative. In the physically relevant case $m_s \gg m_u \sim m_d$ this applies in particular to the K^0 and the K^+ . When the Goldstone boson energy becomes negative the CFL ground

state is reorganized and a Goldstone boson condensate is formed. The physical reason is that a nonzero m_s disfavors strange quarks relative to non-strange quarks. In normal quark matter the system responds to this stress by turning s quarks into (mostly) d quarks. In CFL matter this is difficult, since all quarks are gapped. Instead, the system can respond by populating mesons that contain d quarks and s holes.

The ground state can be determined from the effective potential

$$V_{\text{eff}} = \frac{f_\pi^2}{4} \text{Tr} [2X_L \Sigma X_R \Sigma^\dagger - X_L^2 - X_R^2] \quad (97)$$

$$- A_1 \left\{ [\text{Tr}(M \Sigma^\dagger)]^2 - \text{Tr} [(M \Sigma^\dagger)^2] \right\},$$

where $X_L = MM^\dagger/(2p_F)$, $X_R = M^\dagger M/(2p_F)$ and $M = \text{diag}(m_u, m_d, m_s) = \text{diag}(m, m, m_s)$. Here we only discuss the $T = 0$ case. For nonzero temperature effects, in particular the calculation of the critical temperature of kaon condensation, see (Alford *et al.*, 2007b). The first term on the right-hand side of Eq. (97) contains the effective chemical potential

$$\mu_s \equiv -\mu_{K^0} \simeq \frac{m_s^2}{2p_F} \quad (98)$$

and favors states with a deficit of strange quarks. The second term favors the neutral ground state $\Sigma = 1$. The lightest excitation with positive strangeness is the K^0 meson. We consider the ansatz $\Sigma = \exp(i\alpha\lambda_4)$ which allows the order parameter to rotate in the K^0 direction. The vacuum energy is

$$V(\alpha) = f_\pi^2 \left[-\frac{1}{2} \left(\frac{m_s^2 - m^2}{2p_F} \right)^2 \sin^2 \alpha \quad (99)$$

$$+ m_{K^0}^2 (1 - \cos \alpha) \right],$$

where $m_{K^0}^2 = (4A_1/f_\pi^2)m_u(m_d + m_s) + B(m_d + m_s)/(2f_\pi^2)$. Minimizing the vacuum energy we obtain

$$\cos(\alpha) = \begin{cases} 1 & \mu_s < m_{K^0} \\ \frac{m_{K^0}^2}{\mu_s^2} & \mu_s > m_{K^0} \end{cases} \quad (100)$$

We conclude that there is a second order phase transition to a kaon condensed state at $\mu_s = m_{K^0}$. The strange quark mass breaks the $SU(3)$ flavor symmetry to $SU(2)_I \times U(1)_Y$. In the kaon condensed phase this symmetry is spontaneously broken to $U(1)_{\bar{Q}}$. If $m_u = m_d$, isospin is an exact symmetry and there are two exact Goldstone modes (Miransky and Shovkovy, 2002; Schäfer *et al.*, 2001) with zero energy gap, the K^0 and the K^+ . Isospin breaking leads to a small energy gap for the K^+ .

Using the perturbative result for A_1 , and neglecting instanton effects by setting $B = 0$, we can get an estimate of the critical strange quark mass. The critical strange

quark mass scales as $m_u^{1/3} \Delta^{2/3}$. Taking $\mu = 500$ MeV, $\Delta = 50$ MeV, $m_u = 4$ MeV and $m_d = 7$ MeV, we find $m_s^{\text{crit}} \simeq 68$ MeV, a result that corresponds to $m_{K^0}^{\text{crit}} = 5$ MeV. If instanton contributions increase m_{K^0} by 10 MeV, this would increase m_s^{crit} to 103 MeV, corresponding to the onset of kaon condensation depicted in Fig. 3.

The difference in condensation energy between the CFL phase and the kaon condensed state is not necessarily small. In the limit $\mu_s \rightarrow \Delta$ we have $\sin \alpha \sim 1$ and $V(\alpha) \sim f_\pi^2 \Delta^2/2$. Since f_π^2 is of order $\mu^2/(2\pi^2)$ this is an $\mathcal{O}(1)$ correction to the pairing energy in the CFL phase. Microscopic NJL model calculations of the condensation energy in the kaon condensed phase can be found in (Buballa, 2005b; Forbes, 2005; Kleinhaus *et al.*, 2007; Ruggieri, 2007; Warringa, 2006), see also (Ebert and Klimenko, 2007; Ebert *et al.*, 2007).

The CFL phase also contains a very light flavor neutral mode which can potentially become unstable. This mode is a linear combination of the η and η' and its mass is proportional to $m_u m_d$. Because this mode has zero strangeness it is not affected by the μ_s term in the effective potential. However, since $m_u, m_d \ll m_s$ this state is sensitive to perturbative $\alpha_s m_s^2$ corrections (Kryjevski *et al.*, 2005). The resulting phase diagram is shown in Fig. 7. The precise value of the tetra-critical point (m^*, m_s^*) depends sensitively on the value of the coupling constant. At very high density m^* is extremely small, but at moderate density m^* can become as large as 5 MeV, comparable to the physical values of the up and down quark mass.

E. Fermions in the CFL phase

A single quark excitation with energy close to Δ is long-lived and interacts only weakly with the Goldstone modes in the CFL phase. This means that it is possible to include quarks in the chiral Lagrangian. This Lagrangian not only controls the interaction of quarks with pions and kaons, but it also constrains the dependence of the gap in the fermionic quasiparticle spectrum on the quark masses. This is of interest in connection with the existence and stability of the gapless CFL phase (Alford *et al.*, 2004b), as we have discussed in Secs. I.E, II.B, and III.B.

The effective Lagrangian for fermions in the CFL phase is (Kryjevski and Schäfer, 2005; Kryjevski and Yamada, 2005)

$$\mathcal{L} = \text{Tr} (N^\dagger i v^\mu D_\mu N) - D \text{Tr} (N^\dagger v^\mu \gamma_5 \{ \mathcal{A}_\mu, N \}) \quad (101)$$

$$- F \text{Tr} (N^\dagger v^\mu \gamma_5 [\mathcal{A}_\mu, N]) + \frac{\Delta}{2} \left[(\text{Tr} (N_L N_L) - [\text{Tr} (N_L)]^2) \right.$$

$$\left. - (L \leftrightarrow R) + h.c. \right].$$

$N_{L,R}$ are left and right handed baryon fields in the adjoint

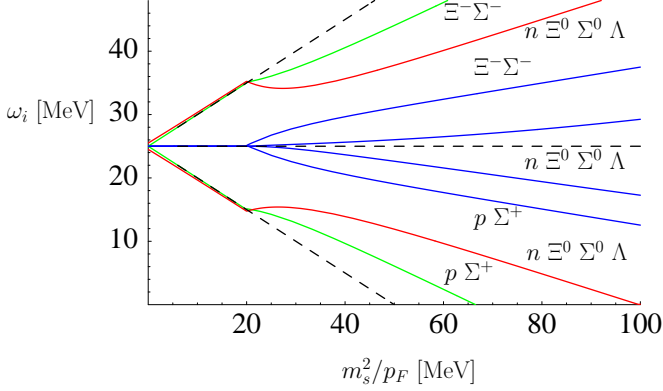


FIG. 8 (Color online) This figure shows the fermion spectrum in the CFL phase. For $m_s = 0$ there are eight fermions with gap Δ (set to 25 MeV as in Fig. 3) and one fermion with gap 2Δ (not shown). As discussed in Sec. III, the octet quasi-particles have the $SU(3)$ and $U(1)_{\tilde{Q}}$ quantum numbers of the octet baryons. Without kaon condensation gapless fermion modes appear at $\mu_s = \Delta$ (dashed lines). With kaon condensation gapless modes appear at $\mu_s = 4\Delta/3$. (Note that the scale on the horizontal axis is $2\mu_s$.)

representation of flavor $SU(3)$. The baryon fields originate from quark-hadron complementarity (Alford *et al.*, 1999a; Schäfer and Wilczek, 1999a). We can think of N as describing a quark which is surrounded by a diquark cloud, $N_L \sim q_L \langle q_L q_L \rangle$. The covariant derivative of the nucleon field is given by $D_\mu N = \partial_\mu N + i[\mathcal{V}_\mu, N]$. The vector and axial-vector currents are

$$\mathcal{V}_\mu = -\frac{i}{2} (\xi \partial_\mu \xi^\dagger + \xi^\dagger \partial_\mu \xi), \quad \mathcal{A}_\mu = -\frac{i}{2} \xi (\nabla_\mu \Sigma^\dagger) \xi, \quad (102)$$

where ξ is defined by $\xi^2 = \Sigma$. It follows that ξ transforms as $\xi \rightarrow L\xi U^\dagger = U\xi R^\dagger$ with $U \in SU(3)_V$. The fermion field transforms as $N \rightarrow UNU^\dagger$. For pure $SU(3)$ flavor transformations $L = R = V$ we have $U = V$. F and D are low energy constants that determine the baryon axial coupling. In QCD at weak coupling, we find $D = F = 1/2$ (Kryjevski and Schäfer, 2005).

The effective theory given in Eq. (101) can be derived from QCD in the weak coupling limit. However, the structure of the theory is completely determined by chiral symmetry, even if the coupling is not weak. In particular, there are no free parameters in the baryon coupling to the vector current. Mass terms are also strongly constrained by chiral symmetry. The effective chemical potentials (X_L, X_R) appear as left and right-handed gauge potentials in the covariant derivative of the nucleon field. We have

$$D_0 N = \partial_0 N + i[\Gamma_0, N], \quad (103)$$

$$\Gamma_0 = -\frac{i}{2} [\xi (\partial_0 + iX_R) \xi^\dagger + \xi^\dagger (\partial_0 + iX_L) \xi],$$

where $X_L = MM^\dagger/(2p_F)$ and $X_R = M^\dagger M/(2p_F)$ as before. (X_L, X_R) covariant derivatives also appears in the axial vector current given in Eq. (102).

We can now study how the fermion spectrum depends on the quark mass. In the CFL state we have $\xi = 1$. For $\mu_s = 0$ the baryon octet has an energy gap Δ and the singlet has gap 2Δ . The leading correction to this result comes from the commutator term in Eq. (103). We find that the gap of the proton and neutron is lowered, $\Delta_{p,n} = \Delta - \mu_s$, while the gap of the cascade particles Ξ^-, Ξ^0 is increased, $\Delta_\Xi = \Delta + \mu_s$. As a consequence we find gapless (p, n) excitations at $\mu_s = \Delta$. This result agrees with the spectrum discussed in Sec. III.B if the identification $p \equiv (bu)$ and $n \equiv (bd)$ is made.

The situation is more complicated when kaon condensation is taken into account. In the kaon condensed phase there is mixing in the ($p, \Sigma^+, \Sigma^-, \Xi^-$) and ($n, \Sigma^0, \Xi^0, \Lambda^8, \Lambda^0$) sector. For $m_{K^0} \ll \mu_s \ll \Delta$ the spectrum is given by

$$\omega_{p\Sigma^\pm \Xi^-} = \begin{cases} \Delta \pm \frac{3}{4}\mu_s, \\ \Delta \pm \frac{1}{4}\mu_s, \end{cases} \quad \omega_{n\Sigma^0 \Xi^0 \Lambda} = \begin{cases} \Delta \pm \frac{1}{2}\mu_s, \\ \Delta, \\ 2\Delta. \end{cases} \quad (104)$$

Numerical results for the eigenvalues are shown in Fig. 8. We observe that mixing within the charged and neutral baryon sectors leads to level repulsion. There are two modes that become light in the CFL window $\mu_s \leq 2\Delta$. One mode is a charged mode which is a linear combination of the proton and the Σ^+ , while the other mode is a linear combination of the neutral baryons ($n, \Sigma^0, \Xi^0, \Lambda^8, \Lambda^0$). The charged mode becomes gapless first, at $\mu_s = 4\Delta/3$. Corrections to this result were studied in the NJL model calculation of (Forbes, 2005), which includes various subleading condensates and obtains $\mu_s = 1.22\Delta$ at $\mu = 500$ MeV. The neutral mode becomes gapless only at $\mu_s = 2\Delta$. The most important difference as compared to the spectrum in the gapless CFL phase without kaon condensation is that for $\mu_s < 2\Delta$ only the charged mode is gapless.

F. Goldstone boson currents

In Sec. IV.G we showed that gapless fermion modes lead to instabilities of the superfluid phase. Here we will discuss how these instabilities arise, and how they can be resolved, in the context of low energy theories of the CFL state, by the formation of the meson supercurrent state introduced in Sec. III.D. The chromomagnetic instability is an instability towards the spontaneous generation of currents, that is to say the spontaneous generation of spatial variation in the phase of the diquark condensate. Consider a spatially varying $U(1)_Y$ rotation of the neutral kaon condensate

$$\xi(\mathbf{x}) = U(\mathbf{x}) \xi_K U^\dagger(\mathbf{x}), \quad (105)$$

where $\xi_K = \exp(i\pi\lambda_4)$ and $U(\mathbf{x}) = \exp(i\phi_K(\mathbf{x})\lambda_8)$. This state is characterized by nonzero vector and axial-vector currents, see Eq. (102). We shall study the dependence

of the vacuum energy on the kaon current $\mathbf{J}_K = \nabla\phi_K$. The gradient term in the meson part of the effective Lagrangian gives a positive contribution

$$\mathcal{E}_m = \frac{1}{2}v_\pi^2 f_\pi^2 \mathbf{J}_K^2. \quad (106)$$

A negative contribution can arise from gapless fermions. In order to determine this contribution we have to calculate the fermion spectrum in the presence of a nonzero current. The relevant couplings are obtained from the covariant derivative of the fermion field in Eq. (103) and the D and F-terms in Eq. (101). The fermion spectrum is quite complicated. The dispersion relation of the lowest mode is approximately given by

$$\omega_l = \Delta + \frac{(l - l_0)^2}{2\Delta} - \frac{3}{4}\mu_s - \frac{1}{4}\mathbf{v} \cdot \mathbf{J}_K, \quad (107)$$

where $l = \mathbf{v} \cdot \mathbf{p} - p_F$ and we have expanded ω_l near its minimum $l_0 = (\mu_s + \mathbf{v} \cdot \mathbf{J}_K)/4$. Eq. (107) shows that there is a gapless mode if $\mu_s > 4\Delta/3 - \mathbf{J}_K/3$. The contribution of the gapless mode to the vacuum energy is

$$\mathcal{E}_q = \frac{\mu^2}{\pi^2} \int dl \int \frac{d\Omega}{4\pi} \omega_l \theta(-\omega_l), \quad (108)$$

where $d\Omega$ is an integral over the Fermi surface. The energy functional $\mathcal{E}_m + \mathcal{E}_q$ was analyzed in (Kryjevski, 2005; Schäfer, 2006). There is an instability near the point $\mu_s = 4\Delta/3$. The instability is resolved by the formation of a Goldstone boson current. If electric charge neutrality is enforced the magnitude of the current is very small, and there is no tendency towards the generation of multiple currents. It was also shown that all gluonic screening masses are real (Gerhold *et al.*, 2007). The situation is more complicated if the neutral fermion mode becomes gapless, too. In this case the magnitude of the current is not small, and multiple currents may appear. This regime corresponds to the portion of the curCFL- K^0 curve in Fig. 3 that is only slightly (invisibly) below the gCFL curve.

G. Other effective theories

Effective Lagrangians have also been constructed for color superconducting phases other than the CFL phase. The effective theory for the light singlet axial mode in the 2SC phase can be found in (Beane *et al.*, 2000). The phonon effective theory in the crystalline color superconducting phase is discussed in Sec. VI.C.

It is also interesting to study effective theories in QCD-like theories at large density. Some of these theories do not have a sign problem and can be studied on the lattice with algorithms that are available today. Of particular interest are QCD with $N_c = 2$ colors (Alles *et al.*, 2006; Fukushima and Iida, 2007; Hands *et al.*, 2006, 1999; Kogut *et al.*, 2001, 1999, 2000, 2002; Nishida *et al.*, 2004) and QCD at finite isospin density (Kogut and Sinclair, 2002; Son and Stephanov, 2001; Splittorff *et al.*, 2001).

VI. NJL MODEL COMPARISONS AMONG CANDIDATE PHASES BELOW CFL DENSITIES

As we have explained in Sec. II, at sufficiently high densities, where the up, down and strange quarks can be treated on an equal footing and the disruptive effects of the strange quark mass can be neglected, quark matter is in the CFL phase. At asymptotic densities, the CFL gap parameter Δ_{CFL} and indeed any property of CFL quark matter can be calculated in full QCD, as described in Sec. IV. At any density at which the CFL phase arises, its low energy excitations, and hence its properties and phenomenology, can be described by the effective field theory of Sec. V, whose form is known and whose parameters can be systematically related to the CFL gap Δ_{CFL} . If we knew that the only form of color superconducting quark matter that arises in the QCD phase diagram were CFL, there would therefore be no need to resort to model analyses. However, as we have discussed in Sec. III, $M_s^2/(\mu\Delta_{\text{CFL}})$ may not be small enough (at $\mu = \mu_{\text{nuc}}$ where the nuclear \rightarrow quark matter transition occurs) for the QCD phase diagram to be this simple.

Even at the very center of a neutron star, μ cannot be larger than about 500 MeV, meaning that the (density dependent) strange quark mass M_s cannot be neglected. In concert with the requirement that bulk matter must be neutral and must be in weak equilibrium, a nonzero M_s favors separation of the Fermi momenta of the three different flavors of quarks, and thus disfavors the cross-species BCS pairing that characterizes the CFL phase. If CFL pairing is disrupted by the heaviness of the strange quark at a higher μ than that at which color superconducting quark matter is superseded by baryonic matter, the CFL phase must be replaced by some phase of quark matter in which there is less, and less symmetric, pairing.

Within a spatially homogeneous ansatz, the next phase down in density is the gapless CFL (gCFL) phase described in Sec. III.B. However, as we have described in Sec. IV.G, such gapless paired states suffer from a chromomagnetic instability: they can lower their energy by the formation of counter-propagating currents. It seems likely, therefore, that a ground state with counter-propagating currents is required. This could take the form of a crystalline color superconductor, that we have introduced in Sec. III.C. Or, given that the CFL phase itself is likely augmented by kaon condensation as described in Secs. II.C and V.D, it could take the form of the phase we have described in Sec. V.F in which a CFL kaon condensate carries a current in one direction balanced by a counter-propagating current in the opposite direction carried by gapless quark quasiparticles.

Determining which phase or phases of quark matter occupy the regime of density between hadronic matter and CFL quark matter in the QCD phase diagram, if there is such a regime, remains an outstanding challenge. Barring a major breakthrough that would allow lattice QCD calculations to be brought to bear despite the fermion sign problem, a from-first-principles determination seems out

of reach. This leaves two possible paths forward. First, as we describe in this section, we can analyze and compare many of the possible phases within a simplified few parameter model, in so doing seeking qualitative insight into what phase(s) are favorable. Second, as we shall describe in Sec. VIII, we can determine the observable consequences of the presence of various possible color superconducting phases in neutron stars, and then seek to use observational data to rule possibilities out or in.

A. Model, pairing ansatz, and homogeneous phases

We shall employ a Nambu–Jona-Lasinio (NJL) model in which the QCD interaction between quarks is replaced by a point-like four-quark interaction, with the quantum numbers of single-gluon exchange, analyzed in mean field theory. This is not a controlled approximation. However, it suffices for our purposes: because this model has attraction in the same channels as in QCD, its high density phase is the CFL phase; and, the Fermi surface splitting effects whose qualitative consequences we wish to study can be built into the model. Note that we shall assume throughout that $\Delta_{\text{CFL}} \ll \mu$. This weak coupling assumption means that the pairing is dominated by modes near the Fermi surfaces. Quantitatively, this means that results for the gaps and condensation energies of candidate phases are independent of the cutoff in the NJL model when expressed in terms of the CFL gap Δ_{CFL} : if the cutoff is changed with the NJL coupling constant adjusted so that Δ_{CFL} stays fixed, the gaps and condensation energies for the candidate crystalline phases also stay fixed. This makes the NJL model valuable for making the comparisons that are our goal. The NJL model has two parameters: the CFL gap Δ_{CFL} which parametrizes the strength of the interaction and $M_s^2/(4\mu)$, the splitting between Fermi surfaces in neutral quark matter in the absence of pairing. The free energy of candidate patterns of pairing can be evaluated and compared as a function of these two parameters.

As a rather general pairing ansatz, we shall consider

$$\begin{aligned} \langle ud \rangle &\sim \Delta_3 \sum_a \exp(2i\mathbf{q}_3^a \cdot \mathbf{r}) \\ \langle us \rangle &\sim \Delta_2 \sum_a \exp(2i\mathbf{q}_2^a \cdot \mathbf{r}) \\ \langle ds \rangle &\sim \Delta_1 \sum_a \exp(2i\mathbf{q}_1^a \cdot \mathbf{r}) . \end{aligned} \quad (109)$$

If we set all the wave vectors \mathbf{q}_I^a to zero, we can use this ansatz to compare spatially homogeneous phases including the CFL phase ($\Delta_1 = \Delta_2 = \Delta_3 \equiv \Delta_{\text{CFL}}$), the gCFL phase ($\Delta_3 > \Delta_2 > \Delta_1 > 0$) and the 2SC phase ($\Delta_3 \equiv \Delta_{2\text{SC}}; \Delta_1 = \Delta_2 = 0$). Choosing different sets of wave vectors will allow us to analyze and compare different crystalline color superconducting phases of quark matter.

NJL models of varying degrees of complexity have been used for a variety of purposes beyond the scope

of this review. For example, whereas we treat Δ_{CFL} and quark masses as parameters and use the NJL model to compare different patterns of pairing at fixed values of these parameters and μ , it is possible instead to fix the NJL coupling or couplings and then self-consistently solve for the gap parameters and the $\langle \bar{s}s \rangle$ condensate as functions of μ (Abuki *et al.*, 2005; Abuki and Kunihiro, 2006; Blaschke *et al.*, 2005; Buballa and Oertel, 2002; Ippolito *et al.*, 2007; Mishra and Mishra, 2004, 2006; Ruster *et al.*, 2005; Steiner *et al.*, 2002; Warringa, 2006). Doing so reintroduces sensitivity to the cutoff in the NJL model and so does not actually reduce the number of parameters. Also, these models tend to find rather larger values of M_s than in analyses that go beyond NJL models, for example the analysis using Dyson-Schwinger equations in (Nickel *et al.*, 2006a). There have also been many investigations of the phase diagram in the μ - T plane in NJL models (either with Δ_{CFL} and M_s as parameters or solved for self-consistently) (Abuki and Kunihiro, 2006; Barducci *et al.*, 2004; Berges and Rajagopal, 1999; Fukushima *et al.*, 2005; He *et al.*, 2007; Iida *et al.*, 2005; Kashiwa *et al.*, 2007; Mishra and Mishra, 2005; Ruster *et al.*, 2004, 2005, 2006; Schwarz *et al.*, 1999; Warringa *et al.*, 2005). Although many of their features are sensitive to the cutoff as well as the chosen couplings, these NJL phase diagrams indicate how rich the QCD phase diagram may turn out to be, as different condensates vanish at different temperatures. One result that has been obtained using the Ginzburg-Landau approximation as well as in NJL models and so is of more general validity is that upon heating the CFL phase at nonzero but small M_s^2/μ , as T increases Δ_2 vanishes first, then Δ_1 , and then Δ_3 (Fukushima *et al.*, 2005; Iida *et al.*, 2004; Ruster *et al.*, 2004). However, it remains to be seen how this conclusion is modified by the effects of gauge-field fluctuations, which for $M_s = 0$ turn the mean-field Ginzburg-Landau second order transition into a strong first order phase transition at a significantly elevated temperature, see Sec. V.B and Eq. (74).

We shall analyze quark matter containing massless u and d quarks and s quarks with an effective mass M_s . The Lagrangian density describing this system in the absence of interactions is given by

$$\mathcal{L}_0 = \bar{\psi}_{i\alpha} \left(i \not{\partial} \delta^{\alpha\beta} \delta_{ij} - M_{ij}^{\alpha\beta} + \mu_{ij}^{\alpha\beta} \gamma_0 \right) \psi_{\beta j} , \quad (110)$$

where $i, j = 1, 2, 3$ are flavor indices and $\alpha, \beta = 1, 2, 3$ are color indices and we have suppressed the Dirac indices, where $M_{ij}^{\alpha\beta} = \delta^{\alpha\beta} \text{diag}(0, 0, M_s)_{ij}$ is the mass matrix, and where the quark chemical potential matrix is given by

$$\mu_{ij}^{\alpha\beta} = (\mu \delta_{ij} - \mu_e Q_{ij}) \delta^{\alpha\beta} + \delta_{ij} \left(\mu_3 T_3^{\alpha\beta} + \frac{2}{\sqrt{3}} \mu_8 T_8^{\alpha\beta} \right) , \quad (111)$$

with $Q_{ij} = \text{diag}(2/3, -1/3, -1/3)_{ij}$ the quark electric-charge matrix and T_3 and T_8 the diagonal color gen-

erators. In QCD, μ_e , μ_3 and μ_8 are the zeroth components of electromagnetic and color gauge fields, and the gauge field dynamics ensure that they take on values such that the matter is neutral (Alford and Rajagopal, 2002; Gerhold and Rebhan, 2003), satisfying the neutrality conditions (3). In the NJL model, quarks interact via four-fermion interactions and there are no gauge fields, so we introduce μ_e , μ_3 and μ_8 by hand, and choose them to satisfy the neutrality constraints (3). The assumption of weak equilibrium is built into the calculation via the fact that the only flavor-dependent chemical potential is μ_e , ensuring for example that the chemical potentials of d and s quarks with the same color must be equal. Because the strange quarks have greater mass, the equality of their chemical potentials implies that the s quarks have smaller Fermi momenta than the d quarks in the absence of BCS pairing. In the absence of pairing, then, because weak equilibrium drives the massive strange quarks to be less numerous than the down quarks, electrical neutrality requires a $\mu_e > 0$, which makes the up quarks less numerous than the down quarks and introduces some electrons into the system. In the absence of pairing, color neutrality is obtained with $\mu_3 = \mu_8 = 0$.

The Fermi momenta of the quarks and electrons in quark matter that is electrically and color neutral and in weak equilibrium are given in the absence of pairing by

$$\begin{aligned} p_F^d &= \mu + \frac{\mu_e}{3} \\ p_F^u &= \mu - \frac{2\mu_e}{3} \\ p_F^s &= \sqrt{\left(\mu + \frac{\mu_e}{3}\right)^2 - M_s^2} \approx \mu + \frac{\mu_e}{3} - \frac{M_s^2}{2\mu} \\ p_F^e &= \mu_e, \end{aligned} \quad (112)$$

where we have simplified p_F^s by working to linear order in μ_e and M_s^2 . To this order, electric neutrality requires $\mu_e = M_s^2/(4\mu)$, yielding

$$\begin{aligned} p_F^d &= \mu + \frac{M_s^2}{12\mu} = p_F^u + \frac{M_s^2}{4\mu} \\ p_F^u &= \mu - \frac{M_s^2}{6\mu} \\ p_F^s &= \mu - \frac{5M_s^2}{12\mu} = p_F^u - \frac{M_s^2}{4\mu} \\ p_F^e &= \frac{M_s^2}{4\mu}, \end{aligned} \quad (113)$$

as illustrated in Fig. 2. We see from (112) that to leading order in M_s^2 and μ_e , the effect of the strange quark mass on unpaired quark matter is as if instead one reduced the strange quark chemical potential by $M_s^2/(2\mu)$. We shall make this approximation throughout. Upon making this assumption, we need no longer be careful about the distinction between p_F 's and μ 's, as we can simply think of the three flavors of quarks as if they have chemical

potentials

$$\begin{aligned} \mu_d &= \mu_u + 2\delta\mu_3 \\ \mu_u &= p_F^u \\ \mu_s &= \mu_u - 2\delta\mu_2 \end{aligned} \quad (114)$$

with

$$\delta\mu_3 = \delta\mu_2 = \frac{M_s^2}{8\mu} \equiv \delta\mu, \quad (115)$$

where the choice of subscripts indicates that $2\delta\mu_2$ is the splitting between the Fermi surfaces for quarks 1 and 3 and $2\delta\mu_3$ is that between the Fermi surfaces for quarks 1 and 2, identifying u, d, s with 1, 2, 3.

As described in (Alford *et al.*, 2004b; Alford and Rajagopal, 2002; Rajagopal and Wilczek, 2001; Steiner *et al.*, 2002), BCS pairing introduces qualitative changes into the analysis of neutrality. For example, in the CFL phase $\mu_e = 0$ and μ_8 is nonzero and of order M_s^2/μ . This arises because wherever BCS pairing occurs between fermions whose Fermi surface would be split in the absence of pairing, the Fermi momenta of these fermions are locked together. This maximizes the pairing energy gain while at the same time exacting a kinetic energy price and changing the relation between the chemical potentials and the particle numbers. This means that the μ 's required for neutrality can change qualitatively as happens in the CFL example.

The NJL interaction term with the quantum numbers of single-gluon exchange that we add to the Lagrangian (110) is

$$\mathcal{L}_{\text{interaction}} = -\frac{3}{8}\lambda(\bar{\psi}\Gamma^{A\nu}\psi)(\bar{\psi}\Gamma_{A\nu}\psi), \quad (116)$$

where we have suppressed the color and flavor indices that we showed explicitly in (110), and have continued to suppress the Dirac indices. The full expression for $\Gamma^{A\nu}$ is $(\Gamma^{A\nu})_{\alpha i, \beta j} = \gamma^\nu (T^A)_{\alpha\beta} \delta_{ij}$. The NJL coupling constant λ has dimension -2, meaning that an ultraviolet cutoff Λ must be introduced as a second parameter in order to fully specify the interaction. We shall define Λ as restricting the momentum integrals to a shell around the Fermi surface, $\mu - \Lambda < |\mathbf{p}| < \mu + \Lambda$.

In the mean-field approximation, the interaction Lagrangian (116) takes on the form

$$\mathcal{L}_{\text{interaction}} = \frac{1}{2}\bar{\psi}\Delta(x)\bar{\psi}^T + \frac{1}{2}\psi^T\bar{\Delta}(x)\psi, \quad (117)$$

where $\Delta(x)$ is related to the diquark condensate by the relations

$$\begin{aligned} \Delta(x) &= \frac{3}{4}\lambda\Gamma^{A\nu}\langle\psi\psi^T\rangle(\Gamma_{A\nu})^T \\ \bar{\Delta}(x) &= \frac{3}{4}\lambda(\Gamma^{A\nu})^T\langle\bar{\psi}^T\bar{\psi}\rangle\Gamma_{A\nu} \\ &= \gamma^0\Delta^\dagger(x)\gamma^0. \end{aligned} \quad (118)$$

The ansatz (109) can now be made precise: we take

$$\Delta(x) = \Delta_{CF}(x) \otimes C\gamma^5, \quad (119)$$

with the color-flavor part

$$\Delta_{CF}(x)_{\alpha i, \beta j} = \sum_{I=1}^3 \sum_{\mathbf{q}_I^a} \Delta(\mathbf{q}_I^a) e^{2i\mathbf{q}_I^a \cdot \mathbf{r}} \epsilon_{I\alpha\beta} \epsilon_{Iij}. \quad (120)$$

We have introduced notation that allows for the possibility of gap parameters $\Delta(\mathbf{q}_I^a)$ with different magnitudes for different I and for different a . In fact, we shall only consider circumstances in which $\Delta(\mathbf{q}_I^a) = \Delta_I$, as in (109).

The full Lagrangian, given by the sum of (110) and (117), is then quadratic and can be written very simply upon introducing the two component Nambu-Gorkov spinors (12) in terms of which

$$\mathcal{L} = \frac{1}{2} \bar{\Psi} \begin{pmatrix} i\bar{\not{\partial}} + \not{\mu} & \Delta(x) \\ \bar{\Delta}(x) & (i\bar{\not{\partial}} - \not{\mu})^T \end{pmatrix} \Psi. \quad (121)$$

Here, $\not{\mu} \equiv \mu\gamma_0$ and μ is the matrix (111).

The propagator corresponding to the Lagrangian (121) is given by

$$\begin{aligned} \langle \Psi(x) \bar{\Psi}(x') \rangle &= \begin{pmatrix} \langle \psi(x) \bar{\psi}(x') \rangle & \langle \psi(x) \psi^T(x') \rangle \\ \langle \bar{\psi}^T(x) \bar{\psi}(x') \rangle & \langle \bar{\psi}^T(x) \psi^T(x') \rangle \end{pmatrix} \\ &= \begin{pmatrix} iG(x, x') & iF(x, x') \\ i\bar{F}(x, x') & i\bar{G}(x, x') \end{pmatrix}, \end{aligned} \quad (122)$$

where G and \bar{G} are the ‘‘normal’’ components of the propagator and F and \bar{F} are the ‘‘anomalous’’ components. They satisfy the coupled differential equations

$$\begin{aligned} \begin{pmatrix} i\bar{\not{\partial}} + \not{\mu} & \Delta(x) \\ \bar{\Delta}(x) & (i\bar{\not{\partial}} - \not{\mu})^T \end{pmatrix} \begin{pmatrix} G(x, x') & F(x, x') \\ \bar{F}(x, x') & \bar{G}(x, x') \end{pmatrix} \\ = \begin{pmatrix} 1 & 0 \\ 0 & 1 \end{pmatrix} \delta^{(4)}(x - x'). \end{aligned} \quad (123)$$

We can now rewrite (118) as

$$\begin{aligned} \Delta(x) &= \frac{3i}{4} \lambda \Gamma^{A\nu} F(x, x) (\Gamma_{A\nu})^T \\ \bar{\Delta}(x) &= \frac{3i}{4} \lambda (\Gamma^{A\nu})^T \bar{F}(x, x) \Gamma_{A\nu}, \end{aligned} \quad (124)$$

either one of which is the self-consistency equation, or gap equation, that we must solve.

Without further approximation, (124) is not tractable. It yields an infinite set of coupled gap equations, one for each $\Delta(\mathbf{q}_I^a)$, because without further approximation it is not consistent to choose finite sets $\{\mathbf{q}_I\}$. When several plane waves are present in the condensate, they induce an infinite tower of higher momentum condensates (Bowers and Rajagopal, 2002). In the next subsection, we shall make a Ginzburg-Landau (i.e. small- Δ) approximation which eliminates these higher harmonics.

Of course, an even more dramatic simplification is obtained if we set all the wave vectors \mathbf{q}_I^a to zero. Still, even in this case obtaining the general solution with $M_s \neq 0$ and $\Delta_1 \neq \Delta_2 \neq \Delta_3$ is somewhat involved (Alford *et al.*, 2004b, 2005c; Fukushima *et al.*, 2005). We shall not present the resulting analysis of the CFL \rightarrow gCFL transition and the gCFL phase here. The free energies of these phases are depicted in Fig. 3, and their gap parameters are depicted below in Fig. 10.

If we simplify even further, by setting $M_s = 0$ and $\Delta_1 = \Delta_2 = \Delta_3 \equiv \Delta_{\text{CFL}}$, the gap equation determining the CFL gap parameter Δ_{CFL} can then be evaluated analytically, yielding (Bowers and Rajagopal, 2002)

$$\Delta_{\text{CFL}} = 2^{\frac{2}{3}} \Lambda \exp \left[-\frac{\pi^2}{2\mu^2 \lambda} \right]. \quad (125)$$

We shall see below that in the limit in which $\Delta \ll \Delta_{\text{CFL}}$, $\delta\mu \ll \mu$, all results for the myriad possible crystalline phases can be expressed in terms of Δ_{CFL} ; neither λ nor Λ shall appear. This reflects the fact that in this limit the physics of interest is dominated by quarks near the Fermi surfaces, not near Λ , and so once Δ_{CFL} is used as the parameter describing the strength of the attraction between quarks, Λ is no longer visible; the cutoff Λ only appears in the relation between Δ_{CFL} and λ , not in any comparison among different possible paired phases. We are using the NJL model in a specific, limited, fashion in which it serves as a two parameter model allowing the comparison among different possible paired phases at a given Δ_{CFL} and M_s . NJL models have also been employed to estimate the value of Δ_{CFL} at a given μ (Alford *et al.*, 1998, 1999b; Berges and Rajagopal, 1999; Carter and Diakonov, 1999; Rajagopal and Wilczek, 2000; Rapp *et al.*, 1998); doing so requires normalizing the four-fermion interaction by calculating some zero density quantity like the vacuum chiral condensate, and in so doing introduces a dependence on the cutoff Λ . Such mean-field NJL analyses are important complements to extrapolation down from an analysis that is rigorous at high density and hence weak coupling, described in Sec. IV, and give us confidence that we understand the magnitude of $\Delta_{\text{CFL}} \sim 10 - 100$ MeV. This estimate receives further support from the lattice-NJL calculation of (Hands and Walters, 2004) which finds diquark condensation and a ~ 60 MeV gap in an NJL model whose parameters are normalized via calculation of f_π , m_π and a constituent quark mass in vacuum. With these as inputs, Δ is then calculated on the lattice, i.e. without making a mean-field approximation. With an understanding of its magnitude in hand, we shall treat Δ_{CFL} as a parameter, thus making our results insensitive to Λ .

We shall focus below on the use of the NJL model that we have introduced to analyze and compare different possible crystalline phases, comparing their free energies to that of the CFL phase as a benchmark. The free energy of the 2SC phase is easily calculable in the same model, and the free energies of the unstable gapless CFL and

gapless 2SC phases can also be obtained (Alford *et al.*, 2005c). These free energies are all shown in Fig. 3. The free energies of phases with various patterns of single-flavor pairing have also been calculated in the same model (Alford *et al.*, 2003). The NJL model is not a natural starting point for an analysis of the kaon condensate in the CFL- K^0 phase, but with considerable effort this has been accomplished in (Buballa, 2005b; Forbes, 2005; Kleinhaus *et al.*, 2007; Warringa, 2006). The curCFL- K^0 phase of Secs. III.D and V.F, in which the K^0 -condensate carries a current, has not been analyzed in an NJL model. But, because both the CFL- K^0 and curCFL- K^0 phases are continuously connected to the CFL phase, they can both be analyzed in a model-independent fashion using the effective field theory described in Sec. V. The CFL- K^0 and curCFL- K^0 curves in Fig. 3 were obtained as described in Sec. V. It remains a challenge for future work to do a calculation in which both curCFL- K^0 and crystalline phases are possible, allowing a direct comparison of their free energies within a single calculation and a study of whether they are distinct as current results seem to suggest or are instead different limits of some more general inhomogeneous color superconducting phase.

B. Crystalline phases

Crystalline color superconductivity (Alford *et al.*, 2001a; Bowers *et al.*, 2001; Bowers and Rajagopal, 2002; Casalbuoni *et al.*, 2006, 2002a, 2005a, 2001a, 2002c; Casalbuoni and Nardulli, 2004; Casalbuoni *et al.*, 2003, 2004; Ciminale *et al.*, 2006; Giannakis *et al.*, 2002; Kundu and Rajagopal, 2002; Leibovich *et al.*, 2001; Mannarelli *et al.*, 2006b) naturally permits pairing between quarks living at split Fermi surfaces by allowing Cooper pairs with nonzero net momentum. In three-flavor quark matter, this allows pairing to occur even with the Fermi surfaces split in the free-energetically optimal way as in the absence of pairing, meaning that neutral crystalline phases are obtained in three-flavor quark matter with the chemical potential matrix (111) simplified to $\mu = \delta^{\alpha\beta} \otimes \text{diag}(\mu_u, \mu_d, \mu_s)$ with the flavor chemical potentials given simply by (114) (Casalbuoni *et al.*, 2005a; Mannarelli *et al.*, 2006b; Rajagopal and Sharma, 2006b), up to higher order corrections that have been investigated in (Casalbuoni *et al.*, 2006). This is the origin of the advantage that crystalline color superconducting phases have over the CFL and gCFL phases at large values of the splitting $\delta\mu$. For example, by allowing u quarks with momentum $\mathbf{p} + \mathbf{q}_3$ to pair with d quarks with momentum $-\mathbf{p} + \mathbf{q}_3$, for any \mathbf{p} , we can pair u and d quarks along rings on their respective Fermi surfaces. In coordinate space, this corresponds to a condensate of the form $\langle ud \rangle \sim \Delta_3 \exp(2i\mathbf{q}_3 \cdot \mathbf{r})$. The net free energy gained due to pairing is then a balance between increasing $|\mathbf{q}_3|$ yielding pairing on larger rings while exacting a greater kinetic energy cost. The optimum choice turns out to be $|\mathbf{q}_3| = \eta\delta\mu_3$ with $\eta = 1.1997$, corresponding

to pairing rings on the Fermi surfaces with opening angle 67.1° (Alford *et al.*, 2001a). Pairing with only a single \mathbf{q}_3 is disadvantaged because the only quarks on each Fermi surface that can then pair are those lying on a single ring. This disadvantage can be overcome in two ways. First, increasing Δ widens the pairing rings on the Fermi surfaces into pairing bands which fill in, forming pairing caps, at large enough Δ (Mannarelli *et al.*, 2006b). Second, it is possible to cover larger areas of the Fermi surfaces by allowing Cooper pairs with the same $|\mathbf{q}_3|$ but various $\hat{\mathbf{q}}_3$, yielding $\langle ud \rangle \sim \Delta_3 \sum_{\mathbf{q}_3^a} \exp(2i\mathbf{q}_3^a \cdot \mathbf{r})$ with the \mathbf{q}_3^a chosen from some specified set $\{\mathbf{q}_3^1, \mathbf{q}_3^2, \mathbf{q}_3^3, \dots\} \equiv \{\mathbf{q}_3\}$. This is a condensate modulated in position space in some crystalline pattern, with the crystal structure defined by $\{\mathbf{q}_3\}$. In this two-flavor context, a Ginzburg-Landau analysis reveals that the best $\{\mathbf{q}_3\}$ contains eight vectors pointing at the corners of a cube, say in the $(\pm 1, \pm 1, \pm 1)$ directions in momentum space, yielding a face-centered cubic structure in position space (Bowers and Rajagopal, 2002).

This subsection describes the analysis of three-flavor crystalline phases in (Rajagopal and Sharma, 2006a). We use the ansatz given by (119) and (120) for the three-flavor crystalline color superconducting condensate. This is antisymmetric in color (α, β) , spin, and flavor (i, j) indices and is a generalization of the CFL condensate to crystalline color superconductivity. We set $\Delta_1 = 0$, neglecting $\langle ds \rangle$ pairing because the d and s Fermi surfaces are twice as far apart from each other as each is from the intervening u Fermi surface. Hence, I can be taken to run over 2 and 3 only. $\{\mathbf{q}_2\}$ and $\{\mathbf{q}_3\}$ define the crystal structures of the $\langle us \rangle$ and $\langle ud \rangle$ condensates respectively. We only consider crystal structures in which all the vectors in $\{\mathbf{q}_2\}$ are equivalent to each other in the sense that any one can be transformed into any other by a symmetry operation of $\{\mathbf{q}_2\}$ and same for $\{\mathbf{q}_3\}$. This justifies our simplifying assumption that the $\langle us \rangle$ and $\langle ud \rangle$ condensates are each specified by a single gap parameter (Δ_2 and Δ_3 respectively), avoiding having to introduce one gap parameter per \mathbf{q} . We furthermore only consider crystal structures which are exchange symmetric, meaning that $\{\mathbf{q}_2\}$ and $\{\mathbf{q}_3\}$ can be exchanged by some combination of rigid rotations and reflections applied simultaneously to all the vectors in both sets. This simplification, together with $\delta\mu_2 = \delta\mu_3$ (an approximation corrected only at order M_s^4/μ^3), guarantees that we find solutions with $\Delta_2 = \Delta_3$.

We analyze and compare candidate crystal structures by evaluating the free energy $\Omega(\Delta_2, \Delta_3)$ for each crystal structure in a Ginzburg-Landau expansion in powers of the Δ 's. This approximation is controlled if $\Delta_2, \Delta_3 \ll \Delta_{\text{CFL}}, \delta\mu$, with Δ_{CFL} the gap parameter in the CFL phase at $M_s^2/\mu = 0$. The terms in the Ginzburg-Landau expansion must respect the global $U(1)$ symmetry for each flavor, meaning that each Δ_I can only appear in the combination $|\Delta_I|^2$. (The $U(1)$ symmetries are spontaneously broken by the condensate, but not explicitly broken.) Therefore, $\Omega(\Delta_2, \Delta_3)$ is given to sextic

order by

$$\begin{aligned} \Omega(\Delta_2, \Delta_3) = & \frac{2\mu^2}{\pi^2} \left[P_2 \alpha_2 |\Delta_2|^2 + P_3 \alpha_3 |\Delta_3|^2 \right. \\ & + \frac{1}{2} \left(\beta_2 |\Delta_2|^4 + \beta_3 |\Delta_3|^4 + \beta_{32} |\Delta_2|^2 |\Delta_3|^2 \right) \\ & + \frac{1}{3} \left(\gamma_2 |\Delta_2|^6 + \gamma_3 |\Delta_3|^6 \right. \\ & \left. \left. + \gamma_{322} |\Delta_3|^2 |\Delta_2|^4 + \gamma_{233} |\Delta_3|^4 |\Delta_2|^2 \right) \right] \quad (126) \end{aligned}$$

where we have chosen notation consistent with that used in the two flavor study of (Bowers and Rajagopal, 2002), which arises as a special case of (126) if we take Δ_2 or Δ_3 to be zero. P_I is the number of vectors in the set $\{\mathbf{q}_I\}$. The form of the Ginzburg-Landau expansion (126) is model-independent, whereas the expressions for the coefficients α_I , β_I , β_{IJ} , γ_I , and γ_{IJJ} for a specific crystal structure are model-dependent. We calculate them in the NJL model described in Sec. VI.A. For exchange symmetric crystal structures, $\alpha_2 = \alpha_3 \equiv \alpha$, $\beta_2 = \beta_3 \equiv \beta$, $\gamma_2 = \gamma_3 \equiv \gamma$ and $\gamma_{233} = \gamma_{322}$.

Because setting one of the Δ_I to zero reduces the problem to one with two-flavor pairing only, we can obtain α , β and γ via applying the two-flavor analysis described in (Bowers and Rajagopal, 2002) to either $\{\mathbf{q}_2\}$ or $\{\mathbf{q}_3\}$ separately. Using α as an example, we learn that

$$\begin{aligned} \alpha_I = \alpha(q_I, \delta\mu_I) = & -1 + \frac{\delta\mu_I}{2q_I} \log \left(\frac{q_I + \delta\mu_I}{q_I - \delta\mu_I} \right) \\ & - \frac{1}{2} \log \left(\frac{\Delta_{2\text{SC}}^2}{4(q_I^2 - \delta\mu_I^2)} \right). \quad (127) \end{aligned}$$

Here, $q_I \equiv |\mathbf{q}_I|$ and $\Delta_{2\text{SC}}$ is the gap parameter for the 2SC (2-flavor, 2-color) BCS pairing obtained with $\delta\mu_I = 0$ and Δ_I nonzero with the other two gap parameters set to zero. Assuming that $\Delta_{\text{CFL}} \ll \mu$, the 2SC gap parameter is given by $\Delta_{2\text{SC}} = 2^{\frac{1}{3}} \Delta_{\text{CFL}}$ (Schäfer, 2000a), see Sec. IV. In the Ginzburg-Landau approximation, in which the Δ_I are assumed small, we must first minimize the quadratic contribution to the free energy, and only then investigate the quartic and sextic contributions. Minimizing α_I fixes the length of all the vectors in the set $\{\mathbf{q}_I\}$, and eliminates the possibility of waves at higher harmonics, yielding $q_I = \eta \delta\mu_I$ with $\eta = 1.1997$ the solution to $\frac{1}{2\eta} \log[(\eta+1)/(\eta-1)] = 1$ (Alford *et al.*, 2001a). Upon setting $q_I = \eta \delta\mu_I$, (127) becomes

$$\alpha_I(\delta\mu_I) = -\frac{1}{2} \log \left(\frac{\Delta_{2\text{SC}}^2}{4\delta\mu_I^2(\eta^2 - 1)} \right). \quad (128)$$

Once the q_I have been fixed, the only dimensionful quantities on which the quartic and sextic coefficients can depend are the $\delta\mu_I$ (Bowers and Rajagopal, 2002; Rajagopal and Sharma, 2006b), meaning that for exchange symmetric crystal structures and with $\delta\mu_2 = \delta\mu_3 = \delta\mu$ we have $\beta = \bar{\beta}/\delta\mu^2$, $\beta_{32} = \bar{\beta}_{32}/\delta\mu^2$, $\gamma =$

$\bar{\gamma}/\delta\mu^4$ and $\gamma_{322} = \bar{\gamma}_{322}/\delta\mu^4$ where the barred quantities are dimensionless numbers which depend only on $\{\hat{\mathbf{q}}_2\}$ and $\{\hat{\mathbf{q}}_3\}$ that must be evaluated for each crystal structure. Doing so requires evaluating one-loop Feynman diagrams with 4 or 6 insertions of Δ_I 's. Each insertion of Δ_I (Δ_I^*) adds (subtracts) momentum $2\mathbf{q}_I^a$ for some a . The vector sum of all these external momenta inserted into a given one-loop diagram must vanish, meaning that the calculation consists of a book-keeping task (determining which combinations of 4 or 6 \mathbf{q}_I^a 's selected from the sets $\{\mathbf{q}_I\}$ satisfy this momentum-conservation constraint) that grows rapidly in complexity with the complexity of the crystal structure, and a loop integration that is nontrivial because the momentum in the propagator changes after each insertion. In (Rajagopal and Sharma, 2006b), this calculation is carried out explicitly for 11 crystal structures in the mean-field NJL model of Sec. VI.A upon making the weak coupling (Δ_{CFL} and $\delta\mu$ both much less than μ) approximation. Note that in this approximation neither the NJL cutoff nor the NJL coupling constant appear in any quartic or higher Ginzburg-Landau coefficient, and as we have seen above they appear in α only within Δ_{CFL} . Hence, the details of the model do not matter as long as one thinks of Δ_{CFL} as a parameter, kept $\ll \mu$.

It is easy to show that for exchange symmetric crystal structures any extrema of $\Omega(\Delta_2, \Delta_3)$ in (Δ_2, Δ_3) -space must either have $\Delta_2 = \Delta_3 = \Delta$, or have one of Δ_2 and Δ_3 vanishing (Rajagopal and Sharma, 2006b). It is also possible to show that the three-flavor crystalline phases with $\Delta_2 = \Delta_3 = \Delta$ are electrically neutral whereas two-flavor solutions in which only one of the Δ 's is nonzero are not (Rajagopal and Sharma, 2006b). We therefore analyze only solutions with $\Delta_2 = \Delta_3 = \Delta$. We find that $\Omega(\Delta, \Delta)$ is positive for large Δ for all the crystal structures that have been investigated to date (Rajagopal and Sharma, 2006b).⁴ This allows us to minimize $\Omega(\Delta, \Delta)$ with respect to Δ , thus evaluating Δ and Ω .

We begin with the simplest three-flavor ‘‘crystal’’ structure in which $\{\mathbf{q}_2\}$ and $\{\mathbf{q}_3\}$ each contain only a single vector, making the $\langle us \rangle$ and $\langle ud \rangle$ condensates each a single plane wave (Casalbuoni *et al.*, 2005a). We call this the 2PW phase. Unlike in the more realistic crystalline phases we describe below, in this ‘‘crystal’’ the magnitude of the $\langle ud \rangle$ and $\langle us \rangle$ condensates are unmodulated. This simple condensate nevertheless yields a qualitative lesson which proves helpful in winnowing the space of multiple plane wave crystal structures (Rajagopal and Sharma, 2006b). For this simple ‘‘crystal’’ structure, all the coefficients in the

⁴ This is in marked contrast with what happens with only two flavors (and upon ignoring the requirement of neutrality.) in that context, many crystal structures have negative γ and hence sextic order free energies that are unbounded from below (Bowers and Rajagopal, 2002).

Ginzburg-Landau free energy can be evaluated analytically (Casalbuoni *et al.*, 2005a; Mannarelli *et al.*, 2006b; Rajagopal and Sharma, 2006b). The terms that occur in the three-flavor case but not in the two-flavor case, namely $\bar{\beta}_{32}$ and $\bar{\gamma}_{322}$, describe the interaction between the two condensates, and depend on the angle ϕ between \mathbf{q}_2 and \mathbf{q}_3 . For any angle ϕ , both $\bar{\beta}_{32}$ and $\bar{\gamma}_{322}$ are positive. And, both increase monotonically with ϕ and diverge as $\phi \rightarrow \pi$. This divergence tells us that choosing \mathbf{q}_2 and \mathbf{q}_3 precisely antiparallel exacts an infinite free energy price in the combined Ginzburg-Landau and weak-coupling limit in which $\Delta \ll \delta\mu, \Delta_{\text{CFL}} \ll \mu$, meaning that in this limit if we chose $\phi = \pi$ we find $\Delta = 0$. Away from the Ginzburg-Landau limit, when the pairing rings on the Fermi surfaces widen into bands, choosing $\phi = \pi$ exacts a finite price meaning that Δ is nonzero but smaller than that for any other choice of ϕ . The high cost of choosing \mathbf{q}_2 and \mathbf{q}_3 precisely antiparallel can be understood qualitatively as arising from the fact that in this case the ring of states on the u -quark Fermi surface that “want to” pair with d -quarks coincides precisely with the ring that “wants to” pair with s -quarks (Mannarelli *et al.*, 2006b). This simple two plane wave ansatz has been analyzed upon making the weak-coupling approximation but without making the Ginzburg-Landau approximation (Mannarelli *et al.*, 2006b). All the qualitative lessons learned from the Ginzburg-Landau approximation remain valid and we learn further that the Ginzburg-Landau approximation always underestimates Δ (Mannarelli *et al.*, 2006b).

The analysis of the simple two plane wave “crystal” structure, together with the observation that in more complicated crystal structures with more than one vector in $\{\mathbf{q}_2\}$ and $\{\mathbf{q}_3\}$ the Ginzburg-Landau coefficient β_{32} (γ_{322}) is given in whole (in part) by a sum of many two plane wave contributions, yields one of two rules for constructing favorable crystal structures for three-flavor crystalline color superconductivity (Rajagopal and Sharma, 2006b): $\{\mathbf{q}_2\}$ and $\{\mathbf{q}_3\}$ should be rotated with respect to each other in a way that best keeps vectors in one set away from the antipodes of vectors in the other set. The second rule is that the sets $\{\mathbf{q}_2\}$ and $\{\mathbf{q}_3\}$ should each be chosen to yield crystal structures which, seen as separate two-flavor crystalline phases, are as favorable as possible. The 11 crystal structures analyzed in (Rajagopal and Sharma, 2006b) allow one to make several pairwise comparisons that test these two rules. There are instances of two structures which differ only in the relative orientation of $\{\mathbf{q}_2\}$ and $\{\mathbf{q}_3\}$ and in these cases the structure in which vectors in $\{\mathbf{q}_2\}$ get closer to the antipodes of vectors in $\{\mathbf{q}_3\}$ are disfavored. And, there are instances where the smallest angle between a vector in $\{\mathbf{q}_2\}$ and the antipodes of a vector in $\{\mathbf{q}_3\}$ are the same for two different crystal structures, and in these cases the one with the more favorable two-flavor structure is more favorable. These considerations, together with explicit calculations, indicate that two structures, which we denote “2Cube45z” and “CubeX”, are

particularly favorable.

In the 2Cube45z crystal, $\{\mathbf{q}_2\}$ and $\{\mathbf{q}_3\}$ each contain eight vectors pointing at the corners of a cube. If we orient $\{\mathbf{q}_2\}$ so that its vectors point in the $(\pm 1, \pm 1, \pm 1)$ directions in momentum space, then $\{\mathbf{q}_3\}$ is rotated relative to $\{\mathbf{q}_2\}$ by 45° about the z -axis. In this crystal structure, the $\langle ud \rangle$ and $\langle us \rangle$ condensates are each given by the most favored two-flavor crystal structure (Bowers and Rajagopal, 2002). The relative rotation maximizes the separation between any vector in $\{\mathbf{q}_2\}$ and the nearest antipodes of a vector in $\{\mathbf{q}_3\}$.

We arrive at the CubeX structure by reducing the number of vectors in $\{\mathbf{q}_2\}$ and $\{\mathbf{q}_3\}$. This worsens the two-flavor free energy of each condensate separately, but allows vectors in $\{\mathbf{q}_2\}$ to be kept farther away from the antipodes of vectors in $\{\mathbf{q}_3\}$. We have not analyzed all structures obtainable in this way, but we have found one and only one which has a condensation energy comparable to that of the 2Cube45z structure. In the CubeX structure, $\{\mathbf{q}_2\}$ and $\{\mathbf{q}_3\}$ each contain four vectors forming a rectangle. The eight vectors together point toward the corners of a cube. The 2 rectangles intersect to look like an “X” if viewed end-on. The color, flavor and position space dependence of the CubeX condensate is given by

$$\begin{aligned} & \epsilon_{2\alpha\beta}\epsilon_{2ij} \left[\cos \frac{2\pi}{a} (x + y + z) + \cos \frac{2\pi}{a} (-x - y + z) \right] + \\ & \epsilon_{3\alpha\beta}\epsilon_{3ij} \left[\cos \frac{2\pi}{a} (-x + y + z) + \cos \frac{2\pi}{a} (x - y + z) \right] \end{aligned} \quad (129)$$

where $a = \sqrt{3}\pi/q = 4.536/\delta\mu = 36.29\mu/M_s^2$ is the lattice spacing. For example, with $M_s^2/\mu = 100, 150, 200$ MeV the lattice spacing is $a = 72, 48, 36$ fm. We depict this condensate in Fig. 9.

In Figs. 10 and 3, we plot Δ and Ω versus M_s^2/μ for the most favorable crystal structures that we have found, namely the CubeX and 2Cube45z structures described above. We have taken the CFL gap parameter $\Delta_{\text{CFL}} = 25$ MeV in these figures, but they can easily be rescaled to any value of $\Delta_{\text{CFL}} \ll \mu$ (Rajagopal and Sharma, 2006b): if the Δ and M_s^2/μ axes are rescaled by Δ_{CFL} and the energy axis is rescaled by Δ_{CFL}^2 . Fig. 10 shows that the gap parameters are large enough that the Ginzburg-Landau approximation is at the edge of its domain of reliability. However, results obtained for the simpler 2PW crystal structures suggest that the Ginzburg-Landau calculation underestimates Δ and the condensation energy and that, even when it breaks down, it is a good qualitative guide to the favorable structure (Mannarelli *et al.*, 2006b). We therefore trust the result, evident in Fig. 3, that these crystalline phases are both impressively robust, with one or other of them favored over a wide swath of M_s^2/μ and hence density. We do not trust the Ginzburg-Landau calculation to discriminate between these two structures, particularly given that although we have a qualitative understanding of why these two are favorable we have

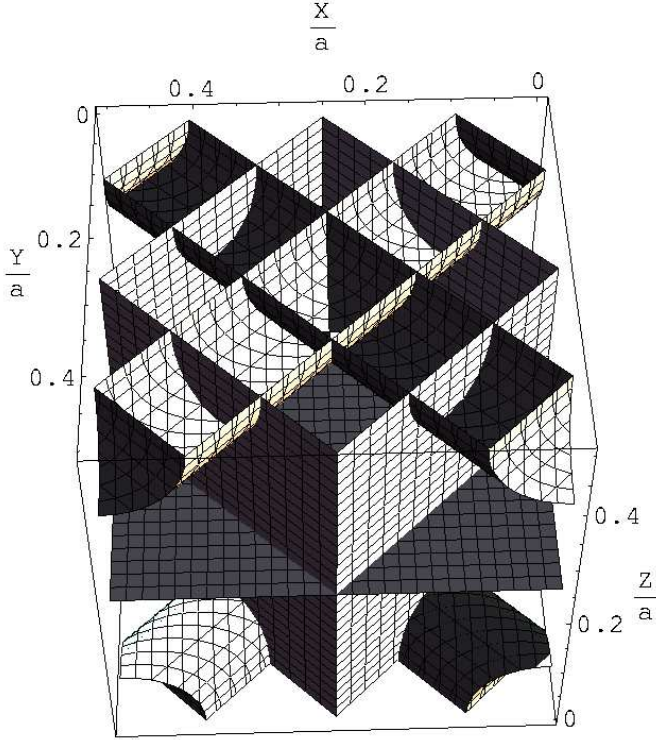


FIG. 9 The CubeX crystal structure of Eq. (129). The figure extends from 0 to $a/2$ in the x , y and z directions. Both $\Delta_2(\mathbf{r})$ and $\Delta_3(\mathbf{r})$ vanish at the horizontal plane. $\Delta_2(\mathbf{r})$ vanishes on the darker vertical planes, and $\Delta_3(\mathbf{r})$ vanishes on the lighter vertical planes. On the upper (lower) dark cylinders and the lower (upper) two small corners of dark cylinders, $\Delta_2(\mathbf{r}) = +3.3\Delta$ ($\Delta_2(\mathbf{r}) = -3.3\Delta$). On the upper (lower) lighter cylinders and the lower (upper) two small corners of lighter cylinders, $\Delta_3(\mathbf{r}) = -3.3\Delta$ ($\Delta_3(\mathbf{r}) = +3.3\Delta$). The largest value of $|\Delta_I(\mathbf{r})|$ is 4Δ , occurring along lines at the centers of the cylinders. The lattice spacing is a when one takes into account the signs of the condensates; if one looks only at $|\Delta_I(\mathbf{r})|$, the lattice spacing is $a/2$.

no qualitative argument for why one should be favored over the other. We are confident that 2Cube45z is the most favorable structure obtained by rotating one cube relative to another. We are not as confident that CubeX is the best possible structure with fewer than 8+8 vectors. Regardless, the 2Cube45z and CubeX crystalline phases together make the case that three-flavor crystalline color superconducting phases are the ground state of cold quark matter over a wide range of densities. If even better crystal structures can be found, this will only further strengthen this case.

Fig. 3 shows that over most of the range of M_s^2/μ where it was once considered a possibility, the gCFL phase can be replaced by a *much* more favorable three-flavor crystalline color superconducting phase. We find that the two most favorable crystal structures have large condensation energies, easily $1/3$ to $1/2$ of that in the CFL phase with $M_s = 0$, which is $3\Delta_{\text{CFL}}^2\mu^2/\pi^2$. This is at first surprising, given that the only quarks that pair are those

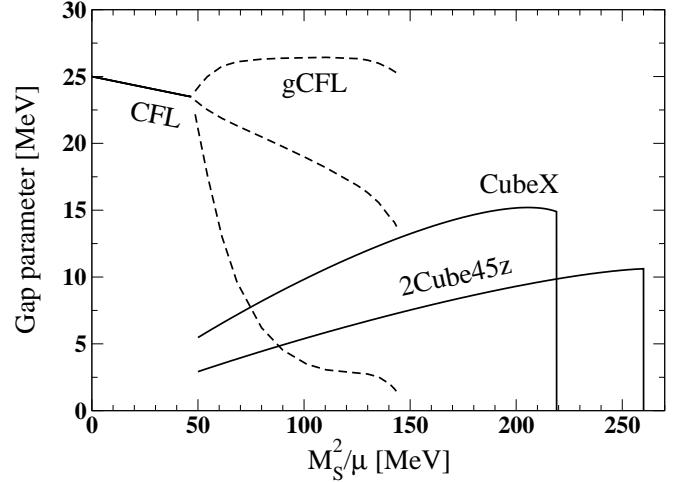


FIG. 10 Gap parameter Δ versus M_s^2/μ for: the CFL gap parameter (set to 25 MeV at $M_s^2/\mu = 0$), the three gap parameters $\Delta_1 < \Delta_2 < \Delta_3$ describing $\langle ds \rangle$, $\langle us \rangle$ and $\langle ud \rangle$ pairing in the gCFL phase, and the gap parameters in the crystalline color superconducting phases with CubeX and 2Cube45z crystal structures. Increasing M_s^2/μ corresponds to decreasing density.

lying on rings on the Fermi surfaces, whereas in the CFL phase with $M_s = 0$ pairing occurs over the entire u , d and s Fermi surfaces. It can to a degree be understood qualitatively once we recall that there are in fact many rings, and note that as Δ increases, the pairing rings spread into bands on the Fermi surfaces, and for Δ as large as that we find to be favored these bands have expanded and filled in, becoming many “polar caps” on the Fermi surfaces (Mannarelli *et al.*, 2006b). In addition to being free-energetically favorable, these crystalline phases are, as far as we know, stable: they do not suffer from the chromomagnetic instability (Ciminale *et al.*, 2006; Gatto and Ruggieri, 2007; Giannakis *et al.*, 2005; Giannakis and Ren, 2005b) and they are also stable with respect to kaon condensation (Anglani *et al.*, 2007). In simplified analogue contexts, it has even been possible to trace the path in configuration space from the unstable gapless phase (analogue of gCFL) downward in free energy to the stable crystalline phase (Fukushima, 2006; Fukushima and Iida, 2007).

Fig. 3 also shows that it is hard to find a crystalline phase with lower free energy than the gCFL phase at the lower values of M_s^2/μ (highest densities) within the “gCFL window”. At these densities, however, the calculations described in Sec. V demonstrate that the gCFL phase is superseded by the stable CFL- K^0 and curCFL- K^0 phases, as shown in Fig. 3.

The three-flavor crystalline color superconducting phases with CubeX and 2Cube45z crystal structures are the lowest free energy phases that we know of, and hence candidates for the ground state of QCD, over a wide range of densities. Within the Ginzburg-Landau approximation to the NJL model that we have employed, one

or other is favored over the CFL, gCFL and unpaired phases for $2.9\Delta_{\text{CFL}} < M_s^2/\mu < 10.4\Delta_{\text{CFL}}$, as shown in Fig. 3. For $\Delta_{\text{CFL}} = 25$ MeV and $M_s = 250$ MeV, this translates to $240\text{MeV} < \mu < 847\text{MeV}$. With these choices of parameters, the lower part of this range of μ (higher part of the range of M_s^2/μ) is certainly superseded by nuclear matter. And, the high end of this range extends beyond the $\mu \sim 500$ MeV characteristic of the quark matter at the densities expected at the center of neutron stars. This qualitative feature persists in the analysis of (Ippolito *et al.*, 2007) in which M_s is solved for rather than taken as a parameter. If neutron stars do have quark matter cores, then, it is reasonable to include the possibility that the *entire* quark matter core could be in a crystalline color superconducting phase on the menu of options that must ultimately be winnowed by confrontation with astrophysical observations. (Recall, that if Δ_{CFL} is larger, say ~ 100 MeV, the entire quark matter core could be in the CFL phase.) As we shall see in the next subsection, crystalline color superconducting quark matter is rigid, with a very large shear modulus, while at the same time being superfluid. This provides a possible origin for pulsar glitches, as we shall discuss in Sec. VIII.F

C. Rigidity of crystalline color superconducting quark matter

The crystalline phases of color superconducting quark matter that we have described in the previous subsection are unique among all forms of dense matter that may arise within neutron star cores in one respect: they are rigid (Mannarelli *et al.*, 2007). They are not solids in the usual sense: the quarks are not fixed in place at the vertices of some crystal structure. Instead, in fact, these phases are superfluid since the condensates all spontaneously break the $U(1)_B$ symmetry corresponding to quark number. We shall always write the condensates as real. This choice of overall phase breaks $U(1)_B$, and spatial gradients in this phase correspond to supercurrents. And yet, we shall see that crystalline color superconductors are rigid solids with large shear moduli. The diquark condensate, although spatially inhomogeneous, can carry supercurrents (Alford *et al.*, 2001a; Mannarelli *et al.*, 2007). It is the spatial modulation of the gap parameter that breaks translation invariance, as depicted for the CubeX phase in Fig. 9, and it is this pattern of modulation that is rigid.⁵ This novel form of rigidity may sound tenuous upon first hearing, but we shall present the effective Lagrangian that describes the

phonons in the CubeX and 2Cube45z crystalline phases, whose lowest order coefficients have been calculated in the NJL model that we are employing (Mannarelli *et al.*, 2007). We shall then extract the shear moduli from the phonon effective action, quantifying the rigidity and indicating the presence of transverse phonons. The fact that the crystalline phases are simultaneously rigid and superfluid means that their presence within neutron star cores has potentially observable consequences, as we shall describe in Sec. VIII.F.

The shear moduli of a crystal may be extracted from the effective Lagrangian that describes phonons in the crystal, namely space- and time-varying displacements of the crystalline pattern. Phonons in two-flavor crystalline phases were first investigated in (Casalbuoni *et al.*, 2002a,c). In the present context, we introduce displacement fields for the $\langle ud \rangle$, $\langle us \rangle$ and $\langle ds \rangle$ condensates by making the replacement

$$\Delta_I \sum_{\mathbf{q}_I^a} e^{2i\mathbf{q}_I^a \cdot \mathbf{r}} \rightarrow \Delta_I \sum_{\mathbf{q}_I^a} e^{2i\mathbf{q}_I^a \cdot (\mathbf{r} - \mathbf{u}_I(\mathbf{r}))} \quad (130)$$

in (120). One way to obtain the effective action describing the dynamics of the displacement fields $\mathbf{u}_I(\mathbf{r})$, including both its form and the values of its coefficients within the NJL model that we are employing, is to begin with the NJL model of Sec. VI.A but with (130) and integrate out the fermion fields. After a lengthy calculation (Mannarelli *et al.*, 2007), this yields

$$\begin{aligned} S[\mathbf{u}] &= \frac{1}{2} \int d^4x \sum_I \kappa_I \\ &\times \left[\left(\sum_{\mathbf{q}_I^a} (\hat{q}_I^a)^m (\hat{q}_I^a)^n \right) (\partial_0 u_I^m) (\partial_0 u_I^n) \right. \\ &\left. - \left(\sum_{\mathbf{q}_I^a} (\hat{q}_I^a)^m (\hat{q}_I^a)^v (\hat{q}_I^a)^n (\hat{q}_I^a)^w \right) (\partial_v u_I^m) (\partial_w u_I^n) \right] \end{aligned} \quad (131)$$

where m, n, v and w are spatial indices running over x, y and z and where we have defined

$$\kappa_I \equiv \frac{2\mu^2 |\Delta_I|^2 \eta^2}{\pi^2 (\eta^2 - 1)}. \quad (132)$$

Upon setting $\Delta_1 = 0$ and $\Delta_2 = \Delta_3 = \Delta$,

$$\kappa_2 = \kappa_3 \equiv \kappa = \frac{2\mu^2 |\Delta|^2 \eta^2}{\pi^2 (\eta^2 - 1)} \simeq 0.664 \mu^2 |\Delta^2|. \quad (133)$$

$S[\mathbf{u}]$ is the low energy effective action for phonons in any crystalline color superconducting phase, valid to second order in derivatives, to second order in the gap parameters Δ_I and to second order in the phonon fields \mathbf{u}_I . Because we are interested in long wavelength, small amplitude, phonon excitations, expanding to second order in derivatives and in the phonon fields is satisfactory. More complicated terms will arise at higher order, for example terms that couple the different \mathbf{u}_I 's, but it is legitimate to neglect these complications (Mannarelli *et al.*,

⁵ Supersolids (Andreev and Lifshitz, 1969; Chester, 1970; Kim and Chan, 2004a,b; Leggett, 1970; Son, 2005) are another example of rigid superfluids, but they differ from crystalline color superconductors in that they are rigid by virtue of the presence of an underlying lattice of atoms.

2007). Extending this calculation to higher order in the Ginzburg-Landau approximation would be worthwhile, however, since as we saw in Sec. VI.B this approximation is at the edge of its domain of reliability.

In order to extract the shear moduli, we need to compare the phonon effective action to the general theory of elastic media (Landau and Lifshitz, 1981), which requires introducing the strain tensor

$$s_I^{mv} \equiv \frac{1}{2} \left(\frac{\partial u_I^m}{\partial x^v} + \frac{\partial u_I^v}{\partial x^m} \right). \quad (134)$$

We then wish to compare the action (131) to

$$\mathcal{S}[\mathbf{u}] = \frac{1}{2} \int d^4x \left(\sum_I \sum_m \rho_I^m (\partial_0 u_I^m) (\partial_0 u_I^m) - \sum_I \sum_{\substack{mn \\ vw}} \lambda_I^{m v n w} s_I^{mv} s_I^{nw} \right) \quad (135)$$

which is the general form of the action in the case in which the effective action is quadratic in displacements and which defines the elastic modulus tensor $\lambda_I^{m v n w}$ for this case. In this case, the stress tensor (in general the derivative of the potential energy with respect to s_I^{mv}) is given by

$$\sigma_I^{mv} = \lambda_I^{m v n w} s_I^{nw}. \quad (136)$$

The diagonal components of σ are proportional to the compression exerted on the system and are therefore related to the bulk modulus of the crystalline color superconducting quark matter. Since unpaired quark matter has a pressure $\sim \mu^4$, it gives a contribution to the bulk modulus that completely overwhelms the contribution from the condensation into a crystalline phase, which is of order $\mu^2 \Delta^2$. We shall therefore not calculate the bulk modulus. On the other hand, the response to shear stress arises only because of the presence of the crystalline condensate. The shear modulus is defined as follows. Imagine exerting a static external stress σ_I having only an off-diagonal component, meaning $\sigma_I^{mv} \neq 0$ for a pair of space directions $m \neq v$, and all the other components of σ are zero. The system will respond with a strain s_I^{nw} . The shear modulus in the mv plane is then

$$\nu_I^{mv} \equiv \frac{\sigma_I^{mv}}{2s_I^{mv}} = \frac{1}{2} \lambda_I^{m v m v}, \quad (137)$$

where the indices m and v are not summed. For a general quadratic potential with σ_I^{mv} given by (136), ν_I^{mv} simplifies partially but the full simplification given by the last equality in (137) only arises for special cases in which the only nonzero entries in $\lambda^{m v n w}$ with $m \neq v$ are the $\lambda^{m v m v}$ entries, as is the case for all the crystal structures that we consider.

For a given crystal structure, upon evaluating the sums in (131) and then using the definition (134) to compare (131) to (135), we can extract expressions for the λ tensor

and thence for the shear moduli. This analysis, described in detail in (Mannarelli *et al.*, 2007), shows that in the CubeX phase

$$\nu_2 = \frac{16}{9} \kappa \begin{pmatrix} 0 & 0 & 1 \\ 0 & 0 & 0 \\ 1 & 0 & 0 \end{pmatrix}, \quad \nu_3 = \frac{16}{9} \kappa \begin{pmatrix} 0 & 0 & 0 \\ 0 & 0 & 1 \\ 0 & 1 & 0 \end{pmatrix}, \quad (138)$$

while in the 2Cube45z phase

$$\nu_2 = \frac{16}{9} \kappa \begin{pmatrix} 0 & 1 & 1 \\ 1 & 0 & 1 \\ 1 & 1 & 0 \end{pmatrix}, \quad \nu_3 = \frac{16}{9} \kappa \begin{pmatrix} 0 & 0 & 1 \\ 0 & 0 & 1 \\ 1 & 1 & 0 \end{pmatrix}. \quad (139)$$

We shall see in Sec. VIII.F that it is relevant to check that both these crystals have enough nonzero entries in their shear moduli ν_I that if there are rotational vortices are pinned within them, a force seeking to move such a vortex is opposed by the rigidity of the crystal structure described by one or more of the nonzero entries in the ν_I . This is demonstrated in (Mannarelli *et al.*, 2007).

We see that all the nonzero shear moduli of both the CubeX and 2Cube45z crystalline color superconducting phases turn out to take on the same value,

$$\nu_{\text{CQM}} = \frac{16}{9} \kappa \quad (140)$$

with κ defined by (133). Evaluating κ yields

$$\begin{aligned} \nu_{\text{CQM}} &= 1.18 \mu^2 \Delta^2 \\ &= 2.47 \frac{\text{MeV}}{\text{fm}^3} \left(\frac{\Delta}{10 \text{ MeV}} \right)^2 \left(\frac{\mu}{400 \text{ MeV}} \right)^2 \end{aligned} \quad (141)$$

From (141) we first of all see that the shear modulus is in no way suppressed relative to the scale $\mu^2 \Delta^2$ that could have been guessed on dimensional grounds. And, second, we discover that a quark matter core in a crystalline color superconducting phase is 20 to 1000 times more rigid than the crust of a conventional neutron star (Mannarelli *et al.*, 2007; Strohmayer *et al.*, 1991). Finally, see (Mannarelli *et al.*, 2007) for the extraction of the phonon dispersion relations from the effective action (131). The transverse phonons, whose restoring force is provided by the shear modulus and which correspond to propagating ripples in a condensation pattern like that in Fig. 9, turn out to have direction-dependent velocities that are typically a substantial fraction of the speed of light, in the specific instances evaluated in (Mannarelli *et al.*, 2007) being given by $\sqrt{1/3}$ and $\sqrt{2/3}$. This is yet a third way of seeing that this superfluid phase of matter is rigid indeed.

VII. TRANSPORT PROPERTIES AND NEUTRINO PROCESSES

In Sec. VIII we shall discuss how the observation of neutron star properties constrains the phase structure of

dense quark matter. A crucial ingredient in these analyses are the transport properties as well as neutrino emissivities and opacities of different phases of quark matter.

Using the methods introduced in Sec. V it is possible to perform rigorous calculations of transport properties of the CFL phase. The results are parameter free predictions of QCD at asymptotically large density, and rigorous consequences of QCD expressed in terms of a few phenomenological parameters (f_π , m_π , ...) at lower density.

In the case of other color superconducting phases we perform calculations using perturbative QCD or models of QCD. For many quantities the results depend mainly on the spectrum of quark modes, and not on details of the quark-quark interaction.

A. Viscosity and thermal conductivity

Viscosity and thermal conductivity determine the dissipated energy \dot{E} in a fluid with nonzero gradients of the velocity \mathbf{v} and the temperature T ,

$$\dot{E} = -\frac{\eta}{2} \int d^3x \left(\partial_i v_j + \partial_j v_i - \frac{2}{3} \delta_{ij} \partial_k v_k \right)^2 - \zeta \int d^3x (\partial_i v_i)^2 - \frac{\kappa}{T} \int d^3x (\partial_i T)^2. \quad (142)$$

The transport coefficients η , ζ and κ are the shear and bulk viscosity and the thermal conductivity, respectively. Eq. (142) is strictly valid only for non-relativistic fluids. In the case of relativistic fluids there is an extra contribution to the dissipated energy which is proportional to κ and the gradient of μ (Landau and Lifshitz, 1987). In terms of its hydrodynamic properties a superfluid can be viewed as a mixture of a normal and a superfluid component characterized by separate flow velocities. The shear viscosity is entirely due to the normal component, but there are contributions to the bulk viscosity which are related to stresses in the superfluid flow relative to the normal one (Andersson and Comer, 2006; Gusakov, 2007; Khalatnikov, 1989). In the following we shall neglect these effects and interpret v_i in Eq. (142) as the normal fluid velocity.

In neutron stars an important contribution to the bulk viscosity arises from electroweak effects. In a bulk compression mode the density changes periodically and electroweak interactions may not be sufficiently fast to reestablish weak equilibrium. Weak effects occur on the same time scale as the oscillation period of the neutron star and the frequency dependence of the bulk viscosity is important. We define

$$\zeta(\omega) = 2 \langle \dot{E} \rangle \left(\frac{V_0}{\delta V_0} \right)^2 \frac{1}{\omega^2}, \quad (143)$$

where ω is the oscillation frequency, $\langle \dots \rangle$ is a time average, and $\delta V_0/V_0$ is the fractional change in the volume. The coefficient ζ in Eq. (142) is the $\omega \rightarrow 0$ limit of $\zeta(\omega)$.

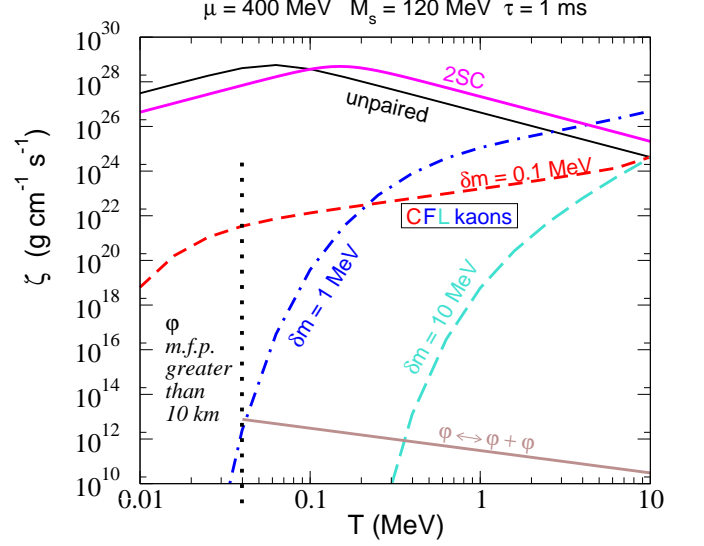


FIG. 11 (Color online) Bulk viscosities as functions of temperature for an oscillation period $\tau = 2\pi/\omega = 1$ ms. CFL phase: contribution from the process $K^0 \leftrightarrow \varphi + \varphi$ for different values of $\delta m \equiv m_{K^0} - \mu_{K^0}$ and contribution from $\varphi \leftrightarrow \varphi + \varphi$, see Eq. (147). 2SC phase and unpaired quark matter: contribution from the process $u + d \leftrightarrow u + s$.

If a single weak process is responsible for reestablishing chemical equilibrium, the frequency dependent bulk viscosity can be written in the form

$$\zeta(\omega) = C \frac{\gamma}{\gamma^2 + \omega^2}. \quad (144)$$

The prefactor C accounts for the dependence of the equilibrium densities (e.g., the net difference between the density of strange and non-strange quarks if the weak process changes strangeness) on the respective chemical potentials, and γ is the characteristic inverse time scale of the flavor changing process. Eq. (144) shows that, for a given ω , ζ has a maximum at $\gamma = \omega$. At this point the time scale of the microscopic process matches the one of the external oscillation. If more than one weak process contributes to reequilibration, Eq. (144) becomes more complicated (Alford and Schmitt, 2007; Haensel *et al.*, 2000)

1. CFL phase

The normal fluid is composed of quasi-particle excitations. In the CFL phase all quark modes are gapped and the relevant excitations are Goldstone bosons. At very low temperature, transport properties are dominated by the massless Goldstone boson φ associated with the breaking of the $U(1)_B$ symmetry. Using the results in Sec. V.C we can compute the mean free path l_φ of the φ due to $\varphi \leftrightarrow \varphi + \varphi$ and $\varphi + \varphi \leftrightarrow \varphi + \varphi$ scattering. Small angle scattering contributions give rise to $l_\varphi \propto \mu^4/T^5$ (Manuel *et al.*, 2005) and $l_\varphi \simeq 1$ km at

$T = 0.1$ MeV, while large angle scattering contributions yield an even longer $l_\varphi \propto \mu^8/T^9$ (Shovkovy and Ellis, 2002). The thermal conductivity κ due to the φ is given by (Shovkovy and Ellis, 2002)

$$\kappa = \frac{2\pi^2 T^3}{45v^2} l_\varphi, \quad (145)$$

where l_φ is the φ mean-free path between large angle scatterings and v is the φ velocity from Eqs. (83) and (84). For temperatures below ~ 1 MeV the thermal conductivity is very large and macroscopic amounts of CFL matter are expected to be isothermal. The electric conductivity in CFL matter is dominated by thermal electrons and positrons and was estimated in (Shovkovy and Ellis, 2003).

At low temperatures, the shear viscosity of the CFL phase is dominated by the φ contribution, which was computed in (Manuel *et al.*, 2005) and is given by

$$\eta = 1.3 \times 10^{-4} \frac{\mu^8}{T^5}. \quad (146)$$

The bulk viscosity ζ vanishes in an exactly scale invariant system. For realistic quark masses the dominant source of scale breaking is the strange quark mass. The contribution to the process $\varphi \leftrightarrow \varphi + \varphi$ is (Manuel and Llanes-Estrada, 2007)

$$\zeta = 0.011 \frac{M_s^4}{T}. \quad (147)$$

We show this contribution in Fig. 11. The other contribution to the CFL bulk viscosity presented in the figure comes from the process $K^0 \leftrightarrow \varphi + \varphi$ and was studied for arbitrary ω in (Alford *et al.*, 2007a). We observe that at $T \simeq (1 - 10)$ MeV the bulk viscosity of CFL matter is comparable to that of unpaired quark matter. For $T < 1$ MeV, ζ is strongly suppressed. Depending on the poorly known value for $\delta m \equiv m_{K^0} - \mu_{K^0}$ (here assumed to be positive, a negative value corresponds to kaon condensation), the pure φ contribution given in Eq. (147) may dominate over the $K^0 \leftrightarrow \varphi + \varphi$ reaction at low enough temperatures. However, for $T < 0.1$ MeV the φ mean free path is on the order of the size of the star, i.e., the system is in the collisionless rather than in the hydrodynamic regime, and the result ceases to be meaningful.

Thermal conductivity and viscosities for the CFL- K^0 phase have not yet been computed. The existence of a gapless K^0 Goldstone mode in this phase will introduce new contributions. However, since the CFL results for κ and η are already dominated by a gapless mode, namely the φ , the modifications to these quantities are not expected to be significant. The modification to ζ will be more significant, since the kaon contribution to this quantity is already important in the CFL phase.

2. Other phases

For unpaired, ultrarelativistic three-flavor quark matter, thermal and electric conductivity as well as shear vis-

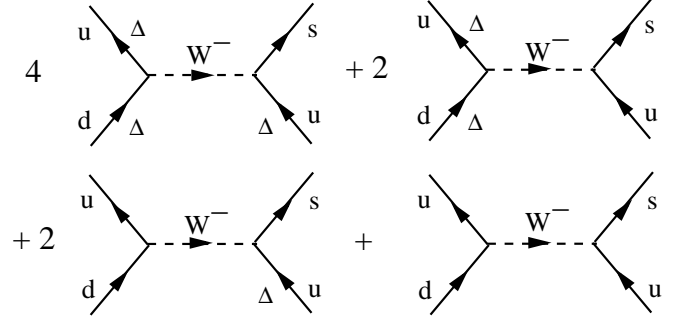


FIG. 12 Contributions to the process $u + d \rightarrow u + s$ in the 2SC phase. A gapped fermion is marked with the gap Δ at the respective line. (We have omitted (small) contributions from anomalous propagators.)

cosity have been computed in (Heiselberg and Pethick, 1993). In the low-temperature limit (in particular $T \ll m_D$ with the electric screening mass $m_D^2 = N_f g^2 \mu^2 / (2\pi^2)$) they are

$$\kappa \simeq 0.5 \frac{m_D^2}{\alpha_s^2}, \quad \sigma_{\text{el}} \simeq 0.01 \frac{e^2 \mu^2 m_D^{2/3}}{\alpha_s^2 T^{5/3}}, \quad (148)$$

and

$$\eta \simeq 4.4 \times 10^{-3} \frac{\mu^4 m_D^{2/3}}{\alpha_s^2 T^{5/3}}. \quad (149)$$

These quantities have not yet been computed for partially gapped color superconductors such as the 2SC phase. The presence of ungapped modes, however, suggests that the results only differ by a numerical factor from the unpaired phase results.

The dominant flavor changing process that contributes to the bulk viscosity in unpaired quark matter is the reaction (Anand *et al.*, 2000; Madsen, 1992)

$$u + d \leftrightarrow u + s. \quad (150)$$

Other relevant processes are the semi-leptonic processes $u + e \leftrightarrow d + \nu_e$ and $u + e \leftrightarrow s + \nu_e$ (Dong *et al.*, 2007; Sa'd *et al.*, 2007b).

In a partially gapped phase the bulk viscosity is also dominated by the process (150). In the 2SC phase of three flavor quark matter, the number of d -quarks produced per unit time and volume, Γ , due to (150) can be computed from the diagrams shown in Fig. 12. The combinatorial factors in front of the diagrams are obtained upon counting color degrees of freedom: one can attach one of three colors to each of the two weak vertices, giving rise to 9 possibilities. In the 2SC phase all blue quarks and all strange quarks are unpaired while all other modes are paired, see Table I. Consequently, 4 of the 9 possibilities contain three gapped modes (red or green for both vertices), 2 contain two gapped modes (red or green for one, blue for the other vertex), 2 contain one gapped mode (blue for one, red or green for

the other vertex), and one contains only unpaired modes (blue for both vertices). Therefore, at very low temperature, $T \ll \Delta$, where the contributions of gapped quarks are exponentially suppressed, Γ is to a very good approximation given by (Madsen, 2000)

$$\Gamma^{2\text{SC}} = \frac{1}{9}\Gamma^{\text{unp}} \quad \text{for } T \ll \Delta, \quad (151)$$

since only the one reaction containing only unpaired modes contributes. The rate Γ^{unp} was computed in (Madsen, 1993).

For larger temperatures, the contribution from gapped modes cannot be neglected. Each diagram yields a contribution which (for one direction of the process) schematically reads

$$\begin{aligned} \Gamma \propto \sum_{\{e_i\}} \int_{\{p_i\}} \mathcal{F} \delta(e_1\varepsilon_1 + e_2\varepsilon_2 - e_3\varepsilon_3 - e_4\varepsilon_4 + \delta\mu) \\ \times f(e_1\varepsilon_1)f(e_2\varepsilon_2)f(-e_3\varepsilon_3)f(-e_4\varepsilon_4). \end{aligned} \quad (152)$$

Here, ε_i are the quasiparticle energies, $\delta\mu = \mu_s - \mu_d$, and f is the Fermi distribution function. \mathcal{F} is a function of the momenta p_i and the signs $e_i = \pm 1$. The sum over the signs e_i is very important in a paired system: the process $u + d \rightarrow u + s$ not only receives contributions from $2 \rightarrow 2$ processes, but also from $3 \rightarrow 1$ and $1 \rightarrow 3$ reactions involving pairs created or absorbed by the condensate.

From the net production rate of d quarks Γ one obtains the characteristic inverse time scale γ needed for the bulk viscosity in Eq. (144). For small external volume oscillations $\delta V_0/V_0$, Γ is linear in the resulting oscillation in chemical potentials, $\Gamma = \lambda\delta\mu$. Then, $\gamma \equiv B\lambda$, where B depends only on the equilibrium flavor densities. The resulting bulk viscosity as a function of temperature for a typical oscillation frequency $\omega/(2\pi) = 1\text{ms}^{-1}$ is shown in Fig. 11. A critical temperature of $T_c = 30$ MeV is assumed. For low temperatures, the time scale of the nonleptonic process is much smaller than the oscillation frequency $\gamma \ll \omega$, implying $\zeta \propto \gamma$. Consequently, from Eq. (151) we conclude $\zeta_{2\text{SC}} = \zeta_{\text{unp}}/9$. For large temperatures, however, we have $\gamma \gg \omega$ and thus $\zeta \propto 1/\gamma$. Consequently, the superconducting phase, which has the slower rate, has the larger bulk viscosity.

The bulk viscosity has also been computed for two-flavor quark matter with single-flavor pairing (Sa'd *et al.*, 2007a). In this case there are also ungapped modes and thus the result is similar to the one of the 2SC phase. The main difference is the lower critical temperature for single-flavor pairing. As a consequence, these phases are unlikely to exist for temperatures larger than that at which the bulk viscosity of the unpaired phase is maximal. Therefore, the bulk viscosity cannot be larger than that of the unpaired phase.

B. Neutrino emissivity and specific heat

Neutrino emissivity determines the rate at which quark matter can lose heat via neutrino emission. For the

purpose of studying how neutron stars with ages ranging from tens of seconds to millions of years cool, as we shall discuss in Sec. VIII.C, it is appropriate to treat the matter as completely transparent to the neutrinos that it emits.

1. CFL phase

In CFL quark matter, all quasifermion modes are gapped and neutrino emissivity is dominated by reactions involving (pseudo)-Goldstone modes such as

$$\pi^\pm, K^\pm \rightarrow e^\pm + \bar{\nu}_e, \quad (153a)$$

$$\pi^0 \rightarrow \nu_e + \bar{\nu}_e, \quad (153b)$$

$$\varphi + \varphi \rightarrow \varphi + \nu_e + \bar{\nu}_e. \quad (153c)$$

These processes were studied in (Jaikumar *et al.*, 2002; Reddy *et al.*, 2003b). The decay rates of the massive mesons π^\pm , K^\pm , and π^0 are proportional to their number densities and are suppressed by Boltzmann factors $\exp(-E/T)$, where E is the energy gap of the meson. Since the pseudo-Goldstone boson energy gaps are on the order of a few MeV, the emissivities are strongly suppressed as compared to unpaired quark matter for temperatures below this scale. Neutrino emission from processes involving the φ is not exponentially suppressed, but it involves a very large power of T ,

$$\epsilon_\nu \sim \frac{G_F^2 T^{15}}{f^2 \mu^4}, \quad (154)$$

and is numerically very small. Reddy *et al.* also studied the neutrino mean free path l_ν . For $T \sim 30$ MeV the mean free path is on the order of 1 m, but for $T < 1$ MeV, $l_\nu > 10$ km (Reddy *et al.*, 2003b). In the CFL- K^0 phase, l_ν is almost the same as in the CFL phase, while the neutrino emissivity is larger (Reddy *et al.*, 2003a).

The specific heat of CFL matter is also dominated by the φ , yielding

$$c_V = \frac{2\pi^2}{15\nu^3} T^3. \quad (155)$$

This is much smaller than the specific heat of any phase containing unpaired quarks, as we shall see below.

2. Other phases

The density of thermally excited ungapped fermions is proportional to $\mu^2 T$ while that of ungapped bosons is T^3 . This means that in any degenerate system ($T \ll \mu$) ungapped fermion modes, if they exist, will dominate the neutrino rates. In unpaired quark matter neutrino emissivity is dominated by the direct Urca processes

$$u + e \rightarrow d + \nu_e \quad (\text{electron capture}), \quad (156a)$$

$$d \rightarrow u + e + \bar{\nu}_e \quad (\beta\text{-decay}). \quad (156b)$$

The radiated energy per unit of time and volume is (Iwamoto, 1980)

$$\epsilon_\nu \simeq \frac{457}{630} \alpha_s G_F^2 T^6 \mu_e \mu_u \mu_d. \quad (157)$$

Note that this result is proportional to the strong coupling constant α_s . The tree-level processes for massless quarks are approximately collinear and the weak matrix element vanishes in the forward direction. A nonzero emissivity arises from strong interaction corrections, which depress quark Fermi momenta relative to their chemical potentials. Because they do not at the same time depress the electron Fermi momentum, this opens up phase space for the reactions (156). A nonzero emissivity can also arise from quark mass effects, or higher order corrections in T/μ . Since strange quark decays are Cabibbo suppressed and T/μ is small the dominant contribution is likely to be that proportional to α_s , namely (157). Note that we have not included non-Fermi liquid corrections of $O(\alpha_s \log(T))$ (Schäfer and Schwenzer, 2004a).

In order to determine the rate at which neutron stars cool we also need to know the specific heat. In unpaired quark matter

$$c_V = \frac{N_c N_f}{3} \mu^2 T, \quad (158)$$

where we have again neglected terms of $O(\alpha_s \log(T))$ (Ipp *et al.*, 2004) and assumed the flavor chemical potentials to be equal. We see that the specific heat (155) in the CFL phase, whose excitations are bosonic, is much smaller than that in unpaired quark matter.

In the case of 2SC matter, the neutrino emissivity at low temperature is 1/3 of that of unpaired quark matter. The 2SC emissivity for arbitrary temperatures can be found in (Jaikumar *et al.*, 2006b). In addition to the direct Urca process neutrino pair production

$$q + q \rightarrow q + q + \nu_\ell + \bar{\nu}_\ell \quad (159)$$

(q is any quark flavor and ℓ denotes neutrino flavor) has also been studied (Jaikumar and Prakash, 2001). The rate of this process is parametrically smaller than the direct Urca process for very small temperatures ($\exp(-2\Delta/T)$ vs. $\exp(-\Delta/T)$), but it may play a significant role for temperatures close to the superconducting phase transition temperature T_c .

For the LOFF phase similar arguments apply. The presence of ungapped modes renders its specific heat (Casalbuoni *et al.*, 2003) and its neutrino emissivity due to direct Urca processes virtually indistinguishable from the unpaired phase (Anglani *et al.*, 2006). However, interesting effects of crystalline structures may be expected for other cooling mechanisms. This is not unlike effects in the crust of a conventional neutron star, where for instance electron-phonon scattering as well as Bragg diffraction of electrons lead to neutrino emission via bremsstrahlung processes, see (Yakovlev *et al.*, 2001) and references therein.

The direct Urca processes have also been considered for the gapless CFL phase. A distinctive feature of this phase is the fact that the energy of one of the quark modes is approximately quadratic in momentum. This implies a strong enhancement in the specific heat, which leads to very slow cooling at very small temperatures when photon emission from the surface dominates the energy loss (Alford *et al.*, 2005b). However, the instability of this phase at small temperatures suggests that this result is most probably of no relevance for astrophysics.

Finally, it is interesting to consider neutrino emission from single flavor paired matter. Single flavor spin-one pairing involves small gaps, as well as nodes in the gap parameter, and the emissivity is expected to be larger than that of matter with spin zero pairing. The emissivity of two-flavor quark matter with $\langle uu \rangle$ and $\langle dd \rangle$ pairing was studied for different spin-one order parameters in (Schmitt *et al.*, 2006; Wang *et al.*, 2006). The result can be written as

$$\epsilon_\nu = \frac{457}{630} \alpha_s G_F^2 T^6 \mu_e \mu_u \mu_d \left[\frac{1}{3} + \frac{2}{3} \mathcal{G}(\Delta/T) \right], \quad (160)$$

where the u -quark and d -quark gaps are assumed to be identical. All spin-one phases analyzed in (Schmitt *et al.*, 2006; Wang *et al.*, 2006) and described by Eq. (160) contain ungapped modes similar to the 2SC phase. Therefore, the emissivity at low temperatures is simply one third of that of unpaired quark matter. (In the case of color-spin locking, all excitations become gapped if one takes into account nonzero quark masses (Aguilera *et al.*, 2005; Schmitt *et al.*, 2006) and/or more complicated structures of the order parameter (Marhauser *et al.*, 2007).) The contribution to (160) that arises from the paired quarks, is described by the nontrivial function $\mathcal{G}(\Delta/T)$; see (Schmitt *et al.*, 2006) for the explicit form and numerical evaluation of this function for arbitrary temperatures. In Table III, we present the behavior of this function for temperatures much smaller than the gap, $T \ll \Delta$, for various single-flavor spin-one color superconducting phases. Although this contribution is small compared to the contribution of the ungapped modes, we can use it to show the effect of different (anisotropic) gap structures on the parametric behavior of the neutrino emissivity. We see that, while fully gapped modes lead to an exponential suppression of the emissivity, nodes in the gap weaken this suppression to a power law. The power law depends on the behavior of the gap in the vicinity of the nodes.

The specific heat can be written as

$$c_V = T(\mu_u^2 + \mu_d^2) \left[\frac{1}{3} + \frac{2}{3} \mathcal{K}(\Delta/T) \right]. \quad (161)$$

We show the suppression function $\mathcal{K}(\Delta/T)$ for the specific heat in Table III. We see that an exponential suppression of the emissivity goes along with an exponential suppression of the specific heat.

phase	gap structure	$\mathcal{G}(\phi) \propto$	$\mathcal{K}(\phi) \propto$
CSL	isotropic (no nodes)	$\phi \exp(-\sqrt{2}\phi)$	$\phi^{5/2} \exp(-\sqrt{2}\phi)$
planar	anisotropic (no nodes)	$\phi^{1/2} \exp(-\phi)$	$\phi^2 \exp(-\phi)$
polar	point nodes (linear)	ϕ^{-2}	ϕ^{-2}
A	point nodes (quadratic)	ϕ^{-1}	ϕ^{-1}

TABLE III Suppression function $\mathcal{G}(\phi)$ for neutrino emissivity in direct Urca processes and suppression function $\mathcal{K}(\phi)$ for specific heat for four spin-one color-superconducting phases (abbreviating $\phi \equiv \Delta/T$, and everything in the limit $\phi \rightarrow \infty$). While fully gapped modes yield exponential suppression, nodes in the gap yield power law suppressions. The gap functions in the polar and A phases differ in the angular direction in the vicinity of the point nodes. A linear behavior leads to a stronger suppression than a quadratic behavior.

VIII. COLOR SUPERCONDUCTIVITY IN NEUTRON STARS

Neutron stars are the densest material objects in the universe, with masses of order that of the sun (M_{\odot}) and radii of order ten km. Depending on their mass and on the stiffness of the equation of state of the material of which they are composed, their central density lies between ~ 3 and ~ 12 times nuclear saturation density ($n_0 = 0.16$ nucleons/fm³) (Lattimer and Prakash, 2001, 2007). Neutron stars consist of an outer crust made of a rigid lattice of positive ions embedded within a fluid of electrons and (in the inner layer of the crust) superfluid neutrons (Negele and Vautherin, 1973). Inside this crust, one finds a fluid “mantle” consisting of neutrons and protons, both likely superfluid, and electrons. Determining the composition of neutron star cores, namely of the densest matter in the universe, remains an outstanding challenge.⁶ If the nuclear equation of state is stiff enough, neutron stars are made of neutrons, protons and electrons all the way down to their centers. If higher densities are reached, other phases of baryonic matter (including either a pion condensate (Bahcall and Wolf, 1965; Baym and Campbell, 1978; Migdal, 1971; Sawyer, 1972; Scalapino, 1972), a kaon condensate (Brown, 1995; Kaplan and Nelson, 1986), or a nonzero density of one or several hyperons (Glendenning, 1985)) may result. Or, neutron star cores may be made of color superconducting quark matter.

The density at which the transition from baryonic matter to quark matter occurs is not known; this depends on a comparison between the equations of state for both, which is not well-determined for either. Very roughly, we expect this transition to occur when the density exceeds one nucleon per nucleon volume, a criterion which suggests a transition to quark matter at densities $\gtrsim 3n_0$. The question we shall pose in this section is how astrophysical observation of neutron stars could determine

whether they do or do not contain quark matter within their cores. We have seen throughout the earlier sections of this review that quark matter at potentially accessible densities may be in the CFL phase, with all quarks paired, or may be in one of a number of possible phases in which there are some unpaired quarks, some of which are spatially inhomogeneous. If quark matter does exist within neutron stars, with their temperatures far below the critical temperatures for these paired phases, it will be in some color superconducting phase. We shall see in this section that these different phases have different observational consequences, making it possible for a combination of different types of observational data to cast light upon the question of which phase of color superconducting quark matter is favored in the QCD phase diagram, if in fact neutron stars do feature quark matter cores.

Before turning to the signatures of quark matter in neutron star cores, we mention here the more radical possibility that nuclear matter in bulk is metastable at zero pressure, with the true ground state of strongly interacting matter in the infinite volume limit being color superconducting three-flavor quark matter. According to this “strange quark matter hypothesis” (Bodmer, 1971; Farhi and Jaffe, 1984; Witten, 1984), ordinary nuclei are either stabilized by virtue of their small size or are metastable with lifetimes vastly exceeding the age of the universe. If this hypothesis is correct, some of the stars that we think are neutron stars may be strange stars, made entirely of quark matter (Alcock *et al.*, 1986; Alcock and Olinto, 1988; Farhi and Jaffe, 1984; Haensel *et al.*, 1986). Strange stars may have a thin crust (of order 100 meters thick) of positive ions suspended above the quark matter surface by an electric field (Alcock *et al.*, 1986), or they may have a comparably thin crust of positive ions embedded within the (negatively charged) outer layer of the quark matter itself (Alford *et al.*, 2006; Jaikumar *et al.*, 2006a). They cannot, however, have a conventional, km thick, crust. And, there are many indications that neutron stars in fact do have conventional crusts. For example, the rich phenomenology of X-ray bursts is well-understood only within this setting. More recent evidence comes from the analysis of the quasi-periodic oscillations with frequencies in the tens of Hz detected in the aftermath of magnetar

⁶ For review articles on neutron stars as laboratories for understanding dense matter, see for instance (Lattimer and Prakash, 2004, 2007; Page and Reddy, 2006; Prakash *et al.*, 2001; Weber, 1999; Weber *et al.*, 2006; Yakovlev and Pethick, 2004).

superbursts (Israel *et al.*, 2005; Strohmayer and Watts, 2005, 2006; Watts and Strohmayer, 2006, 2007), which can be understood as seismic oscillations of a conventional neutron star crust (Strohmayer and Watts, 2005, 2006; Watts and Strohmayer, 2007) whereas the thin crusts of a strange star would oscillate at much higher frequencies (Watts and Reddy, 2007). Even if most compact stars are neutron stars not strange stars, it remains a logical possibility that some strange stars exist, meaning that all ordinary neutron stars are metastable. Although possible this scenario is unlikely, given that merger events in which strange stars in an inspiralling binary are tidally disrupted would litter the universe with small chunks of quark matter (“strangelets”) and one must then understand why these have not catalyzed the conversion of all neutron stars to strange stars (Friedman and Caldwell, 1991). We shall devote the remainder of this section to the more challenging task of using observational data to constrain the more conservative scenario that quark matter exists only above some nonzero transition pressure, namely within the cores of conventional neutron stars.

A. Mass-radius relation

It has long been a central goal of neutron star astrophysics to measure the masses M and radii R of many neutron stars to a reasonable accuracy. Mapping out the curve in the mass-radius plane along which neutron stars are found would yield a strong constraint on the equation of state of dense matter. As this program represents such a large fraction of the effort to use observations of neutron stars to constrain dense matter physics, we begin by considering its implications for the presence of quark matter within neutron star cores.

The larger the maximum mass that can be attained by a neutron star, the stiffer the equation of state of dense matter, and if stars with masses close to $2 M_\odot$ are found then the existence of phases with a soft equation of state, such as baryonic matter with kaon or pion condensation, can be ruled out. However, although the quark matter equation of state is not known from first principles, it may easily be as stiff as the stiffer equations of state posited for ordinary nuclear matter, and neutron stars with quark matter cores can in fact reach masses of order $2 M_\odot$ (Alford *et al.*, 2005a; Baldo *et al.*, 2003; Blaschke *et al.*, 2007; Fraga *et al.*, 2001; R uster and Rischke, 2004).

The equation of state for CFL quark matter can be parametrized to a good approximation as (Alford *et al.*, 2005a)

$$\Omega = -P = -\frac{3}{4\pi^2}(1-c)\mu^4 + \frac{3}{4\pi^2}(M_s^2 - 4\Delta^2)\mu^2 + B_{\text{eff}}. \quad (162)$$

If c were zero, the μ^4 term would be that for noninteracting quarks; c parametrizes the leading effect of interactions, modifying the relation between p_F and μ . At high densities, $c = 2\alpha_s/\pi$ to leading order in the strong

coupling constant. Analysis of higher order corrections suggests that $c \gtrsim 0.3$ at accessible densities (Fraga *et al.*, 2001). B_{eff} can be thought of as parametrizing our ignorance of the μ at which the nuclear matter to quark matter transition occurs. The $M_s^2\mu^2$ term is the leading effect of the strange quark mass, and is common to all quark matter phases. The pressure of a color superconducting phase with less pairing than in the CFL phase would have a smaller coefficient of the $\Delta^2\mu^2$ term, and would also differ at order M_s^4 , here lumped into a change in B_{eff} . Because pairing is a Fermi surface phenomenon, it only modifies the μ^2 term, leaving the larger μ^4 term untouched. However, it can nevertheless be important because at accessible densities the μ^4 term is largely cancelled by B_{eff} , enhancing the importance of the μ^2 term (Alford and Reddy, 2003; Lugones and Horvath, 2002). Remarkably, and perhaps coincidentally, if we make the (reasonable) parameter choices $c = 0.3$, $M_s = 275$ MeV and $\Delta = 100$ MeV and choose B_{eff} such that nuclear matter gives way to CFL quark matter at the relatively low density $1.5 n_0$, then over the entire range of higher densities relevant to neutron stars the quark matter equation of state (162) is almost indistinguishable from the nuclear equation of state due to Akmal, Pandharipande and Ravenhall (APR) (Akmal *et al.*, 1998) that is one of the stiffest nuclear equations of state in the compendium found in (Lattimer and Prakash, 2004, 2007). Neutron stars made entirely of nuclear matter with the APR equation of state and neutron stars with a quark matter core with the equation of state (162) with the parameters just described fall along almost indistinguishable curves on a mass vs. radius plot, with the most significant difference being that the APR equation of state admits neutron stars with maximum mass $2.3M_\odot$, whereas the introduction of a quark matter core reduces the maximum mass slightly, to $2.0M_\odot$ (Alford *et al.*, 2005a).

The similarity between a representative quark matter equation of state and a representative nuclear equation of state makes clear that it will be very hard to use a future determination of the equation of state to discern the presence of quark matter. However, although the numbers in the above paragraph should be taken as indicative rather than definitive, they do suggest that the existence of a neutron star whose mass was reliably determined to be $> 2M_\odot$ would make it hard to envision such a star (and hence any lighter stars) having a quark matter core of any appreciable size. Now that the mass of PSR J0751+1807 has been revised downward from $(2.1 \pm 0.2)M_\odot$ (Nice *et al.*, 2005) to $(1.26^{+0.14}_{-0.12})M_\odot$ (Nice and Stairs, 2007), the heaviest known neutron star orbited by a white dwarf is PSR J0621+1002, whose mass is $(1.69^{+0.11}_{-0.16})M_\odot$ (Nice and Stairs, 2007; Splaver *et al.*, 2002). Also, one of the two pulsars Ter5I and Ter5J (in a globular cluster) must have a mass that is $> 1.68M_\odot$ at the 95% confidence level (Ransom *et al.*, 2005), and the mass of the X-ray pulsar Vela X-1 is above $1.6 M_\odot$ (Barziv *et al.*, 2001).

Given our lack of knowledge of the equations of state for nuclear and quark matter, measuring neutron star masses and radii alone do not allow us to reach our goals.

B. Signatures of the compactness of neutron stars

If we could detect gravity waves from neutron stars spiraling into black holes in binary systems, the gravitational wave form during the last few orbits, when the neutron star is being tidally disrupted, will encode information about the density profile of the neutron star. For example, upon assuming a conventional density profile, the gravity wave form encodes information about the ratio M/R (Faber *et al.*, 2002), essentially via encoding the value of the orbital frequency at which tidal deformation becomes significant. This suggests a scenario in which the presence of an interface separating a denser quark core from a less-dense nuclear mantle could manifest itself via the existence of two orbital frequency scales in the wave form, the first being that at which the outer layers are deformed while the denser quark core remains spherical and the second being the time at which even the quark core is disrupted (Alford *et al.*, 2001b). This idea must be tested in numerical relativity calculations, and it may turn out to be better formulated in some other way. For example, perhaps the gravity wave form can be used to constrain the first few moments of the density profile, and this information can then be used to contrast neutron stars with standard density profiles characterized by a single length scale R with those which are anomalously compact because they have a “step” in their density profile. Whatever the best formulation turns out to be, it seems clear that if LIGO sees events in which the tidal disruption of a neutron star occurs within the LIGO band-width, the gravity wave data will constrain the “compactness” of the neutron star, providing information about the density profile that is complementary to that obtained from a mass-radius relation.

If there is a “step” in the density profile at an interface, LIGO gravity waves may provide evidence for its presence. But, should a density step be expected if color superconducting quark matter is found in the core of a neutron star? There are two qualitatively distinct possibilities for the density profile, depending on the surface tension of the quark matter/nuclear matter interface σ . If σ is large enough, there will be a stable, sharp, interface between two phases having different densities (but the same chemical potential). If σ is small enough, it becomes favorable instead to form a macroscopic volume filled with a net-neutral mixture of droplets of negatively charged quark matter and positively charged nuclear matter, see Sec. III.H, which allows a continuous density profile. The distinction between these two scenarios has been analyzed quantitatively for the case of a first order phase transition from nuclear matter to CFL quark matter (Alford *et al.*, 2001b). This is the simplest possible phase diagram of QCD, with a single transition

between the phases known to exist at nuclear density and at asymptotically high density. We have seen earlier in this review that this simple QCD phase diagram is obtained if Δ_{CFL} is large enough, allowing CFL pairing to fend off stresses that seek to split Fermi surfaces, all the way down in density until the nuclear matter takes over from quark matter. A sharp interface between the (electrically insulating) CFL phase and (electrically conducting) nuclear matter features charged boundary layers on either side of the interface, which play an important role in determining the σ above which this step in the density profile is stable (Alford *et al.*, 2001b). The critical σ is about 40 MeV/fm³, lower than dimensional analysis would indicate should be expected, meaning that the sharp interface with a density step is more likely than a mixture of charged components. The increase in the density at the interface can easily be by a factor of two. The critical σ above which a sharp interface is favored has not been evaluated for the case of a first order phase transition between nuclear matter and color superconducting phases other than the CFL phase.

It is also possible that the long term analysis of the binary double pulsar PSR J0737-3039A (Burgay *et al.*, 2003; Lyne *et al.*, 2004) may yield a measurement of the moment of inertia of this 1.34 solar mass neutron star (Kramer *et al.*, 2004, 2006; Lattimer and Schutz, 2005; Morrison *et al.*, 2004). This could be another route to constraining the compactness of a neutron star, and perhaps gaining evidence for or against a step in the density profile of this star.

C. Cooling

The avenues of investigation that we have described so far may constrain the possible existence of quark matter within neutron star cores, but they are not sensitive to the differences among different color superconducting phases of quark matter. We turn now to the first of three observational signatures that have the potential to differentiate between CFL quark matter and other color superconducting phases.

Within less than a minute of its birth in a supernova, a neutron star cools below about 1 MeV and becomes transparent to neutrinos. For the next million years or so it cools mainly via neutrino emission from its interior. Photon emission from the surface becomes dominant only later than that. This means that information about properties of the interior, in particular its neutrino emissivity and heat capacity, can be inferred from measurements of the temperature and age of neutron stars. Because all forms of dense matter are good heat conductors (Shovkovy and Ellis, 2002), neutron star interiors are isothermal and the rate at which they cool is determined by the volume integrals over the entire interior of the local emissivity and the local specific heat. This means that the cooling tends to be dominated by the properties of whichever phase has the highest neutrino

emissivity and whichever phase has the highest specific heat.

Different forms of dense matter fall into three categories, ordered by decreasing neutrino emissivity. The first category includes any phase of matter that can emit neutrinos via direct Urca processes, yielding an emissivity $\epsilon_\nu \propto T^6$. Examples include unpaired quark matter, phases of quark matter with some unpaired quarks including the crystalline phases and the phases with single flavor pairing in Table III, baryonic matter containing hyperons, nucleonic matter augmented by either a pion or a kaon condensate, and even ordinary nuclear matter at sufficiently high densities that the proton fraction exceeds about 0.1. For the specific case of unpaired quark matter, the emissivity is given by (157) (Iwamoto, 1980, 1982), which can be written as

$$\epsilon_\nu \simeq (4 \times 10^{25} \text{ erg cm}^{-3} \text{ s}^{-1}) \times \frac{\alpha_s}{0.5} \left(\frac{M_s^2/\mu}{100 \text{ MeV}} \right) \left(\frac{\mu}{500 \text{ MeV}} \right)^2 \left(\frac{T}{10^9 \text{ K}} \right)^6 \quad (163)$$

where we have taken $\mu_e = M_s^2/(4\mu)$, appropriate for neutral unpaired quark matter. (Note that $\alpha_s \sim 0.5$ is comparable to the value $c \sim 0.3$ that we used in Sec. VIII.A, according to the lowest order relation $c = 2\alpha_s/\pi$. The $\alpha_s/0.5$ factor in (163) could be replaced by $c/0.3$.) The emissivity of other phases of quark matter in which only some quarks are unpaired, including the crystalline phases, is reduced relative to (163), but only by factors of order unity.

Ordinary nuclear matter at densities not too far above n_0 , where the proton fraction is less than 0.1, falls into a second category in which there is no phase space for direct Urca processes and neutrino emission occurs only via modified Urca processes like $n + X \rightarrow p + X + e + \bar{\nu}$ with X some spectator nucleon, giving the much lower emissivity

$$\epsilon_\nu^{nm} = (1.2 \times 10^{20} \text{ erg cm}^{-3} \text{ s}^{-1}) \left(\frac{n}{n_0} \right)^{2/3} \left(\frac{T}{10^9 \text{ K}} \right)^8 \quad (164)$$

Neutron stars whose interiors emit neutrinos at this rate, perhaps modified by effects of nucleon superfluidity, cool following a family of standard cooling curves (see Page *et al.*, 2004; Yakovlev *et al.*, 2001, 2005) and references therein), taking 10^5 to 10^6 years to cool below 10^8 K.

CFL quark matter constitutes a third category. As we have seen in Sec. VII, it is unique among all phases of dense matter in having an emissivity $\propto T^{15}$ that is many orders of magnitude smaller than (164). Furthermore, whereas all other phases of dense matter have a specific heat $\propto T$, in the CFL phase the specific heat is controlled by bosonic excitations making it $\propto T^3$. This means that if a neutron star has a CFL core, the total neutrino emissivity and the total heat capacity of the star are both utterly dominated by the contributions of the outer layers, whether these are made of nuclear matter

or of some phase that admits direct Urca reactions. The CFL core holds little heat, and emits few neutrinos, but is a good conductor and so stays at the same temperature as the rest of the star. The rest of the star controls how the star cools.

Finally, the single-flavor color superconducting phases are interesting because they represent a potential transition from the first to the third categories (Aguilera *et al.*, 2005; Grigorian *et al.*, 2005): their critical temperatures are so low that if some quarks can only pair in spin-one channels, they will not pair until after the star has cooled through an initial epoch of direct Urca emission; and, in certain cases (Aguilera *et al.*, 2005; Marhauser *et al.*, 2007; Schmitt *et al.*, 2006) all quarks can be gapped below the critical temperature for color-spin locked pairing, meaning that these phases ultimately become like CFL quark matter, playing no role in the cooling of the star which at late times will be controlled by the modified Urca processes in the nuclear matter mantle.

We can now describe a possible future path to the discovery of CFL quark matter cores within neutron stars. Suppose that LIGO detects the gravitational waves from the tidal disruption of a neutron star with some known mass spiralling into a black hole and, as we discussed in Sec. VIII.B, suppose that evidence is found that the density profile of the neutron star has a denser core within a less dense mantle, consistent with the existence of a step in the density profile. Suppose furthermore that it was understood by then that neutron stars with that mass cool following one of the family of standard cooling curves, meaning that there can be no component of their interior within which direct Urca processes are allowed at any time. This combination of observations would rule out the possibility that the dense core, inside the density step, contained any of the color superconducting phases that we have discussed except CFL.

The scenario above may be unlikely, because there are a growing number of lines of evidence that although the cooling of many neutron stars is broadly consistent with the standard cooling curves, some fraction of neutron stars cool much more quickly. Examples of neutron stars that are too cold for their age include those in the supernova remnants 3C58 and CTA1 (Page *et al.*, 2004; Page and Reddy, 2006). A second, less direct, piece of evidence is provided by an unsuccessful search for the X-ray emission from a cooling neutron star in 15 other supernova remnants (Kaplan, 2007; Kaplan *et al.*, 2006, 2004). Although some of these supernovae may have been Type IA supernovae which do not produce neutron stars, and although some may have produced black holes, it is likely that many of these supernovae remnants do contain neutron stars. Their nonobservation results in an upper limit on their temperatures, and in all cases this upper limit falls below the standard cooling curves. A third line of evidence comes from neutron stars that undergo transient bouts of accretion (Brown *et al.*, 1998). X-ray observations of one of these, SAX J1808.4-3658, during its quiescent phase yield an upper limit on the thermal

luminosity of the neutron star (Heinke *et al.*, 2007). The mean accretion rate averaged over many transient accretion episodes is known, meaning that the average accretion heating of the star is known. The fact that the thermal luminosity is as low as it is means that the accretion heating of the star must be balanced by cooling by neutrino emission at a rate that far exceeds (164). The emissivity for unpaired quark matter (157) is consistent with the data, as are the direct Urca rates for sufficiently dense nuclear matter and for hyperon matter. Pion condensation or kaon condensation yield emissivities that are proportional to T^6 but with prefactors that are about two orders of magnitude smaller than that in (157), and are ruled out as explanations for the ability of SAX J1808.4-3658 to keep cool (Heinke *et al.*, 2007). Similar conclusions can also be inferred from the (even lower) limit on the quiescent luminosity of the soft X-ray transient 1H 1905+000 (Chakrabarty, 2007; Jonker *et al.*, 2007, 2006), although in this instance the time-averaged accretion rate is not as well known.

By now it certainly seems clear that some neutron stars cool much faster than others. It is then reasonable to speculate that lighter neutron stars cool following the standard cooling curve and are composed of nuclear matter throughout whereas, based on the three lines of evidence above, heavier neutron stars cool faster because they contain some form of dense matter that can radiate neutrinos via the direct Urca process. This could be quark matter in one of the non-CFL color superconducting phases, but there are other, baryonic, possibilities. If this speculation is correct, then if neutron stars contain CFL cores they must be “inner cores”, within an outer core made of whatever is responsible for the rapid neutrino emission.

D. r -modes limiting pulsar spins

A rapidly spinning neutron star will quickly slow down if it is unstable with respect to bulk flows known as Rossby modes, or r -modes, whose restoring force is due to the Coriolis effect and which transfer the star’s angular momentum into gravitational radiation (Andersson, 1998; Andersson and Comer, 2001; Andersson *et al.*, 1999a,b; Friedman and Morsink, 1998). For any given interior composition and temperature, above some critical spin frequency there is an instability which leads to an exponentially growing r -mode. This means that as a neutron star is spun up by accretion, its spin will be limited by a value very slightly above this critical frequency, at which the accretion torque is balanced by gravitational radiation from the r -mode flows (Andersson *et al.*, 1999a,b; Bildsten, 1998; Lindblom *et al.*, 1998; Owen *et al.*, 1998). From a microphysical point of view, the r -mode instability is limited by viscous damping: the greater the damping, the higher the critical spin above which r -modes become unstable. The critical frequency is controlled by the shear viscos-

ity in some regimes of temperature (typically lower) and by the bulk viscosity in others (typically higher). This means that the existence of pulsars with a given spin, as well as any observational evidence for an upper limit on pulsar spins, can yield constraints on the viscosities of neutron star interiors.

There is observational evidence for a physical limit on pulsar spins. The fastest known pulsar is a recently discovered radio pulsar spinning at 716 Hz (Hessels *et al.*, 2006). However, it is not easy to draw inferences from the distribution of spins of the many known radio pulsars as to whether 716 Hz is close to some physical limit on the spin frequency because there are significant observational biases that make it harder to find faster radio pulsars. The most rapid pulsars are “recycled”, meaning that they were spun-up during an episode of accretion from a binary companion. During such accretion, a neutron star may be visible as an X-ray pulsar. The spin frequencies of the 13 known millisecond X-ray pulsars lie between 270 and 619 Hz. What makes this significant is first of all that the episodes of accretion have long enough durations that they could easily spin a neutron star up beyond 1000 Hz, and second of all that there are no selection biases that preclude the discovery of X-ray pulsars with frequencies as large as 2000 Hz (Chakrabarty, 2004; Chakrabarty *et al.*, 2003). Analysis of the observed distribution of X-ray pulsar spin frequencies leads to two conclusions: first, the distribution is consistent with being uniform;⁷ and, second, there is some physical effect that sets a limit on the allowed spin of a pulsar which (with 95% confidence) is at 730 Hz or lower (Chakrabarty, 2004; Chakrabarty *et al.*, 2003). It is unlikely that a spin-limit in this vicinity can be attributed to centrifugal break-up of the spinning neutron star: unless neutron star radii are larger than anticipated, this “mass shedding limit” is significantly higher, above 1 kHz. On the other hand, if the observed limit on pulsar spin frequencies is attributed to the onset of the r -mode instability, the resulting constraint on the viscosities of neutron star interiors is broadly consistent with the viscosities of nuclear matter, although this consistency is somewhat loose given the

⁷ These data thus rule out a proposal for how small quark matter cores could have been detected (Glendenning and Weber, 2001). If slowly-rotating neutron stars just barely reach quark-matter densities in their center, then rapidly spinning oblate neutron stars, which have slightly lower central density, will not contain quark matter. This “spinning out” of a quark matter core could be detected either by anomalies in braking indices of radio pulsars that are slowing down (Glendenning *et al.*, 1997) or by anomalous population statistics of X-ray pulsars that are being spun up by accretion (Glendenning and Weber, 2001). The data on X-ray pulsars show no sign of such an effect (Chakrabarty, 2004; Chakrabarty *et al.*, 2003) indicating that, if quark matter is present, spinning the star and making it oblate does not get rid of it. If neutron stars do have quark matter cores, therefore, the quark matter must occupy a reasonable fraction of the star.

uncertainties in neutron star densities and in their temperatures while being spun up (Andersson *et al.*, 1999b; Levin and Ushomirsky, 2001).

The physics of the r -mode instability definitively rules out the possibility that accreting X-ray binary pulsars are strange stars that are composed of CFL quark matter throughout (Madsen, 2000). From the results of Sec. VII, we can conclude that CFL quark matter has negligible shear damping, and significantly smaller bulk viscosity than nuclear matter. (See (Haensel *et al.*, 2000, 2001a; Sawyer, 1989), for calculations of bulk viscosity in nuclear matter, (Haensel *et al.*, 2001b; Lindblom and Owen, 2002) for baryonic matter containing hyperons, and (Chatterjee and Bandyopadhyay, 2007) for baryonic matter containing a kaon condensate.) A CFL strange star would therefore have a critical frequency at which the r -mode instability sets in measured in Hz or fractions of Hz, in gross disagreement with the data on spin frequencies of both X-ray and radio pulsars.⁸

It is a very interesting question, at present unresolved, whether the presence of a CFL quark matter core within an ordinary neutron star introduces unstable r -modes at low spin frequencies. If there is a density step at the nuclear/CFL interface, there may be oscillation modes localized near that interface. The question is whether there are r -modes that are sufficiently well localized on the CFL side of the interface that they are undamped, or whether the tails of the mode wave functions that extend into the nuclear matter side of the interface result in enough damping to prevent the modes from becoming unstable. Nobody has solved for the r -mode wave functions for a rotating star whose density profile has a step at an interface, with viscous dissipation occurring on one side of the interface only.⁹ If it were to turn out that a star with a CFL core is even close to as unstable with respect to r -modes as a star that is made entirely of CFL matter, the existence of pulsars spinning with hundreds of Hz frequencies would immediately rule out the possibility that these neutron stars have CFL cores.

E. Supernova neutrinos

The only time when a neutron star emits enough neutrinos to be detectable on earth as a neutrino source is during the first few seconds after the supernova explosion. The time-of-arrival distribution of supernova neutrinos could teach us about possible phase transitions to CFL quark matter (Carter and Reddy, 2000; Jaikumar *et al.*, 2002; Kundu and Reddy, 2004; Reddy *et al.*, 2003a,b). All phases of quark matter and nuclear matter except

CFL have short enough mean free paths that the neutrinos detected from a supernova are emitted from a surface of last scattering called the neutrinosphere, inside of which they were diffusing. This surface of last scattering moves inward to higher densities during the first seconds after the supernova, as the protoneutron star cools. Suppose that a volume in the core of the protoneutron star has made a transition into the CFL phase, in which neutrinos scatter only off Goldstone bosons which are less numerous (number density $\propto T^3$ rather than $\propto \mu^2 T$ for ungapped quark excitations). As this core cools, the neutrino mean free path within a CFL core becomes longer than in any phase of matter in which there are unpaired quarks (or nucleons) off which the neutrinos can scatter. The last supernova neutrinos to arrive could carry information about conditions when the neutrinosphere reaches the CFL core. Perhaps there may even be enhanced neutrino luminosity at the end of an otherwise dropping time-of-arrival distribution, as all those neutrinos that were previously trapped within the transparent core fly out unimpeded (Carter and Reddy, 2000). Determining whether this proposed signature can arise requires implementing the transition to a CFL core, with its long neutrino mean free paths, within a full-fledged simulation of neutrino transport during a supernova.

F. Rigid quark matter and pulsar glitches

The existence of a rigid crystalline color superconducting core within neutron stars may have a variety of observable consequences. For example, if some agency (like magnetic fields not aligned with the rotation axis) could maintain the rigid core in a shape that has a nonzero quadrupole moment, gravity waves would be emitted. The LIGO non-detection of such gravity waves from nearby neutron stars (Abbott *et al.*, 2007) already limits the possibility that they have rigid cores that are deformed to the maximum extent allowed by the shear modulus (165), upon assuming a range of possible breaking strains, and this constraint will tighten as LIGO continues to run (Haskell *et al.*, 2007; Lin, 2007). (The analogous constraint on strange stars that are rigid throughout was obtained in (Owen, 2005).) Perhaps the most exciting implication of a rigid core, however, is the possibility that (some) pulsar “glitches” could originate deep within a neutron star, in its quark matter core.

A spinning neutron star observed as a pulsar gradually spins down as it loses rotational energy to electromagnetic radiation. But, every once in a while the angular velocity at the crust of the star is observed to increase suddenly in a dramatic event called a glitch. The standard explanation (Alpar, 1977; Alpar *et al.*, 1984a, 1996, 1984b; Anderson and Itoh, 1975; Epstein and Baym, 1992; Jones, 1997; Link and Epstein, 1996; Link *et al.*, 1993; Pines and Alpar, 1985) requires the presence of a superfluid in some region of the star which also features a rigid array of spatial inhomogeneities which can pin the

⁸ Strange stars made of unpaired quark matter or of 2SC quark matter can be consistent with the data (Madsen, 2000).

⁹ Certain other oscillation modes (“f-modes” and “g-modes”) of a nonrotating neutron star whose density profile includes a density step have been computed (Sotani *et al.*, 2002).

vortices in the rotating superfluid. In the standard explanation of pulsar glitches, these conditions are met in the inner crust of a neutron star which features a neutron superfluid coexisting with a rigid array of positively charged nuclei that may serve as vortex pinning sites. We shall see below that a rigid core made of crystalline color superconducting quark matter also meets the basic requirements.

The viability of the standard scenario for the origin of pulsar glitches in neutron star crusts has recently been questioned (Link, 2007a). Explaining the issue requires understanding how the basic requirements come into play in the generation of a glitch. As a spinning pulsar slowly loses angular momentum over years, since the angular momentum of any superfluid component of the star is proportional to the density of vortices the vortices “want” to move apart. However, if within the inner crust the vortices are pinned to a rigid structure, these vortices do not move and after a time this superfluid component of the star is spinning faster than the rest of the star. When the “tension” built up in the array of pinned vortices reaches a critical value, there is a sudden “avalanche” in which vortices unpin, move outwards reducing the angular momentum of the superfluid, *and then re-pin*. As this superfluid suddenly loses angular momentum, the rest of the star, including in particular the surface whose angular velocity is observed, speeds up — a glitch. We see that this scenario requires superfluidity coexisting with a rigid structure to which vortices can pin that does not easily deform when vortices pinned to it are under tension. In very recent work, Link has questioned whether this scenario is viable because once neutron vortices are moving through the inner crust, as must happen during a glitch, they are so resistant to bending that they may never re-pin (Link, 2007a). Link concludes that we do not have an understanding of any dynamics that could lead to the re-pinning of moving vortices, and hence that we do not currently understand glitches as a crustal phenomenon.

We have seen in Sec. VI.B that if neutron star cores are made of quark matter but Δ_{CFL} is not large enough for this quark matter to be in the CFL phase, then all of the quark matter core — and hence a significant fraction of the moment of inertia of the star — may be in one of the crystalline phases described in Sec. VI.B. By virtue of being simultaneously superfluids and rigid solids, the crystalline phases of quark matter provide all the necessary conditions to be the locus in which (some) pulsar glitches originate. Their shear moduli (141), namely

$$\nu = 3.96 \times 10^{33} \text{erg/cm}^3 \left(\frac{\Delta}{10 \text{ MeV}} \right)^2 \left(\frac{\mu}{400 \text{ MeV}} \right)^2 \quad (165)$$

with Δ the gap parameter in the crystalline phase as in Fig. 10, make this form of quark matter 20 to 1000 times more rigid than the crust of a neutron star (Mannarelli *et al.*, 2007; Strohmayer *et al.*, 1991), and hence more than rigid enough for glitches to origi-

nate within them. The crystalline phases are at the same time superfluid, and it is reasonable to expect that the superfluid vortices that will result when a neutron star with such a core rotates will have lower free energy if they are centered along the intersections of the nodal planes of the underlying crystal structure, i.e. along lines along which the condensate already vanishes even in the absence of a rotational vortex. A crude estimate of the pinning force on vortices within crystalline color superconducting quark matter indicates that it is sufficient (Mannarelli *et al.*, 2007). So, the basic requirements for superfluid vortices pinning to a rigid structure are all present. The central questions that remain to be addressed are the explicit construction of vortices in the crystalline phase and the calculation of their pinning force, as well as the calculation of the timescale over which sudden changes in the angular momentum of the core are communicated to the (observed) surface, presumably either via the common electron fluid or via magnetic stresses.

Much theoretical work remains before the hypothesis that pulsar glitches originate within a crystalline color superconducting neutron star core is developed fully enough to allow it to confront data on the magnitudes, relaxation timescales, and repeat rates that characterize glitches. Nevertheless, this hypothesis offers one immediate advantage over the conventional scenario that relied on vortex pinning in the neutron star crust. It is impossible for a neutron star anywhere within which rotational vortices are pinned to precess on \sim year time scales (Link, 2006, 2007b; Sedrakian *et al.*, 1999), and yet there is now evidence that several pulsars are precessing (Chukwude *et al.*, 2003; Shabanova *et al.*, 2001; Stairs *et al.*, 2000). Since *all* neutron stars have crusts, the precession of any pulsar is inconsistent with the pinning of vortices within the crust, a requirement in the standard explanation of glitches. On the other hand, perhaps not all neutron stars have crystalline quark matter cores — for example, perhaps the lightest neutron stars have nuclear matter cores. Then, if vortices are never pinned in the crust but are pinned within a crystalline quark matter core, those neutron stars that do have a crystalline quark matter core can glitch but cannot precess while those that don’t can precess but cannot glitch.

Acknowledgments

We acknowledge helpful conversations with N. Andersson, M. Braby, D. Chakrabarty, T. Hatsuda, S. Hughes, D.L. Kaplan, B. Link, M. Mannarelli, C. Manuel, D. Nice, D. Page, A. Rebhan, S. Reddy, R. Sharma, I. Stairs, Q. Wang, and F. Wilczek. This research was supported in part by the Offices of Nuclear Physics and High Energy Physics of the Office of Science of the U.S. Department of Energy under contracts #DE-FG02-91ER40628, #DE-FG02-05ER41375 (OJI), #DE-FG02-94ER40818, #DE-FG02-03ER41260.

References

- Abbott, B., *et al.* (LIGO Scientific), 2007, Phys. Rev. **D76**, 042001.
- Abrikosov, A., L. Gorkov, and I. Dzyaloshinski, 1963, *Methods of Quantum field theory in statistical physics* (Prentice-Hall, Inc., Englewood Cliffs, N.J.).
- Abuki, H., 2003, Prog. Theor. Phys. **110**, 937.
- Abuki, H., T. Hatsuda, and K. Itakura, 2002, Phys. Rev. **D65**, 074014.
- Abuki, H., M. Kitazawa, and T. Kunihiro, 2005, Phys. Lett. **B615**, 102.
- Abuki, H., and T. Kunihiro, 2006, Nucl. Phys. **A768**, 118.
- Aguilera, D. N., 2007, Astrophys. Space Sci. **308**, 443.
- Aguilera, D. N., D. Blaschke, M. Buballa, and V. L. Yudichev, 2005, Phys. Rev. **D72**, 034008.
- Akmal, A., V. R. Pandharipande, and D. G. Ravenhall, 1998, Phys. Rev. **C58**, 1804.
- Alcock, C., E. Farhi, and A. Olinto, 1986, Astrophys. J. **310**, 261.
- Alcock, C., and A. Olinto, 1988, Ann. Rev. Nucl. Part. Sci. **38**, 161.
- Alford, M. G., 2001, Ann. Rev. Nucl. Part. Sci. **51**, 131.
- Alford, M. G., J. Berges, and K. Rajagopal, 1999a, Nucl. Phys. **B558**, 219.
- Alford, M. G., J. Berges, and K. Rajagopal, 2000a, Phys. Rev. Lett. **84**, 598.
- Alford, M. G., J. Berges, and K. Rajagopal, 2000b, Nucl. Phys. **B571**, 269.
- Alford, M. G., J. A. Bowers, J. M. Cheyne, and G. A. Cowan, 2003, Phys. Rev. **D67**, 054018.
- Alford, M. G., J. A. Bowers, and K. Rajagopal, 2001a, Phys. Rev. **D63**, 074016.
- Alford, M. G., M. Braby, M. W. Paris, and S. Reddy, 2005a, Astrophys. J. **629**, 969.
- Alford, M. G., M. Braby, S. Reddy, and T. Schäfer, 2007a, Phys. Rev. **C75**, 055209.
- Alford, M. G., M. Braby, and A. Schmitt, 2007b, eprint arXiv:0707.2389 [nucl-th].
- Alford, M. G., and G. A. Cowan, 2006, J. Phys. **G32**, 511.
- Alford, M. G., and G. Good, 2004, Phys. Rev. **D70**, 036008.
- Alford, M. G., P. Jotwani, C. Kouvaris, J. Kundu, and K. Rajagopal, 2005b, Phys. Rev. **D71**, 114011.
- Alford, M. G., C. Kouvaris, and K. Rajagopal, 2004a, eprint hep-ph/0407257.
- Alford, M. G., C. Kouvaris, and K. Rajagopal, 2004b, Phys. Rev. Lett. **92**, 222001.
- Alford, M. G., C. Kouvaris, and K. Rajagopal, 2005c, Phys. Rev. **D71**, 054009.
- Alford, M. G., and K. Rajagopal, 2002, JHEP **06**, 031.
- Alford, M. G., and K. Rajagopal, 2006, in *Pairing in Fermionic Systems: Basic Concepts and Modern Applications* (World Scientific), pp. 1–36, eprint hep-ph/0606157.
- Alford, M. G., K. Rajagopal, S. Reddy, and A. W. Steiner, 2006, Phys. Rev. **D73**, 114016.
- Alford, M. G., K. Rajagopal, S. Reddy, and F. Wilczek, 2001b, Phys. Rev. **D64**, 074017.
- Alford, M. G., K. Rajagopal, and F. Wilczek, 1998, Phys. Lett. **B422**, 247.
- Alford, M. G., K. Rajagopal, and F. Wilczek, 1999b, Nucl. Phys. **B537**, 443.
- Alford, M. G., and S. Reddy, 2003, Phys. Rev. **D67**, 074024.
- Alford, M. G., and A. Schmitt, 2007, J. Phys. **G34**, 67.
- Alford, M. G., and Q.-h. Wang, 2005, J. Phys. **G31**, 719.
- Alford, M. G., and Q.-h. Wang, 2006, J. Phys. **G32**, 63.
- Alles, B., M. D’Elia, and M. P. Lombardo, 2006, Nucl. Phys. **B752**, 124.
- Alpar, M. A., 1977, Astrophys. J. **213**, 527.
- Alpar, M. A., P. W. Anderson, D. Pines, and J. Shaham, 1984a, Astrophys. J. **278**, 791.
- Alpar, M. A., H. F. Chau, K. S. Cheng, and D. Pines, 1996, Astrophys. J. **459**, 706.
- Alpar, M. A., S. A. Langer, and J. A. Sauls, 1984b, Astrophys. J. **282**, 533.
- Amore, P., M. C. Birse, J. A. McGovern, and N. R. Walet, 2002, Phys. Rev. **D65**, 074005.
- Anand, J. D., N. Chandrika Devi, V. K. Gupta, and S. Singh, 2000, Pramana **54**, 737.
- Anderson, P. W., 1963, Phys. Rev. **130**, 439.
- Anderson, P. W., and N. Itoh, 1975, Nature **256**, 25.
- Andersson, N., 1998, Astrophys. J. **502**, 708.
- Andersson, N., and G. L. Comer, 2001, Mon. Not. Roy. Astron. Soc. **328**, 1129.
- Andersson, N., and G. L. Comer, 2006, eprint gr-qc/0605010.
- Andersson, N., K. D. Kokkotas, and B. F. Schutz, 1999a, Astrophys. J. **510**, 846.
- Andersson, N., K. D. Kokkotas, and N. Stergioulas, 1999b, Astrophys. J. **516**, 307.
- Andreev, A. F., and I. M. Lifshitz, 1969, Sov. Phys. JETP **29**, 2057.
- Anglani, R., R. Gatto, N. D. Ippolito, G. Nardulli, and M. Ruggieri, 2007, eprint arXiv:0706.1781 [hep-ph].
- Anglani, R., G. Nardulli, M. Ruggieri, and M. Mannarelli, 2006, Phys. Rev. **D74**, 074005.
- Anselmino, M., E. Predazzi, S. Ekelin, S. Fredriksson, and D. B. Lichtenberg, 1993, Rev. Mod. Phys. **65**, 1199.
- Bahcall, J. N., and R. A. Wolf, 1965, Phys. Rev. **B140**, 1452.
- Bailin, D., and A. Love, 1979, J. Phys. **A12**, L283.
- Bailin, D., and A. Love, 1984, Phys. Rept. **107**, 325.
- Balachandran, A. P., S. Digal, and T. Matsuura, 2006, Phys. Rev. **D73**, 074009.
- Baldo, M., *et al.*, 2003, Phys. Lett. **B562**, 153.
- Bardeen, J., L. Cooper, and J. Schrieffer, 1957, Phys. Rev. **106**, 162.
- Barducci, A., R. Casalbuoni, G. Pettini, and L. Ravagli, 2004, Phys. Rev. **D69**, 096004.
- Barrois, B. C., 1977, Nucl. Phys. **B129**, 390.
- Barrois, B. C., 1979, *Non-perturbative effects in dense quark matter*, Ph.D. thesis, California Institute of Technology, Pasadena, California, UMI 79-04847.
- Barziv, O., L. Kaper, M. H. van Kerkwijk, J. H. Telling, and J. van Paradijs, 2001, Astron. Astrophys. **377**, 925.
- Baym, G., 1962, Phys. Rev. **127**, 1391.
- Baym, G., and D. K. Campbell, 1978, in *Mesons in Nuclei*, ed. M. Rho, D. Wilkinson, Vol III, 1031. Amsterdam: North Holland.
- Baym, G., H. Monien, C. J. Pethick, and D. G. Ravenhall, 1990, Phys. Rev. Lett. **64**, 1867.
- Beane, S. R., P. F. Bedaque, and M. J. Savage, 2000, Phys. Lett. **B483**, 131.
- Beane, S. R., P. F. Bedaque, and M. J. Savage, 2001, Nucl. Phys. **A688**, 931.
- Bedaque, P. F., H. Caldas, and G. Rupak, 2003, Phys. Rev. Lett. **91**, 247002.
- Bedaque, P. F., and T. Schäfer, 2002, Nucl. Phys. **A697**, 802.
- Berges, J., and K. Rajagopal, 1999, Nucl. Phys. **B538**, 215.
- Bildsten, L., 1998, Astrophys. J. **501**, L89.

- Blaschke, D., S. Fredriksson, H. Grigorian, A. M. Oztas, and F. Sandin, 2005, *Phys. Rev.* **D72**, 065020.
- Blaschke, D. B., D. Gomez Dumm, A. G. Grunfeld, T. Klahn, and N. N. Scoccola, 2007, *Phys. Rev.* **C75**, 065804.
- Boccaletti, D., V. de Sabbata, and C. Gualdi, 1966, *Nuovo Cim.* **45**, 513.
- Bodmer, A. R., 1971, *Phys. Rev.* **D4**, 1601.
- Bowers, J. A., J. Kundu, K. Rajagopal, and E. Shuster, 2001, *Phys. Rev.* **D64**, 014024.
- Bowers, J. A., and K. Rajagopal, 2002, *Phys. Rev.* **D66**, 065002.
- Boyunovsky, D., and H. J. de Vega, 2001a, *Phys. Rev.* **D63**, 034016.
- Boyunovsky, D., and H. J. de Vega, 2001b, *Phys. Rev.* **D63**, 114028.
- Braaten, E., and R. D. Pisarski, 1992, *Phys. Rev.* **D45**, 1827.
- Brown, E. F., L. Bildsten, and R. E. Rutledge, 1998, *Astrophys. J. Lett.* **504**, L95.
- Brown, G. E., 1995, in *Bose-Einstein Condensation*, ed. A. Griffin, et al. 438. Cambridge: Cambridge University Press.
- Brown, W. E., J. T. Liu, and H.-c. Ren, 2000a, *Phys. Rev.* **D62**, 054013.
- Brown, W. E., J. T. Liu, and H.-c. Ren, 2000b, *Phys. Rev.* **D61**, 114012.
- Brown, W. E., J. T. Liu, and H.-c. Ren, 2000c, *Phys. Rev.* **D62**, 054016.
- Buballa, M., 2005a, *Phys. Rept.* **407**, 205.
- Buballa, M., 2005b, *Phys. Lett.* **B609**, 57.
- Buballa, M., J. Hosek, and M. Oertel, 2003, *Phys. Rev. Lett.* **90**, 182002.
- Buballa, M., and M. Oertel, 2002, *Nucl. Phys.* **A703**, 770.
- Buballa, M., and I. A. Shovkovy, 2005, *Phys. Rev.* **D72**, 097501.
- Burgay, M., *et al.*, 2003, *Nature*. **426**, 531.
- Carlson, J., and S. Reddy, 2005, *Phys. Rev. Lett.* **95**, 060401.
- Carter, G. W., and D. Diakonov, 1999, *Phys. Rev.* **D60**, 016004.
- Carter, G. W., and S. Reddy, 2000, *Phys. Rev.* **D62**, 103002.
- Casalbuoni, R., M. Ciminale, R. Gatto, G. Nardulli, and M. Ruggieri, 2006, *Phys. Lett.* **B642**, 350.
- Casalbuoni, R., E. Fabiano, R. Gatto, M. Mannarelli, and G. Nardulli, 2002a, *Phys. Rev.* **D66**, 094006.
- Casalbuoni, R., and R. Gatto, 1999, *Phys. Lett.* **B464**, 111.
- Casalbuoni, R., R. Gatto, N. Ippolito, G. Nardulli, and M. Ruggieri, 2005a, *Phys. Lett.* **B627**, 89.
- Casalbuoni, R., R. Gatto, M. Mannarelli, and G. Nardulli, 2001a, *Phys. Lett.* **B511**, 218.
- Casalbuoni, R., R. Gatto, M. Mannarelli, and G. Nardulli, 2002b, *Phys. Lett.* **B524**, 144.
- Casalbuoni, R., R. Gatto, M. Mannarelli, G. Nardulli, and M. Ruggieri, 2005b, *Phys. Lett.* **B605**, 362.
- Casalbuoni, R., R. Gatto, and G. Nardulli, 2001b, *Phys. Lett.* **B498**, 179.
- Casalbuoni, R., R. Gatto, and G. Nardulli, 2002c, *Phys. Lett.* **B543**, 139.
- Casalbuoni, R., and G. Nardulli, 2004, *Rev. Mod. Phys.* **76**, 263.
- Casalbuoni, R., *et al.*, 2003, *Phys. Lett.* **B575**, 181.
- Casalbuoni, R., *et al.*, 2004, *Phys. Rev.* **D70**, 054004.
- Chakrabarty, D., 2004, 279, in *Binary Radio Pulsars*, ed. F. A. Rasio and I. H. Stairs, (San Francisco: Astron. Soc. Pacific Conf. 328), eprint astro-ph/0408004.
- Chakrabarty, D., 2007, private communication.
- Chakrabarty, D., *et al.*, 2003, *Nature* **424**, 42.
- Chakravarty, S., R. E. Norton, and O. F. Syljuasen, 1995, *Phys. Rev. Lett.* **75**, 1423.
- Chandrasekhar, B. S., 1962, *Appl. Phys. Lett.* **1**, 7.
- Chatterjee, D., and D. Bandyopadhyay, 2007, *Phys. Rev.* **D75**, 123006.
- Chester, G. V., 1970, *Phys. Rev.* **A2**, 256.
- Chin, Y., M. W. Zwiernik, C. H. Schunck, A. Schirotzek, and W. Ketterle, 2006, *Phys. Rev. Lett.* **97**, 030401.
- Chukwude, A. E., A. A. Ubachukwu, and P. N. Okeke, 2003, *Astron. Astrophys.* **399**, 231.
- Ciminale, M., G. Nardulli, M. Ruggieri, and R. Gatto, 2006, *Phys. Lett.* **B636**, 317.
- Clogston, A. M., 1962, *Phys. Rev. Lett.* **9**, 266.
- Close, F. E., and N. A. Tornqvist, 2002, *J. Phys.* **G28**, R249.
- Collins, J. C., and M. J. Perry, 1975, *Phys. Rev. Lett.* **34**, 1353.
- Cornwall, J. M., R. Jackiw, and E. Tomboulis, 1974, *Phys. Rev.* **D10**, 2428.
- Deryagin, D. V., D. Y. Grigoriev, and V. A. Rubakov, 1992, *Int. J. Mod. Phys.* **A7**, 659.
- Dietrich, D. D., and D. H. Rischke, 2004, *Prog. Part. Nucl. Phys.* **53**, 305.
- Dong, H., N. Su, and Q. Wang, 2007, *Phys. Rev.* **D75**, 074016.
- Ebert, D., and K. G. Klimenko, 2007, *Phys. Rev.* **D75**, 045005.
- Ebert, D., K. G. Klimenko, and V. L. Yudichev, 2007, eprint arXiv:0705.2666 [hep-ph].
- Epstein, R. I., and G. Baym, 1992, *Astrophys. J.* **387**, 276.
- Evans, N. J., J. Hormuzdiar, S. D. H. Hsu, and M. Schwetz, 2000, *Nucl. Phys.* **B581**, 391.
- Evans, N. J., S. D. H. Hsu, and M. Schwetz, 1999a, *Nucl. Phys.* **B551**, 275.
- Evans, N. J., S. D. H. Hsu, and M. Schwetz, 1999b, *Phys. Lett.* **B449**, 281.
- Faber, J. A., P. Grandclement, F. A. Rasio, and K. Taniguchi, 2002, *Phys. Rev. Lett.* **89**, 231102.
- Farhi, E., and R. L. Jaffe, 1984, *Phys. Rev.* **D30**, 2379.
- Feng, B., D.-f. Hou, J.-r. Li, and H.-c. Ren, 2006, *Nucl. Phys.* **B754**, 351.
- Ferrer, E. J., and V. de la Incera, 2007a, eprint arXiv:0705.2403 [hep-ph].
- Ferrer, E. J., and V. de la Incera, 2007b, eprint nucl-th/0703034.
- Ferrer, E. J., V. de la Incera, and C. Manuel, 2005, *Phys. Rev. Lett.* **95**, 152002.
- Ferrer, E. J., V. de la Incera, and C. Manuel, 2006, *Nucl. Phys.* **B747**, 88.
- Fetter, A., and J. Walecka, 1971, *Quantum theory of many-particle systems* (McGraw-Hill, New York).
- Forbes, M. M., 2005, *Phys. Rev.* **D72**, 094032.
- Forbes, M. M., and A. R. Zhitnitsky, 2002, *Phys. Rev.* **D65**, 085009.
- Fraga, E. S., R. D. Pisarski, and J. Schaffner-Bielich, 2001, *Phys. Rev.* **D63**, 121702.
- Frautschi, S. C., 1978, presented at Workshop on Hadronic Matter at Extreme Energy Density, Erice, Italy, Oct 13-21, 1978.
- Friedman, J. L., and R. R. Caldwell, 1991, *Phys. Lett.* **B264**, 143.
- Friedman, J. L., and S. M. Morsink, 1998, *Astrophys. J.* **502**, 714.
- Fukushima, K., 2005, *Phys. Rev.* **D72**, 074002.
- Fukushima, K., 2006, *Phys. Rev.* **D73**, 094016.

- Fukushima, K., and K. Iida, 2005, Phys. Rev. **D71**, 074011.
- Fukushima, K., and K. Iida, 2007, eprint arXiv:0705.0792 [hep-ph].
- Fukushima, K., C. Kouvaris, and K. Rajagopal, 2005, Phys. Rev. **D71**, 034002.
- Fukushima, K., and H. J. Warringa, 2007, eprint arXiv:0707.3785 [hep-ph].
- Fulde, P., and R. A. Ferrell, 1964, Phys. Rev. **135**, A550.
- Gatto, R., and M. Ruggieri, 2007, Phys. Rev. **D75**, 114004.
- Gerhold, A., A. Ipp, and A. Rebhan, 2004, Phys. Rev. **D70**, 105015.
- Gerhold, A., and A. Rebhan, 2003, Phys. Rev. **D68**, 011502.
- Gerhold, A., and A. Rebhan, 2005, Phys. Rev. **D71**, 085010.
- Gerhold, A., and T. Schäfer, 2006, Phys. Rev. **D73**, 125022.
- Gerhold, A., T. Schäfer, and A. Kryjevski, 2007, Phys. Rev. **D75**, 054012.
- Giannakis, I., D.-f. Hou, and H.-C. Ren, 2005, Phys. Lett. **B631**, 16.
- Giannakis, I., D.-f. Hou, H.-c. Ren, and D. H. Rischke, 2004, Phys. Rev. Lett. **93**, 232301.
- Giannakis, I., J. T. Liu, and H.-c. Ren, 2002, Phys. Rev. **D66**, 031501.
- Giannakis, I., and H.-c. Ren, 2003, Nucl. Phys. **B669**, 462.
- Giannakis, I., and H.-C. Ren, 2005a, Phys. Lett. **B611**, 137.
- Giannakis, I., and H.-C. Ren, 2005b, Nucl. Phys. **B723**, 255.
- Giorgini, S., L. P. Pitaevskii, and S. Stringari, 2007, eprint arXiv:0706.3360.
- Glendenning, N. K., 1985, Astrophys. J. **293**, 470.
- Glendenning, N. K., 1992, Phys. Rev. **D46**(4), 1274.
- Glendenning, N. K., S. Pei, and F. Weber, 1997, Phys. Rev. Lett. **79**, 1603.
- Glendenning, N. K., and F. Weber, 2001, Astrophys. J. **559**, L119.
- Gorbar, E. V., M. Hashimoto, and V. A. Miransky, 2006a, Phys. Lett. **B632**, 305.
- Gorbar, E. V., M. Hashimoto, and V. A. Miransky, 2007, Phys. Rev. **D75**, 085012.
- Gorbar, E. V., M. Hashimoto, V. A. Miransky, and I. A. Shovkovy, 2006b, Phys. Rev. **D73**, 111502.
- Greiter, M., F. Wilczek, and E. Witten, 1989, Mod. Phys. Lett. **B3**, 903.
- Grigorian, H., D. Blaschke, and D. Voskresensky, 2005, Phys. Rev. **C71**, 045801.
- Gross, D. J., and F. Wilczek, 1973, Phys. Rev. Lett. **30**, 1343.
- Gubankova, E., W. V. Liu, and F. Wilczek, 2003, Phys. Rev. Lett. **91**, 032001.
- Gubankova, E., A. Schmitt, and F. Wilczek, 2006, Phys. Rev. **B74**, 064505.
- Gusakov, M. E., 2007, eprint arXiv:0704.1071 [astro-ph].
- Haensel, P., K. P. Levenfish, and D. G. Yakovlev, 2000, Astron. Astrophys. **357**, 1157.
- Haensel, P., K. P. Levenfish, and D. G. Yakovlev, 2001a, eprint astro-ph/0103290.
- Haensel, P., K. P. Levenfish, and D. G. Yakovlev, 2001b, eprint astro-ph/0110575.
- Haensel, P., J. L. Zdunik, and R. Schaeffer, 1986, Astron. Astrophys. **160**, 121.
- Halperin, B. i., T. C. Lubensky, and S.-k. Ma, 1974, Phys. Rev. Lett. **32**, 292.
- Hands, S., S. Kim, and J.-I. Skullerud, 2006, Eur. Phys. J. **C48**, 193.
- Hands, S., J. B. Kogut, M.-P. Lombardo, and S. E. Morrison, 1999, Nucl. Phys. **B558**, 327.
- Hands, S., and D. N. Walters, 2004, Phys. Rev. **D69**, 076011.
- Hashimoto, M., 2006, Phys. Lett. **B642**, 93.
- Hashimoto, M., and V. A. Miransky, 2007, eprint arXiv:0705.2399 [hep-ph].
- Haskell, B., N. Andersson, D. I. Jones, and L. Samuelsson, 2007, eprint arXiv:0708.2984 [gr-qc].
- Hatsuda, T., M. Tachibana, N. Yamamoto, and G. Baym, 2006, Phys. Rev. Lett. **97**, 122001.
- He, L., M. Jin, and P. Zhuang, 2007, Phys. Rev. **D75**, 036003.
- Heinke, C. O., P. G. Jonker, R. Wijnands, and R. E. Taam, 2007, Astrophys. J. **660**, 1424.
- Heiselberg, H., and C. J. Pethick, 1993, Phys. Rev. **D48**, 2916.
- Hessels, J. W. T., *et al.*, 2006, Science **311**, 1901.
- Higgs, P. W., 1964, Phys. Lett. **12**, 132.
- Holstein, T., A. E. Norton, and P. Pincus, 1973, Phys. Rev. **B8**, 2649.
- Hong, D. K., 2000a, Nucl. Phys. **B582**, 451.
- Hong, D. K., 2000b, Phys. Lett. **B473**, 118.
- Hong, D. K., 2001, Acta Phys. Polon. **B32**, 1253.
- Hong, D. K., 2005, eprint hep-ph/0506097.
- Hong, D. K., V. A. Miransky, I. A. Shovkovy, and L. C. R. Wijewardhana, 2000, Phys. Rev. **D61**, 056001.
- 't Hooft, G., 1976, Phys. Rev. Lett. **37**, 8.
- Hou, D.-f., Q. Wang, and D. H. Rischke, 2004, Phys. Rev. **D69**, 071501.
- Hsu, S. D. H., 2000, eprint hep-ph/0003140.
- Hsu, S. D. H., and M. Schwetz, 2000, Nucl. Phys. **B572**, 211.
- Huang, M., 2005, Int. J. Mod. Phys. **E14**, 675.
- Huang, M., 2006, Phys. Rev. **D73**, 045007.
- Huang, M., and I. Shovkovy, 2003, Nucl. Phys. **A729**, 835.
- Huang, M., and I. A. Shovkovy, 2004a, Phys. Rev. **D70**, 051501.
- Huang, M., and I. A. Shovkovy, 2004b, Phys. Rev. **D70**, 094030.
- Iida, K., and G. Baym, 2001, Phys. Rev. **D63**, 074018.
- Iida, K., and G. Baym, 2002, Phys. Rev. **D66**, 014015.
- Iida, K., and K. Fukushima, 2006, Phys. Rev. **D74**, 074020.
- Iida, K., T. Matsuura, M. Tachibana, and T. Hatsuda, 2004, Phys. Rev. Lett. **93**, 132001.
- Iida, K., T. Matsuura, M. Tachibana, and T. Hatsuda, 2005, Phys. Rev. **D71**, 054003.
- Ipp, A., A. Gerhold, and A. Rebhan, 2004, Phys. Rev. **D69**, 011901.
- Ipp, A., K. Kajantie, A. Rebhan, and A. Vuorinen, 2006, Phys. Rev. **D74**, 045016.
- Ippolito, N. D., G. Nardulli, and M. Ruggieri, 2007, JHEP **04**, 036.
- Israel, G., *et al.*, 2005, Astrophys. J. **628**, L53.
- Itoh, N., 1970, Prog. Theor. Phys. **44**, 291.
- Ivanenko, D. D., and D. F. Kurdgelaidze, 1965, Astrophysics **1**(4), 479.
- Ivanenko, D. D., and D. F. Kurdgelaidze, 1969, Lett. Nuovo Cim. **IIS1**, 13.
- Ivanenko, D. D., and D. F. Kurdgelaidze, 1970, Sov. Phys. J. **13**, 1015.
- Iwamoto, N., 1980, Phys. Rev. Lett. **44**, 1637.
- Iwamoto, N., 1982, Ann. Phys. (N.Y.) **141**, 1.
- Iwasaki, M., 1995, Prog. Theor. Phys. Suppl. **120**, 187.
- Iwasaki, M., and T. Iwado, 1995, Phys. Lett. **B350**, 163.
- Jaffe, R. L., 1977, Phys. Rev. **D15**, 267.
- Jaffe, R. L., and F. Wilczek, 2003, Phys. Rev. Lett. **91**, 232003.
- Jaikumar, P., and M. Prakash, 2001, Phys. Lett. **B516**, 345.
- Jaikumar, P., M. Prakash, and T. Schäfer, 2002, Phys. Rev.

- D66**, 063003.
Jaikumar, P., S. Reddy, and A. W. Steiner, 2006a, Phys. Rev. Lett. **96**, 041101.
Jaikumar, P., C. D. Roberts, and A. Sedrakian, 2006b, Phys. Rev. **C73**, 042801.
Jones, P. B., 1997, Phys. Rev. Lett. **79**, 792.
Jonker, P. G., D. Steeghs, D. Chakrabarty, and A. M. Juett, 2007, eprint arXiv:0706.3421 [astro-ph].
Jonker, P. G., *et al.*, 2006, Mon. Not. Roy. Astron. Soc. **368**, 1803.
Kaplan, D. B., and A. E. Nelson, 1986, Phys. Lett. **B175**, 57.
Kaplan, D. L., 2007, private communication.
Kaplan, D. L., B. M. Gaensler, S. R. Kulkarni, and P. O. Slane, 2006, Astrophys. J. Suppl. **163**, 344.
Kaplan, D. L., *et al.*, 2004, Astrophys. J. Suppl. **153**, 269.
Kashiwa, K., M. Matsuzaki, H. Kouno, and M. Yahiro, 2007, eprint arXiv:0705.1196 [hep-ph].
Khalatnikov, I., 1989, *An Introduction to the Theory of Superfluidity* (Addison-Wesley, New York).
Kim, E., and M. H. W. Chan, 2004a, Nature **427**, 225.
Kim, E., and M. H. W. Chan, 2004b, Science **305**, 1941.
Kiryama, O., 2006a, Phys. Rev. **D74**, 114011.
Kiryama, O., 2006b, Phys. Rev. **D74**, 074019.
Kislinger, M. B., and P. D. Morley, 1976, Phys. Rev. D **13**(10), 2765.
Kitazawa, M., T. Koide, T. Kunihiro, and Y. Nemoto, 2002, Phys. Rev. **D65**, 091504.
Kitazawa, M., T. Koide, T. Kunihiro, and Y. Nemoto, 2004, Phys. Rev. **D70**, 056003.
Kitazawa, M., T. Koide, T. Kunihiro, and Y. Nemoto, 2005a, Prog. Theor. Phys. **114**, 117.
Kitazawa, M., T. Kunihiro, and Y. Nemoto, 2005b, Phys. Lett. **B631**, 157.
Kitazawa, M., D. H. Rischke, and I. A. Shovkovy, 2006, Phys. Lett. **B637**, 367.
Kitazawa, M., D. H. Rischke, and I. A. Shovkovy, 2007, eprint arXiv:0709.2235 [hep-ph].
Kleinhaus, V., M. Buballa, D. Nickel, and M. Oertel, 2007, eprint arXiv:0707.0632 [hep-ph].
Kogut, J. B., and D. K. Sinclair, 2002, Phys. Rev. **D66**, 034505.
Kogut, J. B., D. K. Sinclair, S. J. Hands, and S. E. Morrison, 2001, Phys. Rev. **D64**, 094505.
Kogut, J. B., M. A. Stephanov, and D. Toublan, 1999, Phys. Lett. **B464**, 183.
Kogut, J. B., M. A. Stephanov, D. Toublan, J. J. M. Verbaarschot, and A. Zhitnitsky, 2000, Nucl. Phys. **B582**, 477.
Kogut, J. B., D. Toublan, and D. K. Sinclair, 2002, Nucl. Phys. **B642**, 181.
Kramer, M., *et al.*, 2004, eprint astro-ph/0405179.
Kramer, M., *et al.*, 2006, Science **314**, 97.
Kryjevski, A., 2003, Phys. Rev. **D68**, 074008.
Kryjevski, A., 2005, eprint hep-ph/0508180.
Kryjevski, A., D. B. Kaplan, and T. Schäfer, 2005, Phys. Rev. **D71**, 034004.
Kryjevski, A., and T. Schäfer, 2005, Phys. Lett. **B606**, 52.
Kryjevski, A., and D. Yamada, 2005, Phys. Rev. **D71**, 014011.
Kundu, J., and K. Rajagopal, 2002, Phys. Rev. **D65**, 094022.
Kundu, J., and S. Reddy, 2004, Phys. Rev. **C70**, 055803.
Landau, L. D., and E. M. Lifshitz, 1981, *Theory of Elasticity* (Pergamon, Oxford), 3rd edition.
Landau, L. D., and E. M. Lifshitz, 1987, *Fluid Mechanics* (Pergamon, Oxford), 2nd edition.
Larkin, A. I., and Y. N. Ovchinnikov, 1965, Sov. Phys. JETP **20**, 762.
Lattimer, J. M., and M. Prakash, 2001, Astrophys. J. **550**, 426.
Lattimer, J. M., and M. Prakash, 2004, Science **304**, 536.
Lattimer, J. M., and M. Prakash, 2007, Phys. Rept. **442**, 109.
Lattimer, J. M., and B. F. Schutz, 2005, Astrophys. J. **629**, 979.
Leggett, A. J., 1970, Phys. Rev. Lett. **25**, 1543.
Leibovich, A. K., K. Rajagopal, and E. Shuster, 2001, Phys. Rev. **D64**, 094005.
Levin, Y., and G. Ushomirsky, 2001, Mon. Not. Roy. Astron. Soc. **324**, 917.
Lin, L.-M., 2007, eprint arXiv:0708.2965 [astro-ph].
Lindblom, L., and B. J. Owen, 2002, Phys. Rev. **D65**, 063006.
Lindblom, L., B. J. Owen, and S. M. Morsink, 1998, Phys. Rev. Lett. **80**, 4843.
Link, B., 2006, Astron. Astrophys. **458**, 881.
Link, B., 2007a, talk given at INT workshop on The Neutron Star Crust and Surface, Seattle, and private communication.
Link, B., 2007b, Astrophys. and Space Sci. **308**, 435.
Link, B., and R. I. Epstein, 1996, Astrophys. J. **457**, 854.
Link, B., R. I. Epstein, and G. Baym, 1993, Astrophys. J. **403**, 285.
Litim, D. F., and C. Manuel, 2001, Phys. Rev. **D64**, 094013.
Lugones, G., and J. E. Horvath, 2002, Phys. Rev. **D66**, 074017.
Luttinger, J. M., and J. C. Ward, 1960, Phys. Rev. **118**, 1417.
Lyne, A. G., *et al.*, 2004, Science **303**, 1153.
Madsen, J., 1992, Phys. Rev. **D46**, 3290.
Madsen, J., 1993, Phys. Rev. **D47**, 325.
Madsen, J., 2000, Phys. Rev. Lett. **85**, 10.
Malekzadeh, H., 2006, Phys. Rev. **D74**, 065011.
Malekzadeh, H., and D. H. Rischke, 2006, Phys. Rev. **D73**, 114006.
Mannarelli, M., G. Nardulli, and M. Ruggieri, 2006a, eprint cond-mat/0604579.
Mannarelli, M., K. Rajagopal, and R. Sharma, 2006b, Phys. Rev. **D73**, 114012.
Mannarelli, M., K. Rajagopal, and R. Sharma, 2007, eprint hep-ph/0702021.
Manuel, C., 2000a, Phys. Rev. **D62**, 076009.
Manuel, C., 2000b, Phys. Rev. **D62**, 114008.
Manuel, C., A. Dobado, and F. J. Llanes-Estrada, 2005, JHEP **09**, 076.
Manuel, C., and F. Llanes-Estrada, 2007, eprint arXiv:0705.3909 [hep-ph].
Manuel, C., and K. Rajagopal, 2002, Phys. Rev. Lett. **88**, 042003.
Manuel, C., and M. H. G. Tytgat, 2000, Phys. Lett. **B479**, 190.
Marhauser, F., D. Nickel, M. Buballa, and J. Wambach, 2007, Phys. Rev. **D75**, 054022.
Matsuura, T., K. Iida, T. Hatsuda, and G. Baym, 2004, Phys. Rev. **D69**, 074012.
McLerran, L., and R. D. Pisarski, 2007, eprint arXiv:0706.2191 [hep-ph].
Migdal, A. B., 1971, Zh. Eksp. Teor. Fiz. **61**, 2209.
Miransky, V. A., and I. A. Shovkovy, 2002, Phys. Rev. Lett. **88**, 111601.
Miransky, V. A., I. A. Shovkovy, and L. C. R. Wijewardhana, 2001, Phys. Rev. **D64**, 096002.
Mishra, A., and H. Mishra, 2004, Phys. Rev. **D69**, 014014.

- Mishra, A., and H. Mishra, 2005, Phys. Rev. **D71**, 074023.
- Mishra, A., and H. Mishra, 2006, Phys. Rev. **D74**, 054024.
- Morrison, I. A., T. W. Baumgarte, S. L. Shapiro, and V. R. Pandharipande, 2004, Astrophys. J. **617**, L135.
- Nakano, E., M. Nitta, and T. Matsuura, 2007, eprint arXiv:0708.4096 [hep-ph].
- Nardulli, G., 2002, Riv. Nuovo Cim. **25N3**, 1.
- Nayak, C., and F. Wilczek, 1994, Nucl. Phys. **B430**, 534.
- Negele, J. W., and D. Vautherin, 1973, Nucl. Phys. **A207**, 298.
- Neumann, F., M. Buballa, and M. Oertel, 2003, Nucl. Phys. **A714**, 481.
- Nice, D., and I. Stairs, 2007, private communication.
- Nice, D. J., *et al.*, 2005, Astrophys. J. **634**, 1242.
- Nickel, D., R. Alkofer, and J. Wambach, 2006a, Phys. Rev. **D74**, 114015.
- Nickel, D., J. Wambach, and R. Alkofer, 2006b, Phys. Rev. **D73**, 114028.
- Nishida, Y., K. Fukushima, and T. Hatsuda, 2004, Phys. Rept. **398**, 281.
- Noronha, J. L., H.-c. Ren, I. Giannakis, D. Hou, and D. H. Rischke, 2006, Phys. Rev. **D73**, 094009.
- Noronha, J. L., and I. A. Shovkovy, 2007, eprint arXiv:0708.0307 [hep-ph].
- Ouyed, R., and F. Sannino, 2001, Phys. Lett. **B511**, 66.
- Owen, B. J., 2005, Phys. Rev. Lett. **95**, 211101.
- Owen, B. J., *et al.*, 1998, Phys. Rev. **D58**, 084020.
- Pacini, F., 1966, Nature **209**, 389.
- Page, D., J. M. Lattimer, M. Prakash, and A. W. Steiner, 2004, Astrophys. J. Suppl. **155**, 623.
- Page, D., and S. Reddy, 2006, Ann. Rev. Nucl. Part. Sci. **56**, 327.
- Partridge, G. B., W. Li, R. I. Kamar, Y. Liao, and R. G. Hulet, 2006, Science **311**, 503.
- Pines, D., and M. A. Alpar, 1985, Nature **316**, 27.
- Pisarski, R. D., and D. H. Rischke, 1999a, Phys. Rev. Lett. **83**, 37.
- Pisarski, R. D., and D. H. Rischke, 1999b, Phys. Rev. **D60**, 094013.
- Pisarski, R. D., and D. H. Rischke, 1999c, eprint nucl-th/9907094.
- Pisarski, R. D., and D. H. Rischke, 2000a, Phys. Rev. **D61**, 074017.
- Pisarski, R. D., and D. H. Rischke, 2000b, Phys. Rev. **D61**, 051501.
- Pisarski, R. D., and D. H. Rischke, 2002, Nucl. Phys. **A702**, 177.
- Polchinski, J., 1992, eprint hep-th/9210046.
- Polchinski, J., 1994, Nucl. Phys. **B422**, 617.
- Politzer, H. D., 1973, Phys. Rev. Lett. **30**, 1346.
- Prakash, M., J. M. Lattimer, J. A. Pons, A. W. Steiner, and S. Reddy, 2001, Lect. Notes Phys. **578**, 364.
- Rajagopal, K., and A. Schmitt, 2006, Phys. Rev. **D73**, 045003.
- Rajagopal, K., and R. Sharma, 2006a, J. Phys. **G32**, S483.
- Rajagopal, K., and R. Sharma, 2006b, Phys. Rev. **D74**, 094019.
- Rajagopal, K., and E. Shuster, 2000, Phys. Rev. **D62**, 085007.
- Rajagopal, K., and F. Wilczek, 2000, eprint hep-ph/0011333.
- Rajagopal, K., and F. Wilczek, 2001, Phys. Rev. Lett. **86**, 3492.
- Ransom, S. M., *et al.*, 2005, Science **307**, 892.
- Rapp, R., T. Schäfer, E. V. Shuryak, and M. Velkovsky, 1998, Phys. Rev. Lett. **81**, 53.
- Rapp, R., T. Schäfer, E. V. Shuryak, and M. Velkovsky, 2000, Annals Phys. **280**, 35.
- Ravenhall, D. G., C. J. Pethick, and J. R. Wilson, 1983, Phys. Rev. Lett. **50**(26), 2066.
- Reddy, S., 2002, Acta Phys. Polon. **B33**, 4101.
- Reddy, S., and G. Rupak, 2005, Phys. Rev. **C71**, 025201.
- Reddy, S., M. Sadzikowski, and M. Tachibana, 2003a, Phys. Rev. **D68**, 053010.
- Reddy, S., M. Sadzikowski, and M. Tachibana, 2003b, Nucl. Phys. **A714**, 337.
- Ren, H.-c., 2004, eprint hep-ph/0404074.
- Reuter, P. T., 2006, Phys. Rev. **D74**, 105008.
- Reuter, P. T., Q. Wang, and D. H. Rischke, 2004, Phys. Rev. **D70**, 114029.
- Rho, M., A. Wirzba, and I. Zahed, 2000, Phys. Lett. **B473**, 126.
- Rischke, D. H., 2000a, Phys. Rev. **D62**, 054017.
- Rischke, D. H., 2000b, Phys. Rev. **D62**, 034007.
- Rischke, D. H., 2001, Phys. Rev. **D64**, 094003.
- Rischke, D. H., 2004, Prog. Part. Nucl. Phys. **52**, 197.
- Rischke, D. H., and I. A. Shovkovy, 2002, Phys. Rev. **D66**, 054019.
- Rischke, D. H., D. T. Son, and M. A. Stephanov, 2001, Phys. Rev. Lett. **87**, 062001.
- Ruggieri, M., 2007, JHEP **07**, 031.
- Rüster, S. B., and D. H. Rischke, 2004, Phys. Rev. **D69**, 045011.
- Rüster, S. B., I. A. Shovkovy, and D. H. Rischke, 2004, Nucl. Phys. **A743**, 127.
- Rüster, S. B., V. Werth, M. Buballa, I. A. Shovkovy, and D. H. Rischke, 2005, Phys. Rev. **D72**, 034004.
- Rüster, S. B., V. Werth, M. Buballa, I. A. Shovkovy, and D. H. Rischke, 2006, eprint nucl-th/0602018.
- Sa'd, B. A., I. A. Shovkovy, and D. H. Rischke, 2007a, Phys. Rev. **D75**, 065016.
- Sa'd, B. A., I. A. Shovkovy, and D. H. Rischke, 2007b, Phys. Rev. **D75**, 125004.
- Sawyer, R. F., 1972, Phys. Rev. Lett. **29**, 382.
- Sawyer, R. F., 1989, Phys. Rev. **D39**, 3804.
- Scalapino, D. J., 1972, Phys. Rev. Lett. **29**, 386.
- Schäfer, T., 2000a, Nucl. Phys. **B575**, 269.
- Schäfer, T., 2000b, Phys. Rev. **D62**, 094007.
- Schäfer, T., 2002a, Phys. Rev. **D65**, 094033.
- Schäfer, T., 2002b, Phys. Rev. **D65**, 074006.
- Schäfer, T., 2003a, Nucl. Phys. **A728**, 251.
- Schäfer, T., 2003b, eprint hep-ph/0304281.
- Schäfer, T., 2004, eprint hep-ph/0402032.
- Schäfer, T., 2006, Phys. Rev. Lett. **96**, 012305.
- Schäfer, T., and K. Schwenzer, 2004a, Phys. Rev. **D70**, 114037.
- Schäfer, T., and K. Schwenzer, 2004b, Phys. Rev. **D70**, 054007.
- Schäfer, T., and K. Schwenzer, 2006, Phys. Rev. Lett. **97**, 092301.
- Schäfer, T., D. T. Son, M. A. Stephanov, D. Toublan, and J. J. M. Verbaarschot, 2001, Phys. Lett. **B522**, 67.
- Schäfer, T., and F. Wilczek, 1999a, Phys. Rev. Lett. **82**, 3956.
- Schäfer, T., and F. Wilczek, 1999b, Phys. Lett. **B450**, 325.
- Schäfer, T., and F. Wilczek, 1999c, Phys. Rev. **D60**, 074014.
- Schäfer, T., and F. Wilczek, 1999d, Phys. Rev. **D60**, 114033.
- Schmidt, C., 2006, PoS **LAT2006**, 021.
- Schmitt, A., 2004, *Spin-one color superconductivity in cold and dense quark matter*, Ph.D. thesis, Johann-Wolfgang-Goethe-Universität, Frankfurt/Main, Germany,

- eprint nucl-th/0405076.
- Schmitt, A., 2005, Phys. Rev. **D71**, 054016.
- Schmitt, A., I. A. Shovkovy, and Q. Wang, 2006, Phys. Rev. **D73**, 034012.
- Schmitt, A., Q. Wang, and D. H. Rischke, 2002, Phys. Rev. **D66**, 114010.
- Schmitt, A., Q. Wang, and D. H. Rischke, 2003, Phys. Rev. Lett. **91**, 242301.
- Schmitt, A., Q. Wang, and D. H. Rischke, 2004, Phys. Rev. **D69**, 094017.
- Schwarz, T. M., S. P. Klevansky, and G. Papp, 1999, Phys. Rev. **C60**, 055205.
- Sedrakian, A., I. Wasserman, and J. M. Cordes, 1999, Astrophys. J. **524**, 341S.
- Selem, A., and F. Wilczek, 2006, eprint hep-ph/0602128.
- Shabanova, T. V., A. G. Lyne, and J. O. Urama, 2001, Astrophys. J. **552**, 321.
- Shankar, R., 1994, Rev. Mod. Phys. **66**, 129.
- Sheehy, D. E., and L. Radzihovsky, 2006, Phys. Rev. Lett. **96**, 060401.
- Sheehy, D. E., and L. Radzihovsky, 2007, Ann. Phys. **322**, 1790.
- Shovkovy, I., and M. Huang, 2003, Phys. Lett. **B564**, 205.
- Shovkovy, I. A., 2005, Found. Phys. **35**, 1309.
- Shovkovy, I. A., and P. J. Ellis, 2002, Phys. Rev. **C66**, 015802.
- Shovkovy, I. A., and P. J. Ellis, 2003, Phys. Rev. **C67**, 048801.
- Shovkovy, I. A., and L. C. R. Wijewardhana, 1999, Phys. Lett. **B470**, 189.
- Shuster, E., and D. T. Son, 2000, Nucl. Phys. **B573**, 434.
- Son, D. T., 1999, Phys. Rev. **D59**, 094019.
- Son, D. T., 2002, eprint hep-ph/0204199.
- Son, D. T., 2005, Phys. Rev. Lett. **94**, 175301.
- Son, D. T., and M. A. Stephanov, 2000a, Phys. Rev. **D61**, 074012.
- Son, D. T., and M. A. Stephanov, 2000b, Phys. Rev. **D62**, 059902.
- Son, D. T., and M. A. Stephanov, 2001, Phys. Rev. Lett. **86**, 592.
- Son, D. T., and M. A. Stephanov, 2006, Phys. Rev. A **74**, 013614.
- Son, D. T., M. A. Stephanov, and A. R. Zhitnitsky, 2001, Phys. Rev. Lett. **86**, 3955.
- Sotani, H., K. Tominaga, and K.-i. Maeda, 2002, Phys. Rev. **D65**, 024010.
- Splaver, E. M., *et al.*, 2002, Astrophys. J. **581**, 509.
- Splitteroff, K., D. T. Son, and M. A. Stephanov, 2001, Phys. Rev. **D64**, 016003.
- Srednicki, M., and L. Susskind, 1981, Nucl. Phys. **B187**, 93.
- Stairs, I. H., A. G. Lyne, and S. L. Shemar, 2000, Nature **406**, 484.
- Steiner, A. W., S. Reddy, and M. Prakash, 2002, Phys. Rev. **D66**, 094007.
- Strohmayer, T., H. M. van Horn, S. Ogata, H. Iyetomi, and S. Ichimaru, 1991, Astrophys. J. **375**, 679.
- Strohmayer, T. E., and A. L. Watts, 2005, Astrophys. J. **632**, L111.
- Strohmayer, T. E., and A. L. Watts, 2006, Astrophys. J. **653**, 593.
- Takagi, S., 2003, Prog. Theor. Phys. **109**, 233.
- Vanderheyden, B., and J.-Y. Ollitrault, 1997, Phys. Rev. **D56**, 5108.
- Voskresensky, D. N., 2004, Phys. Rev. **C69**, 065209.
- Wang, Q., and D. H. Rischke, 2002, Phys. Rev. **D65**, 054005.
- Wang, Q., Z.-g. Wang, and J. Wu, 2006, Phys. Rev. **D74**, 014021.
- Warringa, H. J., 2006, eprint hep-ph/0606063.
- Warringa, H. J., D. Boer, and J. O. Andersen, 2005, Phys. Rev. **D72**, 014015.
- Watts, A. L., and S. Reddy, 2007, Mon. Not. Roy. Astron. Soc. **379**, L63.
- Watts, A. L., and T. E. Strohmayer, 2006, Astrophys. J. **637**, L117.
- Watts, A. L., and T. E. Strohmayer, 2007, Astrophys. Space Sci. **308**, 625.
- Weber, F., 1999, *Pulsars as Astrophysical Laboratories for Nuclear and Particle Physics* (IOP Publishing Ltd., Bristol).
- Weber, F., A. Torres i Cuadrat, A. Ho, and P. Rosenfield, 2006, PoS **JHW2005**, 018.
- Witten, E., 1984, Phys. Rev. **D30**, 272.
- Yakovlev, D. G., A. D. Kaminker, O. Y. Gnedin, and P. Haensel, 2001, Phys. Rept. **354**, 1.
- Yakovlev, D. G., and C. J. Pethick, 2004, Ann. Rev. Astron. Astrophys. **42**, 169.
- Yakovlev, D. G., *et al.*, 2005, Nucl. Phys. **A752**, 590.
- Yamamoto, N., M. Tachibana, T. Hatsuda, and G. Baym, 2007, eprint arXiv:0704.2654 [hep-ph].
- Zarembo, K., 2000, Phys. Rev. **D62**, 054003.
- Zwierlein, M. W., A. Schirotzek, C. H. Schunck, and W. Ketterle, 2006, Science **311**, 492.